Fall 12-2020

Relative Attitude Dynamics and Control of Spacecraft Using Electrostatic Torque

John Galjanic
Embry-Riddle Aeronautical University

RELATIVE ATTITUDE DYNAMICS AND CONTROL OF SPACECRAFT USING ELECTROSTATIC TORQUE

By

John Galjanic

A Thesis Submitted to the Faculty of Embry-Riddle Aeronautical University

In Partial Fulfillment of the Requirements for the Degree of

Master of Science in Aerospace Engineering

December 2020

Embry-Riddle Aeronautical University

Daytona Beach, Florida

RELATIVE ATTITUDE DYNAMICS AND CONTROL OF SPACECRAFT USING ELECTROSTATIC TORQUE

By

John Galjanic

This Thesis was prepared under the direction of the candidate's Thesis Committee Chair, Dr. Dongeun Seo, Department of Aerospace Engineering, and has been approved by the members of the Thesis Committee. It was submitted to the Office of the Senior Vice President for Academic Affairs and Provost, and was accepted in partial fulfillment of the requirements for the Degree of Master of Science in Aerospace Engineering.

THESIS COMMITTEE

Dongeun Seo Digitally signed by Dongeun Seo DN: cn=Dongeun Seo, c=US, o=Embry-Riddle Aeronautical University, ou=Aerospace Engineering Department, email=seod@erau.edu Date: 2020.12.03 14:04:24 -05'00'	Morad Nazari Digitally signed by Morad Nazari Date: 2020.12.03 14:49:55 -05'00'
Chairman, Dr. Dongeun Seo	Member, Dr. Morad Nazari
Troy A. Henderson Digitally signed by Troy A. Henderson Date: 2020.12.03 14:41:41 -05'00'	
Member, Dr. Troy Henderson	
Marwan Al-Haik Digitally signed by Marwan Al-Haik DN: cn=Marwan Al-Haik, o=Embry-Riddle Aeronautical University, ou=Aerospace Engineering, email=alhaikm@erau.edu, c=US Date: 2020.12.04 09:20:24 -05'00'	12/4/2020
Graduate Program Coordinator, Dr. Marwan Al-Haik	Date
Maj Mirmirani Digitally signed by Maj Mirmirani Date: 2020.12.04 09:33:21 -05'00'	12/4/2020
Dean of the College of Engineering, Dr. Maj Mirmirani	Date
Christopher Grant Digitally signed by Christopher Grant Date: 2020.12.04 09:44:50 -05'00'	12/4/2020
Associate Provost of Academic Support, Dr. Christopher Grant	Date

ACKNOWLEDGEMENTS

First, I would like to thank my family for the years of support, encouragement, and guidance they have provided me. Without them, I would not have been able to complete my education and chase my dream of working in the field of space exploration. Their presence in my life has been a solid foundation and a bright guiding light, and I am very grateful to them.

I would like to thank my advisor, Dr. Dongeun Seo, for suggesting this topic for research. Throughout this course of study, he has always been available for questions and advice. However, he was also always willing to let me attempt new directions and approaches to problems in ways that seemed most appropriate to me. His guidance has shaped my career as a graduate student and has made me into the professional I am today.

I would like to thank my committee members, Dr. Morad Nazari and Dr. Troy Henderson for their attention to my research and the numerous improvements and enhancements they have suggested to this work. Their guidance has helped shape this thesis into the addition to control theory that it has become.

Finally, I would like to thank Embry-Riddle Aeronautical University as an institution. My time here as both an undergraduate and a graduate student will always be among the most cherished in my life, and I am grateful to this institution, not only for providing the educational foundation upon which my career will be built, but for providing me connection with so many like-minded people that I may call their community a second family.

ABSTRACT

Recent years have seen an increased interest in spacecraft formation flying, with many applications requiring that the members of these formations maintain specific relative attitude configurations. One low-cost method that has been considered to accomplish this is the use of electrostatic torques, which are generated by charging the surfaces of involved spacecraft to allow interaction without physical contact. The research presented in this thesis analyzes a pair of cylindrical-bodied spacecraft operating in deep space. Specifically, the suitability of using electrostatic torques as an actuator to synchronize the two spacecraft's attitude responses is under consideration. The study considers a simplified case, wherein the two spacecraft are restricted to rotate in a single plane, as well as a more practical case where the two are allowed to freely rotate in three dimensions about their centers of mass. These cases are primarily investigated to develop suitable control laws to accomplish the attitude synchronization between the two spacecraft. Additionally, the actuator dynamics required to implement one of these controllers are developed and simulated, in order to investigate the practicality of using the controller in question. Based on the findings of this study, the system was found to be controllable with the presented control laws. In addition, the actuator dynamics required to implement one of these control laws were developed and simulations show that much of the control can be accomplished with small changes in the actuating spacecraft charge. However, with the currently-considered 3D controller in the case that was simulated, the required actuator dynamics are too aggressive at one point for a practical device to accomplish the charging. Thus, future work may consider other 3D control laws.

TABLE OF CONTENTS

LIST OF FIGURES

LIST OF TABLES

NOMENCLATURE

$A(t)$	dynamic matrix for a general linear system
$B(t)$	input-coupling matrix for a general linear system
C	cost function for LQR control
D^+	upper-right Dini time-derivative operator
d	distance between chief and deputy spacecraft
E_{CD}	relative attitude DCM of deputy spacecraft with respect to chief spacecraft
$\vec{e}$	state vector for 2D Case
$\vec{F}_{12}$	electrostatic force between general point charges 1 and 2
$\vec{f}(\vec{x}, t, \vec{u})$	vector of nonlinear state functions for a general system
$H_\gamma(t_0, t_1)$	modified controllability Grammian for use in grammian controller
$\vec{H}_G$	angular momentum about center of mass for a general rotating body
h_m	general scalar for proving stability of Grammian controller
h_M	general scalar for proving stability of Grammian controller
$h(\Phi_{CD})$	potential function of principal rotation angle of relative attitude, used in 3D Case
I_{nxn}	n x n – sized identity matrix
I	moment-of-inertia tensor
I_a	scalar moment of inertia about spacecraft long axis
I_t	scalar moment of inertia about spacecraft transverse axis
$\hat{I}$	first axis unit vector of chief spacecraft body-fixed frame
$\hat{\imath}$	first axis unit vector of deputy spacecraft body-fixed frame
$\hat{J}$	second axis unit vector of chief spacecraft body-fixed frame

$\hat{j}$	second axis unit vector of deputy spacecraft body-fixed frame
$\widehat{K}$	third axis unit vector of chief spacecraft body-fixed frame
$\hat{k}$	third axis unit vector for deputy spacecraft body-fixed frame
$\vec{k}$	principal rotation vector for a general attitude representation
$\vec{k}_{CD}$	principal rotation vector for the relative attitude of the deputy spacecraft with respect to the chief spacecraft
k_C	Coulomb's Constant
L_C	scalar electrostatic torque acting on the chief spacecraft in the 2D Case
L_D	scalar electrostatic torque acting on the deputy spacecraft in the 2D Case
l	distance between two adjacent charged regions on a single spacecraft
$\vec{M}_C^{OL}$	vector open-loop electrostatic torque acting on the chief spacecraft in the 3D Case
$\vec{M}_D^{CL}$	vector closed-loop electrostatic torque acting on the deputy spacecraft in the 3D Case
$\vec{M}_D^{OL}$	vector open-loop electrostatic torque acting on the deputy spacecraft in the 3D Case
$\vec{M}_G$	torque about the center of mass of a general rotating body
$P(t)$	unknown parameter of the Algebraic Riccatti Equation
$Q(t)$	state-weighting matrix for the LQR controller
$Q_{i\to I}$	DCM transforming vectors between the general frames i and I
q_1	electrostatic charge on region 1
q_2	electrostatic charge on region 2
q_3	electrostatic charge on region 3
q_a	electrostatic charge on region a

q_b	electrostatic charge on region b
q_c	electrostatic charge on region c
$R(t)$	input-weighting matrix for the LQR controller
$\hat{r}_{12}$	unit vector pointing from general point charge 1 to general point charge 2
$\vec{r}_{12}$	relative position vector from general point charge 1 to general point charge 2
$\vec{r}_{G2}$	relative position vector from general rotating object's center of mass to general point charge 2
t	time since a reference start time
t_0	start time for time interval of interest
t_1	final time of time interval of interest
$\vec{u}$	input vector to a general system
$V(\vec{x})$	Lyapunov function of a general system's state vector
$\vec{v}^{\hat{\imath}}$	general vector expressed in the general i frame
$\vec{v}^{\hat{I}}$	general vector expressed in the general I frame
$\hat{X}$	first axis unit vector for system reference frame
$\vec{x}$	state vector for a general dynamic system
$\vec{x}_e$	state vector at equilibrium for a general dynamic system
$\delta\vec{x}$	deviation from equilibrium state for a general linearized system
$\hat{Y}$	second axis unit vector for system reference frame
$\hat{Z}$	third axis unit vector for system reference frame
α	first 1-2-1 Euler angle for chief spacecraft
β	first 1-2-1 Euler angle for deputy spacecraft
γ	decay rate for modified Grammian for Grammian controller

Δ	length of time interval of interest, used in stability proof for Grammian controller
ε	relative attitude angle for 2D Case
$\Theta(t_0, \tau)$	state-transition matrix for a general linear system
θ	second 1-2-1 Euler angle for deputy spacecraft
ξ	general state vector used for stability proof of Grammian controller
τ	dummy variable used for time integration in modified grammian calculation
$\vec{\Phi}$	principal rotation vector for a general attitude representation
Φ	principal rotation angle for a general attitude representation
Φ_{CD}	principal rotation angle for the relative attitude of the deputy spacecraft with respect to the chief spacecraft
φ	second 1-2-1 Euler angle for chief spacecraft
ψ_1	first 1-2-1 Euler angle for a general system
ψ_2	second 1-2-1 Euler angle for a general system
ψ_3	third 1-2-1 Euler angle for a general system
$\vec{\omega}$	angular velocity of a general rotating system
ω_1	first component of $\vec{\omega}$
ω_2	second component of $\vec{\omega}$
ω_3	third component of $\vec{\omega}$
$\vec{\omega}_{CD}$	relative angular velocity of deputy spacecraft with respect to chief
$\vec{\omega}_C$	angular velocity of chief spacecraft
$\vec{\omega}_D$	angular velocity of deputy spacecraft
$\vec{\omega}_D^d$	desired angular velocity of deputy spacecraft, used for 3D Case controller

1. Introduction

This chapter introduces the topic of relative attitude control with electrostatic torque as an actuator. It discusses the problem of interest for the research presented in this thesis, as well as the motivation driving the research to solve this problem. After this, a brief layout of the rest of the thesis is presented.

1.1. Research Motivation and Problem Statement

The problem of interest for this research is controlling the relative attitude of the members of a formation of spacecraft. This problem has several applications. One of the primary applications is in remote sensing, both of the Earth and of other celestial bodies. For example, NASA has been considering the development of a spacecraft formation to act as a long-baseline telescope for observing extrasolar bodies (NASA JPL, n.d.). On the other hand, Earth-observing formations can often be used for map-making or espionage applications.

While it is certainly possible to control the relative attitude of member spacecraft of these formations through more traditional means, such as attitude control thrusters or reaction wheels, using electrostatic torque as an actuator offers several unique advantages. Electrostatic torques between formation members are created by electrically charging and discharging portions of the crafts' outer surfaces based on their relative attitudes. The spatial relationship between the charged portions of each spacecraft's surface and their centers of mass turn the natural electrical attraction or repulsion between the charged regions into torques.

One of the principal advantages of this method is that using electrostatic torque removes the need to pack large amounts of propellant into a satellite for attitude control,

as thrusters would require. Additionally, since electrostatic torques are created by spacecraft relative state and electrostatic charge (i.e. they are not dependent on spacecraft angular velocity), they avoid the potential for saturation that reaction wheels struggle with. Electrostatic torques are also remarkably power-efficient to implement, with some estimates placing the required power at the Watt level (Schaub & Stevenson, 2013).

Of course, there are some drawbacks to the technique that need to be addressed. One major drawback is that the control authority that electrostatic torques can exercise is largely dependent on the geometry of the spacecraft (or, more accurately, the locations on the spacecraft that can be charged and discharged and their spatial relationship to the craft's center of mass). This can be mitigated, however, by designing the spacecraft with this actuation system in mind and ensuring that full control authority can be exercised at any time. Additionally, there is the drawback that, if every member of the formation purely uses electrostatic torques, the formation can control the relative attitude of the members, but cannot control the absolute attitude of the entire formation. This can be mitigated by selecting one spacecraft in the formation to possess a traditional attitude control system and use this to set its attitude. Then, the other members can control themselves to align with it.

This thesis seeks to investigate the utility of electrostatic torques as an actuator to control the relative attitude of spacecraft formation members on a more technical level, evaluating potential control laws for their ability to control the relative attitude of the spacecraft. In order to do this, the research analyzes one potential system that this control system could be applied to, a pair of cylindrical spacecraft operating in deep space, far from the influences of celestial bodies.

1.2. Organization of Thesis

With the problem thus described, Chapter 2 presents a review of the findings of several recent studies that have investigated attitude control problems with electrostatic torque actuation systems and discusses their relevance to the research presented in this thesis. The chapter finishes with a discussion of the novel approach of the current study to this problem.

Chapter 3 then provides an overview of some physical concepts that are important to the development of electrostatic torque theory. These are discussed to acquaint unfamiliar readers with details of attitude mechanics, electrostatics, and control theory that are relevant to the research presented in later chapters.

Chapter 4 presents the approach taken to analyze the use of electrostatic torques as relative attitude control actuators. Specifically, it provides a description of the system studied in this research, along with a discussion of the development of this system's equations of motion. These discussions are presented for both a restricted two-dimensional case of the system, as well as the case where the system is allowed the full range of three-dimensional rigid body rotations.

Next, Chapter 5 introduces several control laws that were investigated for use in this system. Both the 2D and 3D Cases of the system are considered. The chapter finishes with a discussion of the necessary actuator dynamics required to implement one of these control laws for the system's 3D Case.

In Chapter 6, numerical simulations of the developed theory are presented to evaluate the effectiveness of these different control laws and actuator dynamics for controlling the relative attitude of the system. These will be presented along with simulations of the

open-loop and equilibrium behavior of the system, in order to demonstrate system controller performance.

Finally, overall conclusions from the research are drawn in Chapter 7. In addition, this chapter makes several recommendations for future work in the field. Some of these recommendations are based on limitations of the present research, while others seek to generalize this topic to other potential systems of application.

2. Review of Relevant Literature

This chapter explores some of the research that has been done on the topic of electrostatic torque control for collections of spacecraft. First, one of the most important techniques that has been developed in the field is discussed. Afterward, a survey of this technique's applications to the problem will be conducted. Finally, the novel elements of the present research will be discussed.

2.1. Multi-Sphere Method for Electrostatic Modelling

Perhaps the most significant research development in the field of electrostatic torque theory in recent years is the development of the Multi-Sphere Method (MSM) (Stevenson & Schaub, 2013). This method enables its users to model the electrostatic interactions between multiple electrically charged bodies of complicated geometries without using computationally-expensive finite element methods that can make simulation and control law development very difficult. The central conceit of the MSM is to approximate an electrically charged object as a finite collection of charge-carrying spheres whose locations are fixed to the object in question. As the charge distribution on the object evolves with time, the charges of the spheres change to continue representing the object.

To apply the MSM to a given spacecraft geometry, the user begins with an initial guess as to the number of spheres necessary to approximate it and the locations in the geometry that those spheres occupy. Then, the electrostatic forces and torques on this initial model are compared to those experienced by a higher-fidelity finite element electrostatic model of the same geometry, and an iterative nonlinear fit algorithm is applied to adjust the initial model until it optimally matches the results of the higher-fidelity model. This process is explained in more detail in (Stevenson & Schaub, 2013).

As mentioned above, the MSM allows for more computationally-efficient modelling of electrostatic torques in spacecraft attitude dynamics. This advantage allows a user to simulate the electrostatic forces and torques between spacecraft in real-time or faster-than-real-time, which is not generally possible for higher-fidelity finite element methods (Stevenson & Schaub, 2013). An additional advantage of the MSM is its reusability. The MSM model of a spacecraft is made for a given geometry, not a specific spacecraft. Therefore, any spacecraft that uses this geometry, with the same dimensions, can utilize the same MSM model of any other spacecraft that uses this geometry. This means that the process of model creation can be performed once to model a member of a spacecraft formation composed of identical member craft, and that model can then be applied to each member of the formation.

Throughout the original research in this thesis, the MSM model of the selected spacecraft geometry will be used as a starting point for developing a model of the system experiencing electrostatic torque. While the authors of (Stevenson & Schaub, 2013) prefer to express the electrostatic model in terms of voltages, as this is a more easily measured control variable, the analysis presented in this thesis expresses the model in terms of sphere charge, instead. This is done for its utility in expressing the electrostatic torques experienced by the system. As this thesis presents functions for the charges on the spacecraft as functions of system state for one of the proposed control laws (see Equations (42) and (43)), the corresponding voltage expressions can be determined by using the conversion presented in Equation (2) of (Stevenson & Schaub, 2013). However, examining this conversion was considered out of scope for the present research. Future work may consider this conversion, however.

2.2. Electrostatic Torque Research to Date

Utilizing the MSM introduced above, several studies have been conducted in recent years to investigate the use of electrostatic torque as an actuator for spacecraft relative attitude control. One of the first of these was conducted by Schaub and Stevenson in 2013, to investigate the use of electrostatic torques to detumble space debris using a spherical servicer craft. This analysis considers two spacecraft, a spherical servicer and a cylindrical debris object, operating in a single plane, with the debris constrained to rotate only in two dimensions. The authors develop a feedback control law, using the spacecraft electrostatic potential as a control variable. This study illustrates the principle that electrostatic torques can, in fact, be used to control the attitude of spacecraft through the use of feedback control theory.

While (Schaub & Stevenson, 2013) is somewhat limited by its planar rotation assumption, it provides several foundational elements to the research presented in this thesis. Not only does it provide the core concept that electrostatic torques can be used for this application, it also provides the MSM model for cylindrical craft that is used in this study (see Section 4.1). The 2D Case of this thesis (see Section 4.1) is a direct generalization of (Schaub & Stevenson, 2013), for the case that both craft are identical.

The planar rotation constraint is lifted from this system in a later study, conducted by Bennett and Schaub (2015). In this study, the authors thoroughly analyze the relationship between spacecraft separation and control authority while using electrostatic torque as an actuator. Additionally, this study develops the stability and equilibrium characteristics of the 3D generalization of the control scheme developed in (Schaub & Stevenson, 2013). While this generalization certainly results in a much more usable control scheme for real-

world applications, it is not as applicable to the problem considered in this thesis, as it still uses the spherical servicer craft from the previous study, whose attitude cannot be meaningfully controlled with the electrostatic torque actuation system (Bennett & Schaub, 2015).

Bennett and Schaub (2018) extend the problem from merely detumbling space debris to also include altering the orbit of the debris in order to either service or dispose of it. The study accomplishes this by considering different nominal charge values for the servicer spacecraft. This results in the servicer spacecraft exerting a net pull or push on the debris, dependent on the sign of the nominal charge. This is used to tug the debris from its current orbit to the desired target orbit. One of the most notable developments of this study was an analysis of the different steady-state attitudes of the debris object, depending on whether the nominal pulling or pushing configuration was used. When in the pulling configuration, the debris object (still modelled as a cylinder) comes to equilibrium with its long axis pointed along the inter-craft axis, while the pushing configuration results in an equilibrium condition where the debris object is oriented perpendicularly to the inter-craft axis (Bennett & Schaub, 2018). Owing to this discovery, the simulations in this thesis were conducted with nominal charges set up to create a pushing configuration, as this results in equilibria more useful to spacecraft formations with pointing applications in mind.

Following on the concept of the electrostatic tug spacecraft, (Aslanov & Schaub, 2019) focuses in on the utility of the pushing configuration, specifically. This study continues to utilize the system model of the previous studies: with a spherical servicer spacecraft and a cylindrical debris object. It also returns to the constrained planar rotation

considered by (Schaub & Stevenson, 2013). The primary concern of the study is to evaluate the stability of several feedback control laws that the attitude-stabilizing tug craft can use to constrain the attitude motion of the debris object.

2.3. Novelty of Present Research

As can be seen from the references discussed above, much of the current research in electrostatic torque actuation turns its attention to the control of space debris for servicing or disposal. However, the research presented in this thesis turns the developments in these references to a new application: namely, the relative attitude control of two identical spacecraft, with an eye toward one day using similar techniques on larger formations of spacecraft. The two identical spacecraft considered by this study are a pair of cylindrical spacecraft, allowing the study to leverage the MSM model for cylindrical spacecraft from the previous work as a starting point for the analysis.

Additionally, this study also adds an additional factor to the system: considering spacecraft purpose-built to use the electrostatic actuation, being able to independently control the charge on differing parts of their surfaces. This study assumes that the outer surfaces of the spacecraft have charge-carrying regions which are separated by electrically insulating regions that allow the charge-carrying regions to be independently charged and discharged. Meanwhile, the previous studies considered a debris object whose entire surface was made of conducting material, meaning that the entire surface would hold approximately the same electrical potential.

Finally, as stated above, this study focuses on the charge of the various chargeable regions as a control variable, whereas the previous research used the electrical potential as the control variable. This was done for the ease with which the actuator dynamics

could be developed from the system's equations of motion. Additionally, using this control variable allows more direct actuation if the particle gun concept, as described in (Schaub & Stevenson, 2013), is used to conduct the charging and discharging of the member spacecraft.

3. Overview of Relevant Concepts

This chapter discusses some of the important principles of physics and control theory that are used throughout the research presented in this thesis. First, some of the salient features of attitude mechanics are discussed, including Euler's rigid body rotational kinetics equation and several attitude kinematic representations that are useful in the following discussions. Next, a brief primer on the relevant portions of electrostatic theory are presented. This is to acquaint the reader with their use in constructing expressions for the torques due to electrostatic interaction that are used as actuators for this research. Finally, various aspects of control theory that are used throughout this investigation are discussed.

3.1. Attitude Mechanics

Attitude mechanics, at its core, is the field of dynamics that concerns itself with the evolution of the orientation (or attitude) of objects over time, subject to the conditions that induce that evolution. In three-dimensional space, the attitude of an object is usually mathematically reckoned as a relationship between two coordinate frames.

A coordinate frame is, in essence, a mathematical object that consists of a set of basis vectors that can be used to define the location of a point in the space that the problem takes place in. In a three-dimensional problem, such as attitude mechanics, a coordinate frame is a set of three linearly-independent basis vectors. While, theoretically, any type of coordinate system can be used to define these coordinate frames, the following discussions are only concerned with Cartesian three-dimensional coordinate frames. This type of coordinate frame can be thought of, spatially, as a set of three mutually-perpendicular vectors originating from a single point. The simplest attitude mechanics

problems are concerned with modelling the time-history of the attitude between a single coordinate frame, defined to be fixed to a specific physical object, with respect to a reference coordinate frame, defined in a manner useful to the specific problem at hand.

3.1.1. Attitude Representations

There are several ways to mathematically represent the attitude between two coordinate frames. This discussion presents three of them that are of particular importance to the research presented in this thesis: principal rotation vectors, direction cosine matrices, and Euler angles. The introductions of these three concepts that follow assume that the problem of interest takes place in three-dimensional Cartesian space.

The simplest of these three, conceptually, is the principal rotation vector representation. This representation relies on the fact that the attitude between any two coordinate frames can be represented as a single-axis rotation between the two of them. The principal rotation vector is then defined by the following relation:

$$\vec{\Phi} = \Phi\vec{k} \tag{1}$$

where $\vec{\Phi} \in \mathbb{R}^3$ is the principal rotation vector representation, $\Phi \in \mathbb{R}$ is the magnitude of that vector (referred to as the principal rotation angle), and $\vec{k} \in \mathbb{R}^3$ is the unit vector parallel to the principal rotation vector, known as the principal rotation axis. As the name suggests, the principal rotation axis is the unit vector that describes the spatial orientation of the single axis about which one of the coordinate frames in question must be revolved to align with the other coordinate frame. Similarly, the principal rotation angle is the amount by which the first coordinate frame must be revolved about the principal rotation axis to align the two coordinate frames. The principal rotation axis is a dimensionless

quantity, while the principal rotation angle (and thus, the principal rotation vector) has angular units, usually degrees or radians.

The second attitude representation used in this thesis, and the most widely used one in it, is the direction cosine matrix (DCM). However, this is also one of the most complicated ones. A DCM is a 3x3 matrix whose elements are the cosines of the angles between each possible pair of axes between the two coordinate frames in the problem of interest. To illustrate this, consider a pair of coordinate frames, $\hat{I}\hat{J}\hat{K}$ and $\hat{\imath}\hat{\jmath}\hat{k}$. The names of these coordinate frames indicate the names of the axes that comprise them. For example, the $\hat{I}\hat{J}\hat{K}$ frame is the coordinate frame whose first axis is defined by the unit vector $\hat{I} \in \mathbb{R}^3$, second axis is defined by the unit vector $\hat{J} \in \mathbb{R}^3$, and third axis is defined by the unit vector $\hat{K} \in \mathbb{R}^3$. Let the symbol $\angle$ denote the angle between the following two vectors. Then, the DCM between these two coordinate frames is defined by the following.

$$Q_{i\to I} = \begin{bmatrix} cos(\angle \hat{I}\hat{\imath}) & cos(\angle \hat{I}\hat{\jmath}) & cos(\angle \hat{I}\hat{k}) \\ cos(\angle \hat{J}\hat{\imath}) & cos(\angle \hat{J}\hat{\jmath}) & cos(\angle \hat{J}\hat{k}) \\ cos(\angle \hat{K}\hat{\imath}) & cos(\angle \hat{K}\hat{\jmath}) & cos(\angle \hat{K}\hat{k}) \end{bmatrix} \tag{2}$$

Not only does the DCM define the relationship between the two coordinate frames, it also provides a tool to convert any given vector between its expression in the two frames. Using the DCM defined above, a general vector $\vec{v} \in \mathbb{R}^3$, expressed in the $\hat{\imath}\hat{\jmath}\hat{k}$ frame, can be converted to its equivalent expression in the $\hat{I}\hat{J}\hat{K}$ frame by pre-multiplying it by the DCM. That is to say,

$$\vec{v}^{\hat{I}} = Q_{i\to I}\vec{v}^{\hat{\imath}} \tag{3}$$

where the superscript denotes which of the two coordinate frame expressions is being used, based on the first axis of that coordinate frame, and the product shown is the matrix product.

The final, and perhaps best-known, attitude representation used in this study is the Euler angle representation. This representation prescribes a series of rotations about a coordinate frame's instantaneous axes that must be performed to align it with the reference coordinate frame. One of the most familiar of these rotation sequences is the sequence about the first axis, then second, then third, often referred to as the roll, pitch, yaw sequence or the 1-2-3 sequence, though many others exist. It is important to stress that these rotations are applied to the *instantaneous* axes of the frame. So, after the first rotation is applied, the second rotation is applied about the *current* second axis, not the original one. For the research presented in this thesis, the less-conventional 1-2-1 rotation sequence will be used, as explained in Section 4.3.

A given attitude can be expressed in any of these three representations and, if desired, can be converted from one to another. For the three presented here, it is easiest to convert between Euler angles and DCMs, which can be converted in either direction. That is to say, one can convert from Euler angles to DCMs, or from DCMs to Euler angles, with little difficulty. This conversion is accomplished by constructing the DCM that represents the single-axis rotation prescribed by each Euler angle and then multiplying these in sequence to produce the DCM representation of the full rotation. The sequence in question is to have the first rotation as the right-most matrix and then include the following ones to the left of it, in succession. Representing the 1-2-1 rotation sequence mentioned above as the angles ψ_1, ψ_2, and ψ_3, this is done as follows:

$$Q = \begin{bmatrix} 1 & 0 & 0 \\ 0 & \cos\psi_3 & \sin\psi_3 \\ 0 & -\sin\psi_3 & \cos\psi_3 \end{bmatrix} \begin{bmatrix} \cos\psi_2 & 0 & -\sin\psi_2 \\ 0 & 1 & 0 \\ \sin\psi_2 & 0 & \cos\psi_2 \end{bmatrix} \begin{bmatrix} 1 & 0 & 0 \\ 0 & \cos\psi_1 & \sin\psi_1 \\ 0 & -\sin\psi_1 & \cos\psi_1 \end{bmatrix} =$$

$$\begin{bmatrix} \mathrm{c}\,\psi_2 & \mathrm{s}\,\psi_2\,\mathrm{s}\,\psi_1 & -\mathrm{s}\,\psi_2\,\mathrm{c}\,\psi_1 \\ \mathrm{s}\,\psi_2\,\mathrm{s}\,\psi_3 & \mathrm{c}\,\psi_1\,\mathrm{c}\,\psi_3 - \mathrm{c}\,\psi_2\,\mathrm{s}\,\psi_1\,\mathrm{s}\,\psi_3 & \mathrm{s}\,\psi_1\,\mathrm{c}\,\psi_3 + \mathrm{c}\,\psi_2\,\mathrm{c}\,\psi_1\,\mathrm{s}\,\psi_3 \\ \mathrm{s}\,\psi_2\,\mathrm{c}\,\psi_3 & -\mathrm{c}\,\psi_1\,\mathrm{s}\,\psi_3 - \mathrm{c}\,\psi_2\,\mathrm{s}\,\psi_1\,\mathrm{c}\,\psi_3 & -\mathrm{s}\,\psi_1\,\mathrm{s}\,\psi_3 + \mathrm{c}\,\psi_2\,\mathrm{c}\,\psi_1\,\mathrm{c}\,\psi_3 \end{bmatrix} \quad (4)$$

where, for brevity, the prefix *c* indicates the cosine of the following angle and the prefix *s* indicates the sine of the following angle. To convert from the DCM representation to the Euler angle representation, it is simplest to use the above expression to derive the relations in terms of elements of the DCM, as follows:

$$\psi_1 = -tan^{-1}\frac{Q_{1,2}}{Q_{1,3}}, \quad \psi_2 = cos^{-1}Q_{1,1}, \quad \psi_3 = -tan^{-1}\frac{Q_{2,1}}{Q_{3,1}} \quad (5)$$

where the first subscript refers to the row index of the element of the DCM, the second subscript refers to the column index of the element of the DCM, and the superscript -1 refers to the inverse of the trigonometric function to which it is attached.

While it is a simple task to convert an attitude expressed with DCMs into the principal rotation vector representation, it is far more difficult to convert back from a principal rotation vector to a DCM. However, since the research presented below only requires the conversion from DCM to principal rotation vector, the conversion back is neglected, here. To obtain the principal rotation vector representation of an attitude from its DCM representation, the principal rotation angle and principal rotation axis are obtained separately and then combined. The formulas for these are given by (Song, Tang, Hong, & Hu, 2017):

$$\Phi = cos^{-1}\left(\frac{tr(Q)-1}{2}\right), \qquad \vec{k} = \frac{\widetilde{(Q-Q^T)}}{2\,sin\,\Phi} \quad (6)$$

where $tr(Q)$: $\mathbb{R}^{3x3} \rightarrow \mathbb{R}$ refers to the trace of the DCM, which is the sum of its diagonal terms, the superscript T refers to the transpose of the matrix to which it is attached, and the $\check{}$: $\mathbb{R}^{3x3} \rightarrow \mathbb{R}^3$ operator denotes the following operation:

$$\check{Q} = \begin{bmatrix} Q_{3,2} \\ Q_{1,3} \\ Q_{2,1} \end{bmatrix} \tag{7}$$

3.1.2. Attitude Kinematics

Out of the three attitude representations presented above, one was used in this study to track the evolution of the system attitude with respect to time. This is the DCM representation. However, before the expression for the attitude DCM's evolution with respect to time (or "kinematics") can be presented, there is one other important concept to discuss. This is the angular velocity vector.

As its name suggests, angular velocity is the rotational equivalent of velocity in translational motion. That is to say, it defines the rate at which the attitude changes over time. In three-dimensional Cartesian space, the angular velocity is a vector that points in the direction of the axis that the rotating body is instantaneously rotating about. The magnitude of the angular velocity vector defines the instantaneous rate at which the rotating body is rotating about that axis. For the simplest case, that of constant-rate rotation about a single axis, the angular velocity vector is a constant vector. However, in more complicated cases, it can change over time due to the application of moments or torques to the system. This is the topic of the next section.

At any given instant during rotational motion, the instantaneous angular velocity vector can be used with the current DCM of the system's attitude to define the

instantaneous rate at which the DCM changes over time. Expressed mathematically, this defines the attitude kinematic equation of a system using the DCM attitude representation (Song, Tang, Hong, & Hu, 2017):

$$\dot{Q} = \tilde{\omega}Q = \begin{bmatrix} 0 & -\omega_3 & \omega_2 \\ \omega_3 & 0 & -\omega_1 \\ -\omega_2 & \omega_1 & 0 \end{bmatrix} Q \tag{8}$$

where the dot over a symbol indicates the derivative with respect to time of the quantity the symbol represents, $\vec{\omega} = [\omega_1 \quad \omega_2 \quad \omega_3]^T$ is the angular velocity vector of the system, expressed in the body-fixed coordinate frame of the rotating object, and the $\tilde{}: \mathbb{R}^3 \rightarrow \mathbb{R}^{3x3}$ operator converts the three-term angular velocity vector into the skew-symmetric matrix shown in the equation. Note that the operators $\tilde{}$ and $\check{}$ denote inverse operations of one another.

3.1.3. Attitude Kinetics

Equation (8) describes how the attitude of a system evolves over time due to its instantaneous angular velocity vector. However, as mentioned above, the angular velocity vector, itself, can evolve over time. This occurs when a torque or moment is applied to the system. In a manner analogous to Newton's Second Law, which describes the relationship between a translational force and the time-derivative of the linear momentum of a translating system, the net torque or moment ("moment" will be used from now on for simplicity) applied to the system about its center of mass can be mathematically equated to the time-derivative of a rotating system's angular momentum about its center of mass. Mathematically, this is written in the following manner (Curtis, 2005).

$$\vec{M}_G = \dot{\vec{H}}_G \tag{9}$$

where $\vec{M}_G \in \mathbb{R}^3$ is the net moment on the rotating body about its center of mass, expressed in the body-fixed coordinate frame of the rotating body, $\vec{H}_G \in \mathbb{R}^3$ is the angular momentum of the rotating body about its center of mass, expressed in the body-fixed coordinate frame of the rotating body, the subscript G clarifies that the center of mass is the point about which the moments and angular momentum are reckoned, and the dot operator is as defined above.

To develop the relationship between the net moment and the angular velocity's rate of change, the right-hand side of this equation must be expanded. This is done by taking the definition of the angular momentum vector of the body about its center of mass in three-dimensional Cartesian space and differentiating with respect to time. This definition is given by the following (Curtis, 2005).

$$\vec{H}_G = I\vec{\omega} \tag{10}$$

where $I \in \mathbb{R}^{3x3}$ is the moment of inertia tensor of the rotating body about its center of mass, and the product shown between it and the angular velocity vector is the matrix product.

Using the transport theorem, the time derivative of angular momentum is then found to be the following (Curtis, 2005).

$$\dot{\vec{H}}_G = \dot{I}\vec{\omega} + I\dot{\vec{\omega}} + \vec{\omega} \times I\vec{\omega} \tag{11}$$

where the × symbol denotes the cross-product operation. However, since the bodies in this study are assumed to expend negligible mass during their operation, the first term of the right-hand side of this equation goes to zero. Substituting this expression into

Equation (9) and dropping the aforementioned term, the following result, known as Euler's equation for rigid body rotations, is obtained.

$$\vec{M}_G = I\dot{\vec{\omega}} + \vec{\omega} \times I\vec{\omega} \tag{12}$$

Note that this expression can be generalized for cases where the moments and angular momentum are taken about a point other than the rotating body's center of mass. However, these cases are not used in the research presented in this thesis, and so the equations for this case are not explored here. For a discussion of this topic, see (Curtis, 2005). Equation (12) can be solved for the time-derivative of the angular velocity vector in order to obtain an expression for how the angular velocity vector evolves over time due to the applied moments and the current angular velocity vector, known as the kinetic equation of a rotating system.

$$\dot{\vec{\omega}} = I^{-1}\left(\vec{M}_G - \vec{\omega} \times I\vec{\omega}\right) \tag{13}$$

where the superscript -1 refers to the matrix inverse of the matrix it is applied to.

3.2. Electrostatics

In order to model the generation of moments on the spacecraft in this study due to the use of electrostatic torques, a brief discussion of electrostatics is helpful. Of particular interest is the description of the forces produced by the proximity of electric charges.

Without treating the concept at a quantum level, electrical charge is a fundamental property of matter that causes matter to both create and react to electric fields in space. The most commonly-encountered particles that carry electric charge are the subatomic particles known as protons (positive charge) and electrons (negative charge). Most

modern electrical technology operates by the movement of electrons, as carriers of negative electrical charge. For certain applications, such as the charging of spacecraft surfaces used in this research and the studies mentioned in the literature review above, larger, conducting objects can be charged or discharged by bombarding them with charged particles. The resulting balance of positively and negatively charged particles in the conducting object then determines the charge of the object, overall.

When in proximity with one another, electrically charged objects exert forces on one another. For point-sized objects, such as single protons or electrons, this force is described by Coulomb's Law, below.

$$\vec{F}_{12} = \frac{k_C q_1 q_2 \hat{r}_{12}}{\|\vec{r}_{12}\|^2} \tag{14}$$

Where $\vec{F}_{12} \in \mathbb{R}^3$ is the vector force exerted on point charge 2 by point charge 1, $\vec{r}_{12} \in \mathbb{R}^3$ is the position vector of point charge 2 with respect to point charge 1, $\hat{r}_{12} \in \mathbb{R}^3$ is the unit vector parallel to the same, $q_1 \in \mathbb{R}$ and $q_2 \in \mathbb{R}$ are the electrical charges of the two point charges, the $\| \ \|: \mathbb{R}^3 \to \mathbb{R}^+$ operator denotes the magnitude of the vector it acts on, and k_C is Coulomb's Constant, with value 8.99E9 $\frac{Nm^2}{C^2}$. While, in general, objects larger than points require a finite element summation to accurately compute the electrostatic force that they exert on one another, if the charged objects are sufficiently far away and they are symmetrically charged, the electrostatic force they exert on one another can be modelled as that between two point charges, located at the centers of the objects in question and with charge magnitude equal to the total net charge in the object.

In the research presented in this thesis, the electrostatic forces are modeled as interactions between point charges due to this distance consideration. These forces then

create torques on the spacecraft based on the distance between the location where the forces are applied and the spacecraft centers of mass. This is done by the cross-product definition of torque. That is to say, that torque is the cross product of a force and its moment arm. This results in the following expression for the electrostatic torque on one object due to the interactions of one pair of charged regions between the two spacecraft.

$$\vec{M}_G = \vec{r}_{G2} \times \frac{k_C q_1 q_2 \hat{r}_{12}}{\|\vec{r}_{12}\|^2} \tag{15}$$

where $\vec{r}_{G2} \in \mathbb{R}^3$ refers to the relative position vector of charged region 2 with respect to the center of mass of the spacecraft that it is part of. This expression can then be summed over every combination of charged regions across the two spacecraft to determine the total electrostatic torque that one spacecraft produces on the other.

3.3. Control Theory

Finally, as this research is fundamentally centered around the concept of controlling the behavior of a system, it is beneficial to include a discussion of some of the important concepts of control theory. Fundamentally, control theory studies the methods by which certain parameters of interest of a system can be brought to desired values or be kept within acceptable limits by acting on that system in an appropriate manner. In general, there are two basic methods by which to control a system, referred to as open-loop control and closed-loop control.

Open-loop control is when a system is acted on to produce the desired result without taking into account the current state of the system in how that control effort is applied. A common example is a sprinkler system, in which the water flows for a specified time, independent of the degree of moisture of the ground that is being watered.

The other method is called closed-loop control, where measurements of the current state of the system are used to inform and modify the amount of control effort expended on the system. An example of this would be a human operator braking a car to come to a stop sign, taking into account the current distance from the stop sign and the car's current velocity to know how much to depress the brake pedal. It is important to mention that open-loop control is different than open-loop dynamics, which is a similar term. However, the latter refers to the behavior of a system in the absence of a controller, as opposed to a system whose control does not depend on the system state. All of the control laws presented in this thesis are closed-loop controllers, as they depend on the current state of the system to modify the control effort applied to the system

3.3.1. State-Space Modeling

For the 2D Case of the research presented below, the system dynamics and control were accomplished via state-space modeling techniques, which use matrix equations to model systems with more than one parameter of interest. These parameters of interest are known as state variables, and the collection of all state variables for a system is referred to as the system state. Often, the system state is represented as a vector with each of the terms being one of the state variables. The dynamics of the system are then modeled as a differential matrix equation of this state vector in order to study how the system evolves with respect to one or more independent variables, usually including time. These equations can be either linear or nonlinear.

For the nonlinear case, the state equations that describe the evolution of the system state are nonlinear functions of the state variables. In mathematical terms, this is often rendered by the following expression.

$$\dot{\vec{x}} = \vec{f}(\vec{x}, t, \vec{u}) \tag{16}$$

where $\vec{x}$ is a general state vector, $\vec{u}$ is a general vector of control inputs, $\vec{f}$ is a vector of nonlinear functions of the state vector, input vector, and the independent variables (in this example, time is assumed to be the only independent variable, as it is in many dynamics applications), t represents the time since a reference start time, and the dot operator is as defined above. Often, nonlinear systems are very difficult to derive control systems for. When possible, then, nonlinear systems are often locally approximated by related linear systems in order to create control laws that are valid within a neighborhood of a desired system state.

Often, this desired state takes the form of an equilibrium state of the system, which is a state where the derivative of the state is null. That is to say, $\dot{\vec{x}} = \vec{0}$. Physically, this means that the state variables do not change without input to the system at this point. The system state at an equilibrium is commonly denoted $\vec{x}_e$ to distinguish it from other states. Since an equilibrium state is often the desired final state of a controlled system, they are also often used in the process of linearization, which approximates a nonlinear system with a linear system that makes fairly accurate predictions of behavior within a small neighborhood of the state about which the system was linearized.

One common way that nonlinear systems can be linearized (which is used in this thesis) is to take the Jacobian of the expression for the state's derivative with respect to the system state vector and use this as the linear relationship between a small deviation of the state from the equilibrium condition and the derivative of that small deviation. This is then added to the Jacobian of the state's time derivative with respect to the input vector, multiplied by the input vector.

To give an example, consider a nonlinear system with two state variables x_1 and x_2, two inputs u_1 and u_2, and two functions of those state and input variables in the right-hand side of Equation (16), denoted f_1 and f_2. The linearized form of this system is given by the following equation.

$$\delta\dot{\vec{x}} = \left[\begin{matrix} \frac{\partial f_1}{\partial x_1} & \frac{\partial f_1}{\partial x_2} \\ \frac{\partial f_2}{\partial x_1} & \frac{\partial f_2}{\partial x_2} \end{matrix}\right]_{\vec{x}_e} \delta\vec{x} + \left[\begin{matrix} \frac{\partial f_1}{\partial u_1} & \frac{\partial f_1}{\partial u_2} \\ \frac{\partial f_2}{\partial u_1} & \frac{\partial f_2}{\partial u_2} \end{matrix}\right]_{\vec{x}_e} \vec{u} = A(t)\delta\vec{x} + B(t)\vec{u} \tag{17}$$

where $\delta\vec{x} = \vec{x} - \vec{x}_e$. Additional details of this process can be found in Chapter 1 of (Wie, 2008).

Fundamentally, this linearized structure also represents the structure of a system with linear state equations, where the derivative of the state vector is related by multiplication with a matrix of values (which may be constant or vary with respect to the independent variable(s) only) to the current state vector. Whether the system was linear to begin with, or has been linearized from a nonlinear system, many well-described control laws can now be derived from this linear form, as functions of the matrices $A(t)$ and $B(t)$. When these control laws define $\vec{u}$ as a function of the state vector, the resulting control is closed-loop control. Otherwise, it is open-loop. Once a control law is derived for this linearized state equation, the control is then applied to the nonlinear system.

3.3.2. Stability

One final topic in control theory that must be discussed is that of stability theory. At its core, stability theory is concerned with whether or not a system will tend to return to an equilibrium condition after it has been disturbed. If a system tends to return to equilibrium after a disturbance, it is called a stable system. Systems that tend away from

the equilibrium after a disturbance are called unstable, and systems that tend to remain within a neighborhood of the equilibrium condition, but do not necessarily converge to the equilibrium, itself, are termed marginally stable. Often, in controls applications, stability theory is applied to the closed-loop dynamics of the system to determine whether the applied control law will make the system converge to its desired state.

One of the more common methods to prove stability of the system, and the one used in this thesis, is known as Lyapunov's Direct Method. This involves defining a scalar function of the system state, known as a Lyapunov function (often given the symbol $V(\vec{x})$), that satisfies the following conditions:

$$V(\vec{x}) = 0, \qquad iff \quad \vec{x} = \vec{x}_e$$
$$V(\vec{x}) > 0, \qquad iff \quad \vec{x} \neq \vec{x}_e \tag{18}$$

With the Lyapunov function so defined, the stability of the system can then be investigated by taking its time derivative. If the time derivative of the Lyapunov function is less than or equal to zero at all states, the system is marginally stable. If it is strictly less than zero at all states other than the equilibrium state, the system is locally stable. If neither of these conditions are met, no conclusions about stability can be drawn, and a different Lyapunov function must be investigated. For more details on this procedure, see Chapter 1 of (Wie, 2008).

4. System Model Development

The next four chapters cover new research in the field of relative spacecraft attitude control with electrostatic torques. This chapter starts by describing the system analyzed for this research, a pair of cylindrical spacecraft interacting in deep space, and listing the assumptions that were used to analyze it. After this, the equations of motion for the system are developed, using two different paradigms: a case where the two spacecraft are assumed to rotate in a single plane, referred to as the 2D Case of the system, and a case where the spacecraft freely experience three-dimensional rigid body rotations about their centers of mass, referred to as the 3D Case of the system.

4.1. System Description and Assumptions

The system under consideration in this research is represented in Figure 4.1. The system is a pair of cylindrical spacecraft, whose centers of mass are separated by a distance *d*. The two craft are free to rotate about their centers of mass, but the nature of this rotation is dependent on the particular paradigm being analyzed. For the 2D Case, this rotation is constrained to be that about the spacecraft $\hat{J}$ and $\hat{j}$ axes, defined below. For the 3D Case, the rotations are three-dimensional rigid body rotations. Using the multi-sphere method described above in Section 2.1, the spacecraft are electrically approximated by three charge-carrying spheres each. For the chief, these spheres are called sphere 1, sphere 2, and sphere 3. For the deputy, they are referred to as sphere a, sphere b, and sphere c. The details of this approximation are the same as that used for the cylindrical deputy spacecraft analyzed in (Schaub & Stevenson, 2013).

This analysis uses three coordinate frames to develop the dynamics of the system. For ease of visualization, these are shown in Figure 4.1. The $\hat{X}\hat{Y}\hat{Z}$ coordinate frame is the

reference frame of the system, whose $\hat{X}$ axis is defined to lie along the line connecting the centers of mass of the two spacecraft, pointing from chief to deputy. The $\hat{Y}$ and $\hat{Z}$ axes are defined arbitrarily, but such that the reference frame is orthogonal and right-handed.

The $\hat{I}\hat{J}\hat{K}$ coordinate frame is the body-fixed coordinate frame for the chief spacecraft. The $\hat{I}$ axis is defined to lie along the long axis of the spacecraft, pointing from sphere 2 to sphere 1. This alignment allows a convenient Euler angle attitude representation to be used for the 3D Case of this system: the 1-2-1 sequence introduced in Section 4.2.2. The $\hat{J}$ and $\hat{K}$ axes are defined to make an orthogonal right-handed coordinate frame.

Finally, the $\hat{\imath}\hat{\jmath}\hat{k}$ coordinate frame is the body-fixed coordinate frame for the deputy spacecraft. Similarly, the $\hat{\imath}$ axis is defined to lie along the long axis of the spacecraft, with the other two defined to form an orthogonal right-handed coordinate frame. For the special case depicted in Figure 4.1, all three coordinate frames are aligned.

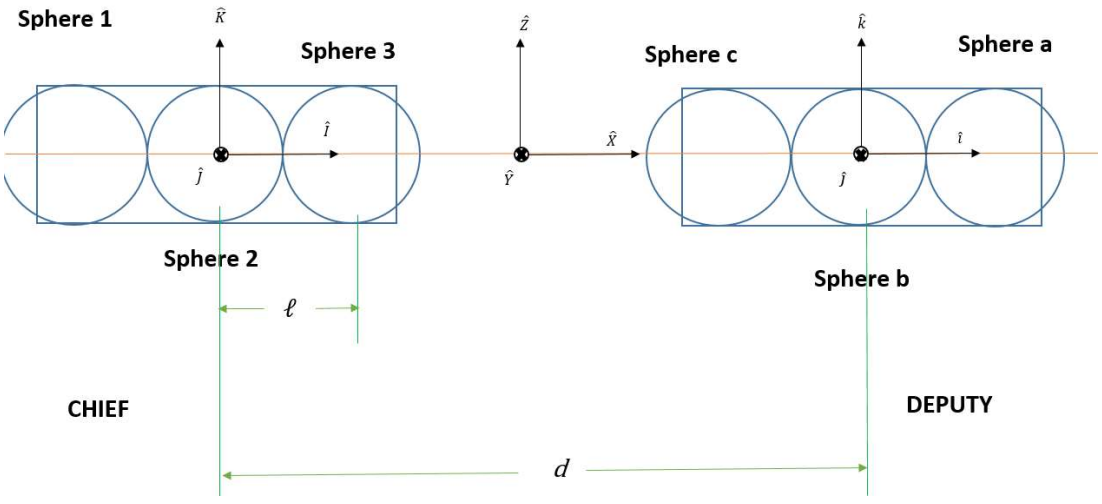

Figure 4.1 System Free-Body Diagram, All Coordinate Frames Aligned

The following assumptions are used in the remainder of the study presented here:

1. The two spacecraft are assumed to be operating in deep space, away from the gravitational or magnetic influence of celestial bodies
2. The two spacecraft maintain a fixed distance between each other in a fixed direction (this is possible by using thrusters, as shown in (Schaub & Stevenson, 2013), and is taken for granted here)
3. The charge-carrying regions on individual spacecraft are assumed to be separated by insulating material, so that charge does not flow between them
4. The distance between the spacecraft is assumed to be sufficient to treat the interactions between charge-carrying spheres as interactions between point charges.
5. The two spacecraft are assumed to be of identical construction, so that their mass properties and physical dimensions are considered the same for this analysis.

While these assumptions will decrease the fidelity of the analysis for Earth-orbit applications, they are valid for deep-space interferometer applications, such as those proposed in (NASA JPL, n.d.). Additionally, they allow the use of a simpler model to develop the initial theory. In future work, higher-fidelity models will be considered to ensure that the conclusions made are more applicable to the real world.

4.2. Equation of Motion Development

In this section, the equation of motion of the system described above is developed for both cases of the system. That is to say, the 2D and 3D Cases outlined above. The 2D Case will be discussed first.

4.2.1. 2D Case

To represent the constrained rotation of the spacecraft for the 2D Case, a single angle

is used for each spacecraft. For the chief spacecraft, this angle is denoted $\varphi \in [0, 2\pi)$, and it defines the rotation of the $\hat{I}\hat{J}\hat{K}$ coordinate frame relative to the $\hat{X}\hat{Y}\hat{Z}$ coordinate frame, about the $\hat{J}$ axis. Similarly, the attitude angle for the deputy spacecraft is denoted $\theta \in [0, 2\pi)$, and it defines the rotation of the $\hat{\imath}\hat{\jmath}\hat{k}$ coordinate frame with respect to the $\hat{X}\hat{Y}\hat{Z}$ coordinate frame, about the $\hat{\jmath}$ axis. The relative attitude between the two spacecraft is then defined by the angle $\varepsilon = \varphi - \theta$. These three angles allow us to construct expressions for the electrostatic torques that each spacecraft experiences. The expression for this torque on the deputy spacecraft, for the 2D Case, is shown below. Details of this derivation are given in Appendix A.

$$
\begin{aligned}
L_D = k_C \Bigg(& \frac{q_1 q_a (dl\ sin\ (\varepsilon+\varphi) - l^2 sin\ \varepsilon)}{((d + l\ cos\ (\varepsilon+\varphi) - l\ cos\ \varphi)^2 + (l\ sin\ (\varepsilon+\varphi) - l\ sin\ \varphi)^2)^{3/2}} \\
& + \frac{q_1 q_c (-dl\ sin\ (\varepsilon+\varphi) + l^2 sin\ \varepsilon)}{((d - l\ cos\ (\varepsilon+\varphi) - l\ cos\ \varphi)^2 + (-l\ sin\ (\varepsilon+\varphi) - l\ sin\ \varphi)^2)^{3/2}} \\
& + \frac{q_2 q_a (dl\ sin\ (\varepsilon+\varphi))}{((d - l\ cos\ (\varepsilon+\varphi))^2 + (-l\ sin\ (\varepsilon+\varphi))^2)^{3/2}} \\
& + \frac{q_2 q_c (-dl\ sin\ (\varepsilon+\varphi))}{((d - l\ cos\ (\varepsilon+\varphi))^2 + (-l\ sin\ (\varepsilon+\varphi))^2)^{3/2}} \\
& + \frac{q_3 q_a (dl\ sin\ (\varepsilon+\varphi) + l^2 sin\ \varepsilon)}{((d + l\ cos\ (\varepsilon+\varphi) + l\ cos\ \varphi)^2 + (l\ sin\ (\varepsilon+\varphi) + l\ sin\ \varphi)^2)^{3/2}} \\
& + \frac{q_3 q_c (l^2\ sin\ \varepsilon - ld\ sin\ \varphi)}{((d - l\ cos\ (\varepsilon+\varphi) + l\ cos\ \varphi)^2 + (-l\ sin\ (\varepsilon+\varphi) + l\ sin\ \varphi)^2)^{3/2}} \Bigg)
\end{aligned}
\tag{19}
$$

where $L_D \in \mathbb{R}$ is the scalar torque acting on the deputy spacecraft, $d \in \mathbb{R}^+$ is the distance between the centers of sphere 2 and sphere b as explained above, $l \in \mathbb{R}^+$ is the distance between the centers of any two adjacent spheres on the same spacecraft, k_C is

Coulomb's Constant, and $q_n \in \mathbb{R}$ refers to the electrical charge on sphere $n \in \{1 \quad 2 \quad 3 \quad a \quad b \quad c\}$. A similar expression can be derived for the torque acting on the chief spacecraft for the 2D Case.

$$L_C = k_C \left(\frac{q_1 q_a(-ld \sin\varphi + l^2 sin\,\varepsilon)}{((d + l\,cos\,(\varepsilon+\varphi) - l\,cos\,\varphi)^2 + (l\,sin\,(\varepsilon+\varphi) - l\,sin\,\varphi)^2)^{3/2}} \right.$$
$$+ \frac{q_1 q_c(-ld \sin\varphi - l^2 sin\,\varepsilon)}{((d - l\,cos\,(\varepsilon+\varphi) - l\,cos\,\varphi)^2 + (-l\,sin\,(\varepsilon+\varphi) - l\,sin\,\varphi)^2)^{3/2}}$$
$$+ \frac{q_1 q_b(-ld \sin\varphi)}{((-d + l\,cos\,\varphi)^2 + (l\,sin\,\varphi)^2)^{3/2}} \tag{20}$$
$$+ \frac{q_3 q_b(ld\,sin\,\varphi)}{((-d - l\,cos\,\varphi)^2 + (-l\,sin\,\varphi)^2)^{3/2}}$$
$$+ \frac{q_3 q_a(ld \sin\varphi - l^2 sin\,\varepsilon)}{((d + l\,cos\,(\varepsilon+\varphi) + l\,cos\,\varphi)^2 + (l\,sin\,(\varepsilon+\varphi) + l\,sin\,\varphi)^2)^{3/2}}$$
$$\left. + \frac{q_3 q_c(ld \sin\varphi + l^2 sin\,\varepsilon)}{((d - l\,cos\,(\varepsilon+\varphi) + l\,cos\,\varphi)^2 + (-l\,sin\,(\varepsilon+\varphi) + l\,sin\,\varphi)^2)^{3/2}} \right)$$

where $L_C \in \mathbb{R}$.

These torque expressions can be used to construct the system's open loop dynamics for the relative attitude between the spacecraft in the 2D Case. These open loop dynamics are given, in state-space form, by the following equation.

$$\vec{e} = \begin{bmatrix} \varepsilon \\ \dot{\varepsilon} \end{bmatrix}, \quad \dot{\vec{e}} = \begin{bmatrix} \dot{\varepsilon} \\ f(\varepsilon, \varphi) \end{bmatrix} \tag{21}$$

where $f(\varepsilon, \varphi)$ is given by the equation which follows, on the next page. This state-space form is convenient for the development of the 2D Case control laws. These will be explored in Chapter 5.

$$f(\varepsilon,\varphi)=\frac{k_C}{I_t}\left(\frac{q_1q_a(dl\,sin\,(\varepsilon+\varphi)-2l^2sin\,\varepsilon+ld\,\sin\varphi)}{((d+l\,cos\,(\varepsilon+\varphi)-l\,cos\,\varphi)^2+(l\,sin\,(\varepsilon+\varphi)-l\,sin\,\varphi)^2)^{3/2}}\right.$$

$$+\frac{q_1q_c(-dl\,sin\,(\varepsilon+\varphi)+2l^2sin\,\varepsilon+ld\,\sin\varphi)}{((d-l\,cos\,(\varepsilon+\varphi)-l\,cos\,\varphi)^2+(-l\,sin\,(\varepsilon+\varphi)-l\,sin\,\varphi)^2)^{3/2}}$$

$$+\frac{q_2q_a(dl\,sin\,(\varepsilon+\varphi))}{((d-l\,cos\,(\varepsilon+\varphi))^2+(-l\,sin\,(\varepsilon+\varphi))^2)^{3/2}}$$

$$+\frac{q_2q_c(-dl\,sin\,(\varepsilon+\varphi))}{((d-l\,cos\,(\varepsilon+\varphi))^2+(-l\,sin\,(\varepsilon+\varphi))^2)^{3/2}}$$

$$+\frac{q_3q_a(dl\,sin\,(\varepsilon+\varphi)+2l^2sin\,\varepsilon-ld\,\sin\varphi)}{((d+l\,cos\,(\varepsilon+\varphi)+l\,cos\,\varphi)^2+(l\,sin\,(\varepsilon+\varphi)+l\,sin\,\varphi)^2)^{3/2}}$$

$$+\frac{q_3q_c(2l^2\,sin\,\varepsilon-ld\,sin\,\varphi-ld\,\sin(\varepsilon+\varphi))}{((d-l\,cos\,(\varepsilon+\varphi)+l\,cos\,\varphi)^2+(-l\,sin\,(\varepsilon+\varphi)+l\,sin\,\varphi)^2)^{3/2}}$$

$$-\frac{q_1q_b(-ld\,\sin\varphi)}{((-d+l\,cos\,\varphi)^2+(l\,sin\,\varphi)^2)^{3/2}}$$

$$\left.-\frac{q_3q_b(ld\,sin\,\varphi)}{((-d-l\,cos\,\varphi)^2+(-l\,sin\,\varphi)^2)^{3/2}}\right)$$

where $I_t \in \mathbb{R}^+$ denotes the scalar moment-of-inertia of each spacecraft (recall that identical construction of the two craft is assumed) about their short principal axes. Note that these axes are parallel for the 2D Case. Details of the derivation of this equation are given in Appendix B. For the purposes of the 2D Case study, the chief tumble angle φ is considered to depend only on time and its control is not explored.

4.2.2. 3D Case

For the 3D Case, the spacecraft attitudes, with respect to the reference frame, are expressed in terms of two angles, each. The first is the first-axis rotation between the body-fixed frame of each spacecraft and the reference frame. For the chief spacecraft, this is termed $\alpha \in [0, 2\pi)$, while it is called $\beta \in [0, 2\pi)$ for the deputy spacecraft. The

second angle is the second-axis rotation between the body-fixed frame of each spacecraft and the reference frame, executed after the first-axis rotation. This is referred to as $\varphi \in [0, \pi]$ for the chief spacecraft and $\theta \in [0, \pi]$ for the deputy spacecraft. These angles are physically the same as those defined for the 2D Case, above, though the axes they are defined about are no longer always parallel, and their domains have changed, as a result.

A final rotation about the first axis of each spacecraft would complete an Euler angle sequence of 1-2-1 for each spacecraft. But, for the purposes of this system, this final rotation angle is meaningless, due to the spacecrafts' cylindrical shape. Thus, this final rotation is ignored. These angles are used to construct the following expression for the open-loop electrostatic torque on the deputy spacecraft, expressed in its body-fixed frame. Full details of the derivation are given in Appendix D.

$$\begin{aligned}\vec{M}_D^{OL} = k_C \Bigg(& \frac{q_1 q_a \vec{A}}{\left(d^2 + 2l(d\cos\varphi - d\cos\theta - l\cos\theta\cos\varphi + l - \Omega - \Gamma)\right)^{3/2}} \\ & + \frac{q_3 q_a \vec{B}}{\left(d^2 - 2l(d\cos\varphi + d\cos\theta - l\cos\theta\cos\varphi - l - \Omega - \Gamma)\right)^{3/2}} \\ & + \frac{q_2 q_a \vec{C}}{(d^2 - 2ld\cos\theta + l^2)^{3/2}} + \frac{q_2 q_c \vec{F}}{(d^2 + 2ld\cos\theta + l^2)^{3/2}} \\ & + \frac{q_1 q_c \vec{D}}{\left(d^2 + 2l(d\cos\varphi + d\cos\theta + l\cos\theta\cos\varphi + l + \Omega + \Gamma)\right)^{3/2}} \\ & + \frac{q_3 q_c \vec{E}}{\left(d^2 - 2l(d\cos\varphi - d\cos\theta + l\cos\theta\cos\varphi - l + \Omega + \Gamma)\right)^{3/2}} \Bigg)\end{aligned} \tag{22}$$

$$\Omega = l\sin\theta\sin\beta\sin\varphi\sin\alpha$$

$$\Gamma = l\sin\theta\cos\beta\sin\varphi\cos\alpha$$

where $\vec{M}_D^{OL} \in \mathbb{R}^3$ is the open-loop electrostatic torque on the deputy spacecraft, q_n, k_C, l, and d are as defined for the 2D Case, and the vectors $\vec{A}$, $\vec{B}$, $\vec{C}$, $\vec{D}$, $\vec{E}$, and $\vec{F}$ are defined by the following vector expressions.

$$\vec{A} = \begin{bmatrix} 0 \\ -l\sin\theta\left(d - l\cos\varphi + \cos\theta\left(l - l\sin^2\beta + l\cos^2\beta\right)\right) + l\cos\theta\,\Lambda \\ l\left(-l\cos\beta\sin\varphi\sin\alpha + 2l\sin\theta\sin\beta\cos\beta - l\sin\varphi\cos\alpha\sin\beta\right) \end{bmatrix}$$

$$\vec{B} = \begin{bmatrix} 0 \\ -l\sin\theta\left(d + l\cos\varphi + \cos\theta\left(l - l\sin^2\beta + l\cos^2\beta\right)\right) - l\cos\theta\,\Lambda \\ l\left(l\cos\beta\sin\varphi\sin\alpha + 2l\sin\theta\sin\beta\cos\beta + l\sin\varphi\cos\alpha\sin\beta\right) \end{bmatrix}$$

$$\vec{C} = \begin{bmatrix} 0 \\ -l\left(d\sin\theta + l\cos\theta\sin\theta - l\sin\theta\cos\theta\sin^2\beta + l\sin\theta\cos\theta\cos^2\beta\right) \\ 2l^2\sin\theta\sin\beta\cos\beta \end{bmatrix}$$

$$\vec{D} = \begin{bmatrix} 0 \\ -l\sin\theta\left(-d + l\cos\varphi + \cos\theta\left(l - l\sin^2\beta + l\cos^2\beta\right)\right) - l\cos\theta\,\Lambda \\ l\left(l\cos\beta\sin\varphi\sin\alpha + 2l\sin\theta\sin\beta\cos\beta + l\sin\varphi\cos\alpha\sin\beta\right) \end{bmatrix}$$

$$\vec{E} = \begin{bmatrix} 0 \\ -l\sin\theta\left(-d - l\cos\varphi + \cos\theta\left(l - l\sin^2\beta + l\cos^2\beta\right)\right) + l\cos\theta\,\Lambda \\ l\left(-l\cos\beta\sin\varphi\sin\alpha + 2l\sin\theta\sin\beta\cos\beta - l\sin\varphi\cos\alpha\sin\beta\right) \end{bmatrix}$$

$$\vec{F} = \begin{bmatrix} 0 \\ -l\left(-d\sin\theta + l\cos\theta\sin\theta - l\sin\theta\cos\theta\sin^2\beta + l\sin\theta\cos\theta\cos^2\beta\right) \\ 2l^2\sin\theta\sin\beta\cos\beta \end{bmatrix}$$

$$\Lambda = \sin\beta\sin\varphi\sin\alpha - \cos\beta\sin\varphi\cos\alpha$$

The equivalent torque on the chief spacecraft is developed by an identical method, which is also documented in Appendix D. The mathematical expression for this torque is very similar in structure, being a sum of six vectors, one for each pair of interacting charges between the two spacecraft. It is given by the equation which is shown on the following page.

$$\vec{M}_C^{OL} = k_C \left(\frac{q_1 q_a \vec{U}}{\left(d^2 + 2l(d\cos\theta - d\cos\varphi - l\cos\theta\cos\varphi + l - \Omega - \Gamma)\right)^{3/2}} \right.$$

$$+ \frac{q_1 q_c \vec{V}}{\left(d^2 - 2l(d\cos\theta + d\cos\varphi - l\cos\theta\cos\varphi - l - \Omega - \Gamma)\right)^{3/2}}$$

$$+ \frac{q_1 q_b \vec{W}}{(d^2 - 2ld\cos\varphi + l^2)^{3/2}} + \frac{q_3 q_b \vec{Z}}{(d^2 + 2ld\cos\varphi + l^2)^{3/2}} \qquad (23)$$

$$+ \frac{q_3 q_a \vec{X}}{\left(d^2 + 2l(d\cos\theta + d\cos\varphi + l\cos\theta\cos\varphi + l + \Omega + \Gamma)\right)^{3/2}}$$

$$\left. + \frac{q_3 q_c \vec{Y}}{\left(d^2 - 2l(d\cos\theta - d\cos\varphi + l\cos\theta\cos\varphi - l + \Omega + \Gamma)\right)^{3/2}} \right)$$

$$\Omega = l\sin\theta\sin\beta\sin\varphi\sin\alpha$$

$$\Gamma = l\sin\theta\cos\beta\sin\varphi\cos\alpha$$

$$\vec{U} = \begin{bmatrix} 0 \\ -l\sin\varphi\left(-d - l\cos\theta + \cos\varphi\left(l + l\sin^2\alpha + l\cos^2\alpha\right)\right) - l\cos\varphi\,\Xi \\ l\left(-l\cos\alpha\sin\theta\sin\beta + 2l\sin\varphi\sin\alpha\cos\alpha - l\sin\theta\cos\beta\sin\alpha\right) \end{bmatrix}$$

$$\vec{V} = \begin{bmatrix} 0 \\ -l\sin\varphi\left(-d + l\cos\theta + \cos\varphi\left(l - l\sin^2\alpha + l\cos^2\alpha\right)\right) - l\cos\varphi\,\Xi \\ l\left(l\cos\alpha\sin\theta\sin\beta + 2l\sin\varphi\sin\alpha\cos\alpha + l\sin\theta\cos\beta\sin\alpha\right) \end{bmatrix}$$

$$\vec{W} = \begin{bmatrix} 0 \\ -l\left(-d\sin\varphi + l\cos\varphi\sin\varphi - l\sin\varphi\cos\varphi\sin^2\alpha + l\sin\varphi\cos\varphi\cos^2\alpha\right) \\ 2l^2\sin\varphi\sin\alpha\cos\alpha \end{bmatrix}$$

$$\vec{X} = \begin{bmatrix} 0 \\ -l\sin\varphi\left(d + l\cos\theta + \cos\varphi\left(l + l\sin^2\alpha - l\cos^2\alpha\right)\right) + l\cos\varphi\,\Xi \\ l\left(l\cos\alpha\sin\theta\sin\beta + 2l\sin\varphi\sin\alpha\cos\alpha + l\sin\theta\cos\beta\sin\alpha\right) \end{bmatrix}$$

$$\vec{Y} = \begin{bmatrix} 0 \\ -l\sin\varphi\left(d - l\cos\theta + \cos\varphi\left(l - l\sin^2\alpha + l\cos^2\alpha\right)\right) + l\cos\varphi\,\Xi \\ l\left(-l\cos\alpha\sin\theta\sin\beta + 2l\sin\varphi\sin\alpha\cos\alpha - l\sin\theta\cos\beta\sin\alpha\right) \end{bmatrix}$$

$$\vec{Z} = \begin{bmatrix} 0 \\ -l\,(d\,sin\,\varphi + l\,cos\,\varphi\,sin\,\varphi - l\,sin\,\varphi\,cos\,\varphi\,sin^2\alpha + l\,sin\,\varphi\,cos\,\varphi\,cos^2\alpha) \\ 2l^2 sin\,\varphi\,sin\,\alpha\,cos\,\alpha \end{bmatrix}$$

$$\Xi = sin\,\beta\,sin\,\theta\,sin\,\alpha - cos\,\alpha\,sin\,\theta\,cos\,\beta$$

Using these torques, the open loop spacecraft relative kinetics are described by the following. Full details of this derivation are given in Appendix E.

$$\begin{aligned} \dot{\vec{\omega}}_{CD} = E_{CD}^T I_D^{-1} \left(\vec{M}_D^{OL} - E_{CD}(\widetilde{\vec{\omega}_{CD}} + \vec{\omega}_C) I_D \left(E_{CD}(\vec{\omega}_{CD} + \vec{\omega}_C) \right) \right) \\ -I_C^{-1} \left(\vec{M}_C^{OL} - \tilde{\omega}_C I_C \vec{\omega}_C \right) \end{aligned} \tag{24}$$

where the subscripts C and D refer to the chief and deputy spacecraft, respectively, $E_{CD} \in \mathbb{R}^{3x3}$ is the relative attitude DCM of the deputy spacecraft with respect to the chief spacecraft, $\vec{\omega}_{CD} \in \mathbb{R}^3$ is the relative angular velocity of the deputy spacecraft with respect to the chief spacecraft, the $\tilde{}$ operator is as defined in Section 3.1, and $I_N \in \mathbb{R}^{3x3}$ denotes the moment-of-inertia tensor of spacecraft N, calculated in its own body-fixed frame.

Since identical construction was assumed, both moment-of-inertia tensors have the same value, which is as follows.

$$I_N = \begin{bmatrix} I_a & 0 & 0 \\ 0 & I_t & 0 \\ 0 & 0 & I_t \end{bmatrix} \tag{25}$$

where $I_a \in \mathbb{R}^+$ is the scalar moment-of-inertia of the spacecraft about its long axis, and I_t is as defined above. Since each moment-of-inertia term is calculated in the spacecraft's body-fixed frame, their numerical values are identical, due to their identical construction. The relative attitude kinematics are represented using the error DCM defined above, with the kinematic equation defined, in (Galjanic & Seo, 2020), by the following expression.

$$\dot{E}_{CD} = \widetilde{\omega}_{CD} E_{CD} \tag{26}$$

Taken together, Equations (24) and (26) describe the open-loop equations of motion of the relative dynamics of the system in its 3D Case. These will be used with the controllers defined in the next chapter to derive the closed-loop dynamics of the system.

5. Controller Development

With the open-loop dynamics of both cases described, this chapter presents the investigated control laws to derive the closed-loop dynamics of this system, in both its 2D Case and its 3D Case.

5.1. 2D Case

In order to control the relative attitude of the two spacecraft for the 2D Case, two controllers were developed based on a linearized equation of motion and applied to the full equation of motion. Equation (21) was linearized by the Jacobian method about $\vec{e} = [0 \quad 0]^T$, as the goal of this research is to synchronize the spacecraft attitude responses. The linearized dynamics are as follows.

$$\dot{\vec{e}} = \begin{bmatrix} 0 & 1 \\ g(\varphi) & 0 \end{bmatrix} \vec{e} + \begin{bmatrix} 0 \\ \frac{1}{I_t} \end{bmatrix} u(t) \tag{27}$$

where the function $g(\varphi)$ is given by the following expression.

$$g(\varphi) = \frac{k_C}{I_t}\left(\frac{q_{1,e}q_{a,e}\left(6l^2 sin^2\varphi - 2l^2 + ld\ cos\ \varphi\right)}{d^3} + \frac{q_{1,e}q_{c,e}\left(2l^2 - ld\ cos\ \varphi\ \right)}{((d-2l\ cos\ \varphi)^2 + (-2l\ sin\ \varphi)^2)^{3/2}} \right.$$

$$+ \frac{q_{2,e}q_{a,e}(ld\ cos\ \varphi\ \left((d-l\ cos\ \varphi)^2 + (-l\ sin\ \varphi)^2\right)^{3/2})}{((d-l\ cos\ \varphi)^2 + (-l\ sin\ \varphi)^2)^3}$$

$$- \frac{3\ q_{2,e}q_{a,e}\ l^2 d^2\ sin^2\varphi\ \left((d-l\ cos\ \varphi)^2 + (-l\ sin\ \varphi)^2\right)^{1/2}}{((d-l\ cos\ \varphi)^2 + (-l\ sin\ \varphi)^2)^3}$$

$$+ \frac{q_{2,e}q_{c,e}(-ld\ cos\ \varphi\ \left((d+l\ cos\ \varphi)^2 + (-l\ sin\ \varphi)^2\right)^{3/2})}{((d+l\ cos\ \varphi)^2 + (-l\ sin\ \varphi)^2)^3}$$

$$+ \frac{3q_{2,e}q_{c,e}\ l^2 d^2 sin^2\varphi\ \left((d+l\ cos\ \varphi)^2 + (-l\ sin\ \varphi)^2\right)^{1/2}}{((d+l\ cos\ \varphi)^2 + (-l\ sin\ \varphi)^2)^3} + \frac{q_{3,e}q_{a,e}(ld\ cos\ \varphi + 2l^2)}{((d+2l\ cos\ \varphi)^2 + (2l\ sin\ \varphi)^2)^{3/2}}$$

$$\left. + \frac{q_{3,e}q_{c,e}(6l^2 sin^2\varphi + 2l^2 - ld\ cos\ \varphi)}{d^3} \right)$$

and $q_{ne} \in \mathbb{R}$ indicates the equilibrium charge on sphere $n \in \{1 \quad 2 \quad 3 \quad a \quad b \quad c\}$. The pseudo-input signal $u \in \mathbb{R}$ represents the torque experienced by the system due to manipulating the charges on the spacecraft. Details of this linearization are given in Appendix C.

For the first controller, it is designed to have the structure $u(t) = -K\vec{e}$, where $K \in \mathbb{R}^2$ is a row vector of gains. K is designed based on the minimum control energy approach, using a modified controllability Grammian function, similar to what is shown in (Desoer & Callier, 1990). For the normal Grammian, see (Hespanha, 2009).

$$H_\gamma(t_0, t_1) = \int_{t_0}^{t_1} \Theta(t_0, \tau) B(\tau) B^T(\tau) \Theta^T(t_0, \tau) e^{-4\gamma(\tau - t_0)} d\tau \tag{28}$$

where $[t_0, \ t_1]$ defines the time interval of interest, $\Theta(t_0, \tau)$ is the linearized system's state transition matrix, $B(\tau)$ is the linearized system's input-coupling matrix, and γ defines the rate of decay for the linearized system response, which, in the 2D Case study, was tuned to provide the smallest error in the steady state (see Chapter 6).

It can be seen that, at $\gamma = 0$, H_γ is the controllability Grammian for the system (Rugh, 1996). K was then proposed as $K = B^T H_\gamma^{-1}(t_0, t_1)$. The stability for this controller can be proven, by noticing that $\xi = \vec{e}$, $t = t_0$, and $\Delta = t_1 - t_0$ in (Desoer & Callier, 1990), using the following Lyapunov function.

$$V(\xi) = \xi^T {H_\gamma}^{-1}(t_0, t_1) \xi \tag{29}$$

$$\dot{V} \leq -2\gamma \xi^T {H_\gamma}^{-1}(t_0, t_1) \xi \leq -2\gamma h_M^{-1} \|\xi\|^2 \tag{30}$$

where $\Delta \in \mathbb{R}^+$ is the length of the interval of interest, $\xi \in \mathbb{R}^n$ is the state vector of a general system under control by this controller, and $h_M > 0 \in \mathbb{R}$ satisfies $H_0(t_0, t_1) \leq$

$h_M I_{nxn}$, where I_{nxn} is an identity matrix.

Using this Lyapunov function and its derivative, the following inequality can be constructed by simple division.

$$\frac{\dot{V}}{V} \leq -2\gamma \frac{h_m}{h_M} exp(-4\gamma \Delta) \tag{31}$$

where $h_m > 0 \in \mathbb{R}$ satisfies $h_m \leq h_M$ and $h_m I_{nxn} \leq H_0(t_0, t_1)$. From Equation (31), $V(\xi)$ can be shown to decay exponentially. Therefore, the controller is stable. The more detailed version of the proof follows the same steps as in (Desoer and Callier, 1990) with $\xi = \vec{e}$, $t = t_0$, and $\Delta = t_1 - t_0$.

The second controller developed for the 2D Case is a time-periodic LQR controller, since some of the simulations conducted (see Chapter 6) used a time-periodic chief tumble angle φ. The time-periodic LQR controller is designed to minimize the following state and input cost function.

$$C = \frac{1}{2}\int_0^\infty (\vec{e}^T(t)Q(t)\,\vec{e}(t) + u(t)R(t)u(t))dt \tag{32}$$

where $Q(t) \geq 0 \in \mathbb{R}^{2x2}$ and $R(t) > 0 \in \mathbb{R}$ are weighting matrices with the same period as the open-loop system. The controller is designed by solving the periodic Algebraic Riccati Equation, which is given by the following.

$$-(A^T(t)P(t) + P(t)A(t) + Q(t)) + P(t)B(t)R^{-1}(t)B^T(t)P(t) = 0 \tag{33}$$

This equation is solved for $P(t) \in \mathbb{R}^{2x2}$. This is then used to construct the feedback control signal presented on the following page. It is important to note that this feedback control signal is essentially a state-feedback controller with time-periodic gain.

$$u(t) = -R^{-1}(t)B^T(t)P(t)\vec{e}(t) \tag{34}$$

The results of these two controllers are simulated in Chapter 6, below. In addition, their performance is compared, in order to determine which is more effective at effecting the control of the 2D Case system.

5.2. 3D Case

In order to accomplish the control of the relative attitude between the two satellites for the 3D Case, the nonlinear swarm controller proposed in (Song, Tang, Hong, & Hu, 2017) is used. Similar to the 2D Case, this controller is applied to the motion of the deputy spacecraft as a pseudo-input signal. Meanwhile, the attitude of the chief spacecraft is assumed to be controlled by a separate system, to maintain the motions specified in Chapter 6, below.

The control law for this controller is given in (Song, Tang, Hong, & Hu, 2017) by the following mathematical expression.

$$\vec{\omega}_D = \vec{\omega}_D^d + h'(\Phi_{CD})\vec{k}_{CD} \tag{35}$$

where $\vec{\omega}_D^d \in \mathbb{R}^3$ is the desired angular velocity of the deputy spacecraft observed from the inertial reference frame and expressed in the deputy's body-fixed frame, $\Phi_{CD} \in [0, \pi]$ is the principal rotation angle between the deputy spacecraft's attitude and the chief spacecraft's attitude, $\vec{k}_{CD} \in \mathbb{R}^3$ is the principal rotation axis between the deputy spacecraft's attitude and the chief spacecraft's attitude, and $h(\cdot)$: $[0, \pi] \rightarrow \mathbb{R}^+$ defines a potential function satisfying the following assumptions: h must be twice continuously differentiable on $[0, \pi]$, $h(0) = h'(0) = 0$, and $h' > 0$ on $(0, \pi)$.

For the purposes of this investigation, a modified form of the second h suggested by

(Song, Tang, Hong, & Hu, 2017) was used. Namely, $h(\Phi_{CD}) = 0.8sin^2(\Phi_{CD}^2)$. By using this control law with Euler's Equation for the motion of rigid bodies, Equation (12), the following expression was found for the control torque that this law exerts. Full details of this derivation are provided in Appendix F.

$$\vec{M}_D^{CL} = I_D\left(\dot{\vec{\omega}}_C + \dot{\Phi}_{CD}h''(\Phi_{CD})\vec{k}_{CD} + h'(\Phi_{CD})\dot{\vec{k}}_{CD}\right) + \left(\vec{\omega}_C + h'(\Phi_{CD})\vec{k}_{CD}\right) \times I_D\left(\vec{\omega}_C + h'(\Phi_{CD})\vec{k}_{CD}\right) \quad (36)$$

where $\vec{M}_D^{CL} \in \mathbb{R}^3$ denotes the control moment on the deputy spacecraft, expressed in its body-fixed frame. This control torque is applied to the system to create the closed-loop equations of motion that follow.

$$\dot{\vec{\omega}}_{CD} = E_{CD}^T I_D^{-1}\left(\vec{M}_D^{CL} + \vec{M}_D^{OL} - E_{CD}(\widetilde{\vec{\omega}_{CD}} + \vec{\omega}_C)I_D\left(E_{CD}(\vec{\omega}_{CD} + \vec{\omega}_C)\right)\right) - I_C^{-1}\left(\vec{M}_C^{OL} - \tilde{\omega}_C I_C \vec{\omega}_C\right) \quad (37)$$

$$\dot{E}_{CD} = \tilde{\omega}_{CD}E_{CD} \quad (38)$$

This controller can be shown to stabilize the system by the following, which is adapted from the proof offered in (Song, Tang, Hong, & Hu, 2017), for the case of two spacecraft. We begin by defining the following function.

$$V(E_{CD}) = h(\Phi_{CD}) \quad (39)$$

The upper-right Dini time-derivative of this equation is then taken, and can be expressed as the following.

$$D^+V(E_{CD}) = -2h'(\Phi_{CD})^2\vec{k}_{CD}^T\vec{k}_{CD} \quad (40)$$

Note that this expression is a simplification of the corresponding expression in the reference, made for the system under consideration in this study. The function $V(E_{CD})$ can be considered a Lyapunov candidate function for this system, as one of the assumptions listed above for h is that $h' > 0$ on $(0, \pi)$, and another is that $h(0) = h'(0) = 0$. This implies that $V(E_{CD}) > 0$ for $\Phi_{CD} \neq 0$ and $V(E_{CD}) = 0$ for $\Phi_{CD} = 0$. Additionally, by Equation (40), and the assumption on h', $D^+V(E_{CD}) < 0$ for $\Phi_{CD} \neq 0$, and $D^+V(E_{CD}) = 0$ for $\Phi_{CD} = 0$. Therefore, this Lyapunov function can be used to conclude that the closed-loop system is stable with respect to $\Phi_{CD} = 0$, which is the state of the two spacecraft being aligned.

5.2.1. Actuator Dynamics

As the previous sections use pseudo-input control vectors to model the closed-loop dynamics, this section details the necessary actuator response required to generate the control signal given in Equation (36). This is accomplished by means of a dynamic inversion, whereby the expression for electrostatic torque on the deputy spacecraft, Equation (22), is equated to the control torque expression, Equation (36), and the result is solved for the electrostatic charges, q_n. That is to say, the following equation is made.

$$\vec{M}_D^{OL} = \vec{M}_D^{CL} \tag{41}$$

However, careful readers will note that this vector expression results in a system of three equations with six unknowns. In order to facilitate solving for these unknowns, an additional constraint is introduced to the system. Namely, the electrostatic charges on the chief spacecraft are assumed to be held fixed at a nominal value, with the deputy spacecraft charges remaining variable, to accomplish control over the deputy's attitude.

Given this new constraint, Equation (41) is solved for the charges on the deputy spacecraft, (q_a, q_b, and q_c) and the results, as functions of system state, are shown below. Full details of this derivation are given in Appendix G.

$$q_a = \frac{\lambda \vec{M}_{D,2}^{CL} - \chi \vec{M}_{D,3}^{CL}}{\eta\lambda - \chi\mu} \tag{42}$$

$$q_b \; free$$

$$q_c = \frac{\eta \vec{M}_{D,3}^{CL} - \mu \vec{M}_{D,2}^{CL}}{\eta\lambda - \chi\mu} \tag{43}$$

where the subscripts 2 and 3 denote the 2nd and 3rd terms of the vectors to which they are attached, and the following expressions define the other variables.

$$\lambda = \frac{q_1 l\,(l\cos\beta\sin\varphi\sin\alpha + 2l\sin\theta\sin\beta\cos\beta + l\sin\varphi\cos\alpha\sin\beta)}{\left(d^2 + 2l(d\cos\varphi + d\cos\theta + l\cos\theta\cos\varphi + l + \Omega + \Gamma)\right)^{3/2}} + \frac{q_3 l\,(-l\cos\beta\sin\varphi\sin\alpha + 2l\sin\theta\sin\beta\cos\beta - l\sin\varphi\cos\alpha\sin\beta)}{\left(d^2 - 2l(d\cos\varphi - d\cos\theta + l\cos\theta\cos\varphi - l + \Omega + \Gamma)\right)^{3/2}} + \frac{2q_2 l^2 \sin\theta\sin\beta\cos\beta}{(d^2 + 2ld\cos\theta + l^2)^{3/2}}$$

$$\chi = \frac{-q_1 l\,\sin\theta\left(-d + l\cos\varphi + \cos\theta\,(l - l\sin^2\beta + l\cos^2\beta)\right) - l\cos\theta\,\Lambda}{\left(d^2 + 2l(d\cos\varphi + d\cos\theta + l\cos\theta\cos\varphi + l + \Omega + \Gamma)\right)^{3/2}} - \frac{q_3 l\sin\theta\left(-d - l\cos\varphi + \cos\theta\,(l - l\sin^2\beta + l\cos^2\beta)\right) + l\cos\theta\,\Lambda}{\left(d^2 - 2l(d\cos\varphi - d\cos\theta + l\cos\theta\cos\varphi - l + \Omega + \Gamma)\right)^{3/2}} - \frac{q_2 l\,(-d\sin\theta + l\cos\theta\sin\theta - l\sin\theta\cos\theta\sin^2\beta + l\sin\theta\cos\theta\cos^2\beta)}{(d^2 + 2ld\cos\theta + l^2)^{3/2}}$$

$$\eta = \frac{-q_1 l\sin\theta\left(d - l\cos\varphi + \cos\theta\,(l - l\sin^2\beta + l\cos^2\beta)\right) + l\cos\theta\,\Lambda}{\left(d^2 + 2l(d\cos\varphi - d\cos\theta - l\cos\theta\cos\varphi + l - \Omega - \Gamma)\right)^{3/2}} - \frac{q_3 l\,\sin\theta\left(d + l\cos\varphi + \cos\theta\,(l - l\sin^2\beta + l\cos^2\beta)\right) - l\cos\theta\,\Lambda}{\left(d^2 - 2l(d\cos\varphi + d\cos\theta - l\cos\theta\cos\varphi - l - \Omega - \Gamma)\right)^{3/2}} - \frac{q_2 l\,(d\sin\theta + l\cos\theta\sin\theta - l\sin\theta\cos\theta\sin^2\beta + l\sin\theta\cos\theta\cos^2\beta)}{(d^2 - 2ld\cos\theta + l^2)^{3/2}}$$

$$\mu = \frac{q_1 l\ (-l\ cos\ \beta\ sin\ \varphi\ sin\ \alpha + 2l\ sin\ \theta\ sin\ \beta\ cos\ \beta - l\ sin\ \varphi\ cos\ \alpha\ sin\ \beta)}{\left(d^2 + 2l(d\ cos\ \varphi - d\ cos\ \theta - l\ cos\ \theta\ cos\ \varphi + l - \Omega - \Gamma)\right)^{3/2}}$$

$$+ \frac{q_3 l\ (l\ cos\ \beta\ sin\ \varphi\ sin\ \alpha + 2l\ sin\ \theta\ sin\ \beta\ cos\ \beta + l\ sin\ \varphi\ cos\ \alpha\ sin\ \beta)}{\left(d^2 - 2l(d\ cos\ \varphi + d\ cos\ \theta - l\ cos\ \theta\ cos\ \varphi - l - \Omega - \Gamma)\right)^{3/2}}$$

$$+ \frac{2q_2 2l^2 sin\ \theta\ sin\ \beta\ cos\ \beta}{(d^2 - 2ld\ cos\ \theta + l^2)^{3/2}}$$

In the above solution, it is notable that the value for the middle charge, q_b, does not have an expression associated with it. This is due to the fact that this sphere is centered at the deputy's center of mass and, therefore, cannot contribute to any torque about the center of mass. Close inspection of Equation (22) confirms this, as the term does not appear in that equation. In order to determine the practicality of the functions for the other two charges, they are simulated numerically and the results are discussed in Chapter 6, below.

6. Numerical Simulations

This chapter presents numerical simulations of several important equations presented above, to observe the behavior of the system. The geometric parameters for these simulations were taken from the system considered in (Schaub & Stevenson, 2013). That is, $d = 15$ m, $l = 1.1569$ m, $I_a = 29.45\ \text{kgm}^2$, and $I_t = 191.4\ \text{kgm}^2$. The equilibrium charge of each sphere was arbitrarily set to 1 mC.

6.1. 2D Case

The following simulations address the system in its 2D Case. These simulations will examine the open-loop and closed-loop dynamics of the 2D Case system. Most importantly, the behavior of the two controllers will be compared.

6.1.1. Open-Loop Dynamics

Equation (21) was simulated to observe the natural, open-loop, behavior of the system. This system was simulated for 100 s with an initial state vector of $\vec{e} = [20\ (\text{degree}),\ 20\ (\text{degree/sec})]^T$. The chief spacecraft was arbitrarily assumed to rotate at $\dot{\varphi} = 10\ \text{deg/sec}$. The response of the system is shown in Figure 6.1, below.

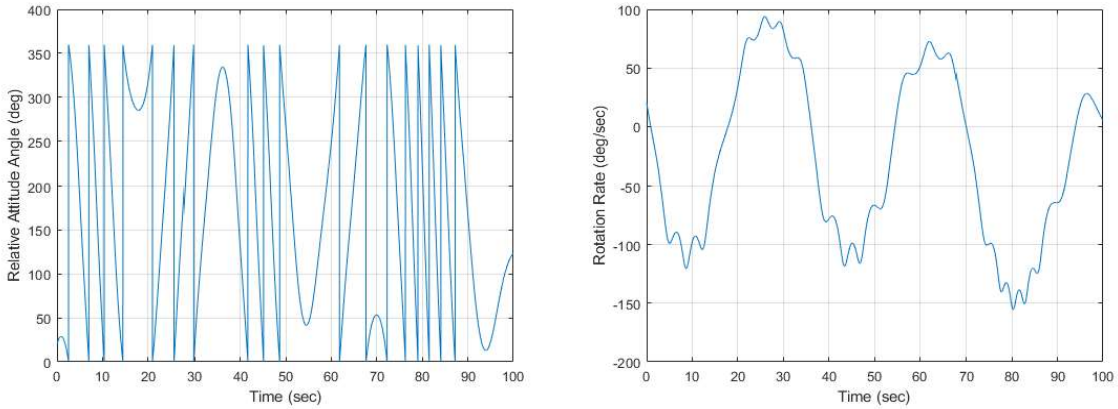

(a) Relative Angle ϵ Response (b) Relative Angle Rate $\dot{\epsilon}$ Response

Figure 6.1 Open-Loop System Response for 2D Case

It can be plainly seen from Figure 6.1 that the relative attitude of the two spacecraft is naturally far from zero and fluctuates periodically. This contrasts with the behavior of the closed-loop system. This will be presented in the following sections.

6.1.2. Grammian Controller

Using $\gamma = 10$ in Equation (28), the gain matrix for the controller became $K = [192.2959,\ 19.9667]$. The response of the closed-loop system using this controller is shown in Figure 6.2.

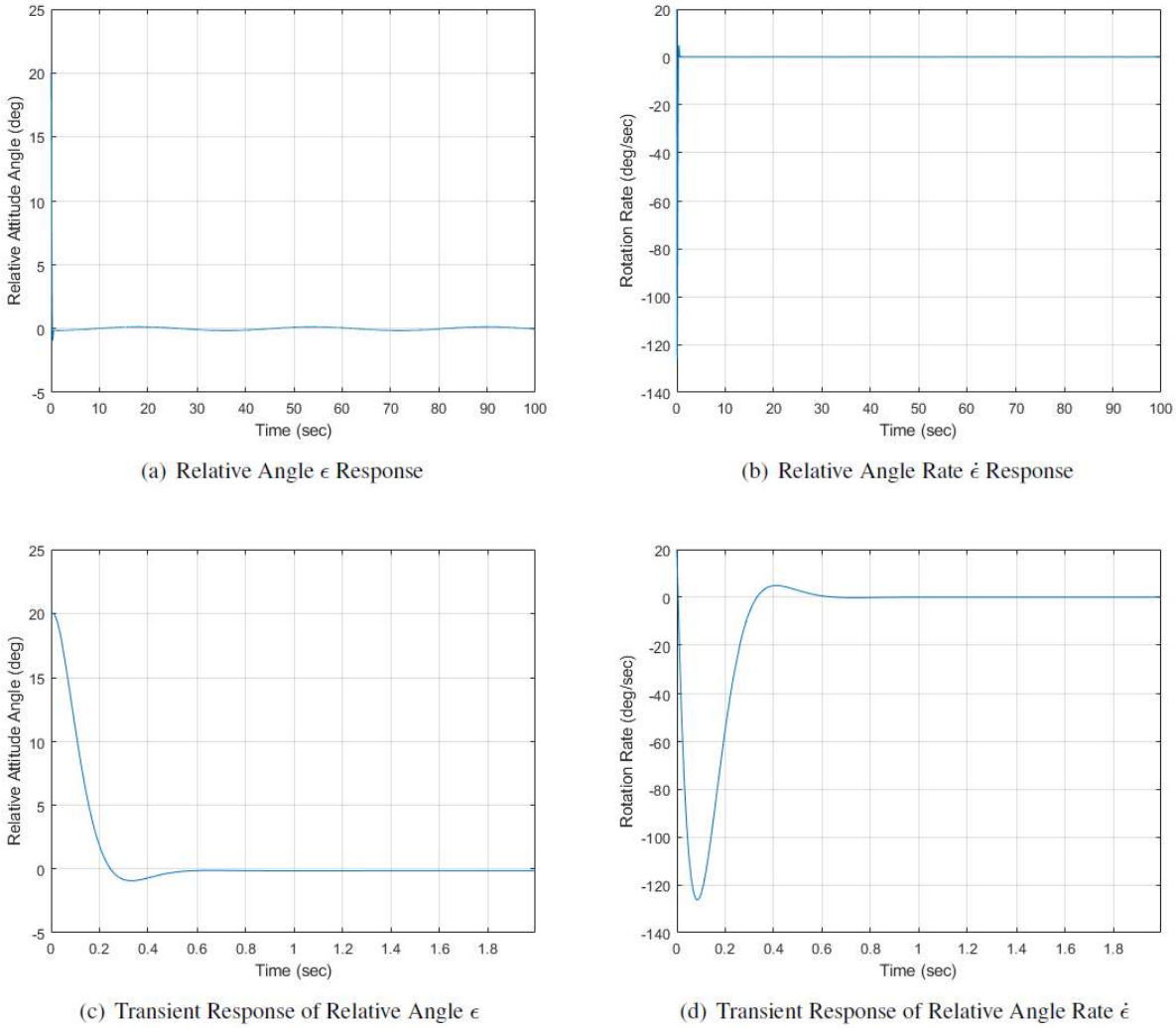

(a) Relative Angle ϵ Response

(b) Relative Angle Rate $\dot{\epsilon}$ Response

(c) Transient Response of Relative Angle ϵ

(d) Transient Response of Relative Angle Rate $\dot{\epsilon}$

Figure 6.2 Closed-Loop System Response for 2D Case and Grammian Controller

It can be seen in Figure 6.2 that the relative attitude response remains very near to zero under this controller. However, there is still some oscillation about the equilibrium condition. This is due to the continued rotation of the two spacecraft, which, as mentioned previously, was set to $\dot{\varphi} = 10$ deg/sec.

A numerical simulation was also conducted with the chief angle φ oscillating about $\varphi = 90$ deg. The exact function used to simulate the angle's behavior was $\varphi(t) = \frac{\pi}{180} cos(2\pi t) + \frac{\pi}{2}$. The mechanism driving this φ behavior was not explored, but was assumed to be a reaction wheel or similar device onboard the chief spacecraft. Using this configuration and the grammian approach with $\gamma = 10$, the gain matrix was found to be $K = [192.4860,\ 19.9667]$. The response of the system is shown in Figure 6.3.

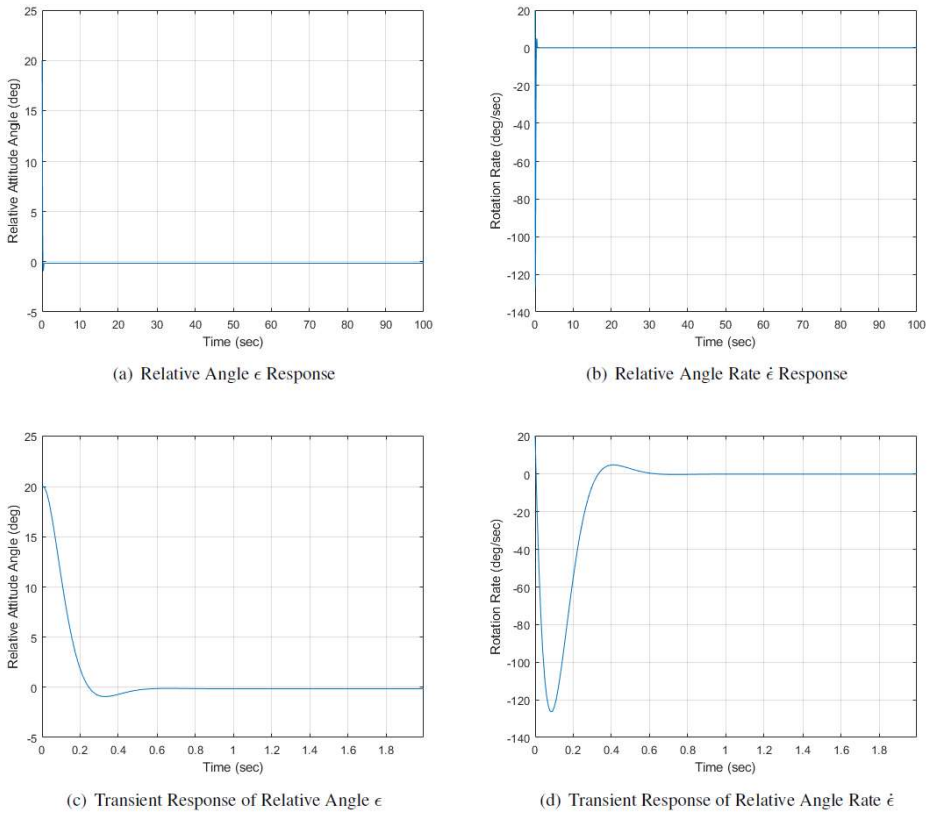

(a) Relative Angle ϵ Response

(b) Relative Angle Rate $\dot{\epsilon}$ Response

(c) Transient Response of Relative Angle ϵ

(d) Transient Response of Relative Angle Rate $\dot{\epsilon}$

Figure 6.3 Grammian-Controlled Response with Oscillating φ for 2D Case

It can be seen from Figure 6.3 that, in the absence of wide variations in φ, the closed-loop system is very well-behaved. The values for both ε and $\dot{\varepsilon}$ are brought near to zero and remain there with little variation. However, it is important to note the presence of steady-state error in the relative angle. The value settles at $\varepsilon = -0.1439$ deg. Though this may not appear to be a large error, for some pointing applications it is significant.

6.1.3. Time-Varying LQR Controller

For simplicity, constants were used for the weighting matrices for the LQR controller. The system under consideration was simulated, with linearly varying φ ($\dot{\varphi} = 10$ deg/sec), using the LQR controller with weighting matrices $Q = \begin{bmatrix} 100 & 1 \\ 1 & 100 \end{bmatrix}$ and $R = 0.001$. The initial conditions were set to be identical to those in the grammian controller simulations, in order to compare the two. The results are shown in Figure 6.4.

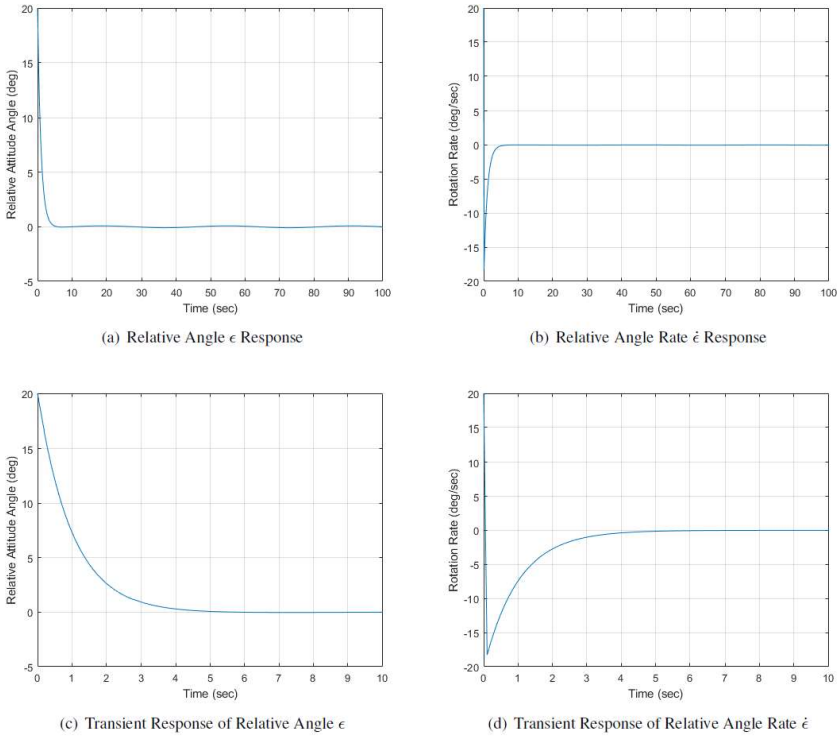

Figure 6.4 System Response for LQR Controller and Linearly Varying φ for 2D Case

It can be seen from Figure 6.4 that the time-varying LQR controller drives the relative angle to a small oscillation in the steady-state, like the grammian control in Figure 6.2. However, the amplitude of this oscillation is visibly smaller. A direct numerical comparison between these responses is given in Table 6.1.

Additionally, the response for the system with oscillating φ angle was simulated under the influence of the time-varying LQR controller given above. This was done in order to compare with the grammian control with oscillating φ. The response is shown in Figure 6.5.

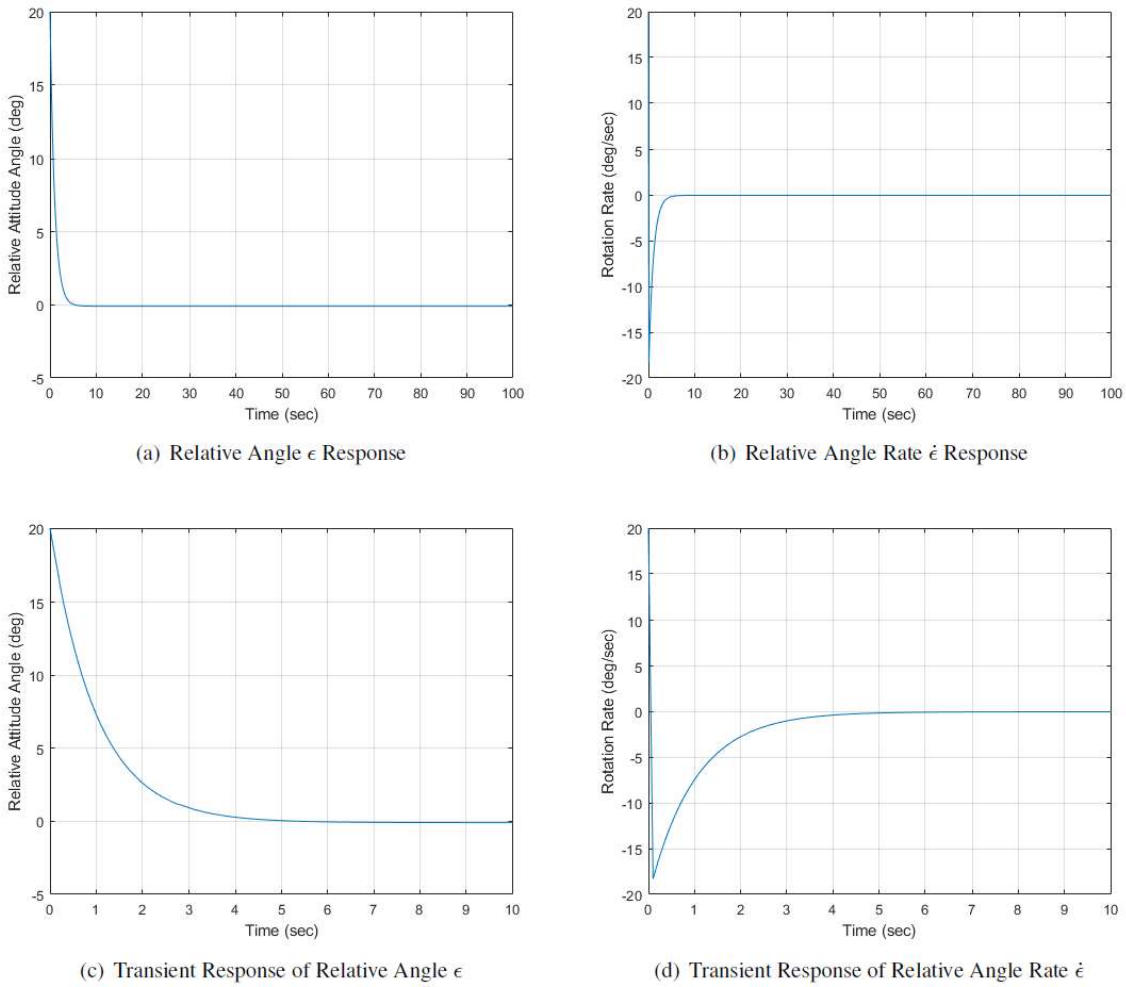

(a) Relative Angle ϵ Response

(b) Relative Angle Rate $\dot{\epsilon}$ Response

(c) Transient Response of Relative Angle ϵ

(d) Transient Response of Relative Angle Rate $\dot{\epsilon}$

Figure 6.5 Simulation for Time-Varying LQR Controller and Oscillating φ for 2D Case

Table 6.1

Comparison of Relative Angle ε Responses Between Grammian Control and Time-Varying LQR Control for 2D Case

φ Behavior	Response Property	Grammian Controller	Time-Varying LQR Controller
Linear	Max. Overshoot (deg)	0.926	N/A
	Avg. Steady-State Error (deg)	0	0
	Steady-State Oscillation Amplitude (deg)	0.144	0.08627
	Steady-State Oscillation Frequency (Hz)	0.0277	0.0278
Oscillating	Max. Overshoot (deg)	0.9288	N/A
	Avg. Steady-State Error (deg)	-0.1439	-0.08747
	Steady-State Oscillation Amplitude (deg)	0	0

Figure 6.5 shows near-identical transient behavior to Figure 6.4. The most notable difference is the long-term behavior of the relative angle, which shows a constant steady-state. This is similar to the behavior of the system under the influence of the grammian control law as shown in Figure 6.3, except that the steady-state error is far lower. A numerical comparison of these behaviors is given in Table 6.1. Additionally, the behaviors are plotted together in Figure 6.6.

Overall, Table 6.1 shows superior performance for the system under influence of the time-varying LQR controller. For the linearly varying φ angle responses, it shows a lower oscillation amplitude in the steady state and, for both φ behaviors, shows no overshoot in the response. The steady-state error for the oscillating φ angle case is lower for the time-varying LQR controller, as well. Most likely, these discrepancies are due to the fact that the time-varying LQR controller was designed to minimize the controller

energy. With this strategy in mind, the controller would logically reduce oscillation amplitude and avoid overshoot, if possible. Meanwhile, the Grammian controller was designed using an arbitrary decay rate, which did not take these parameters into consideration. However, the major shortfall of the time-varying LQR controller is that the structure detailed above applies to periodic systems only, whereas the Grammian-based controller is capable of controlling the system with arbitrary φ behavior. If future study of this system's 2D Case is conducted for periodic cases only, the time-varying LQR controller is likely to be the best approach. Otherwise, the Grammian controller is recommended.

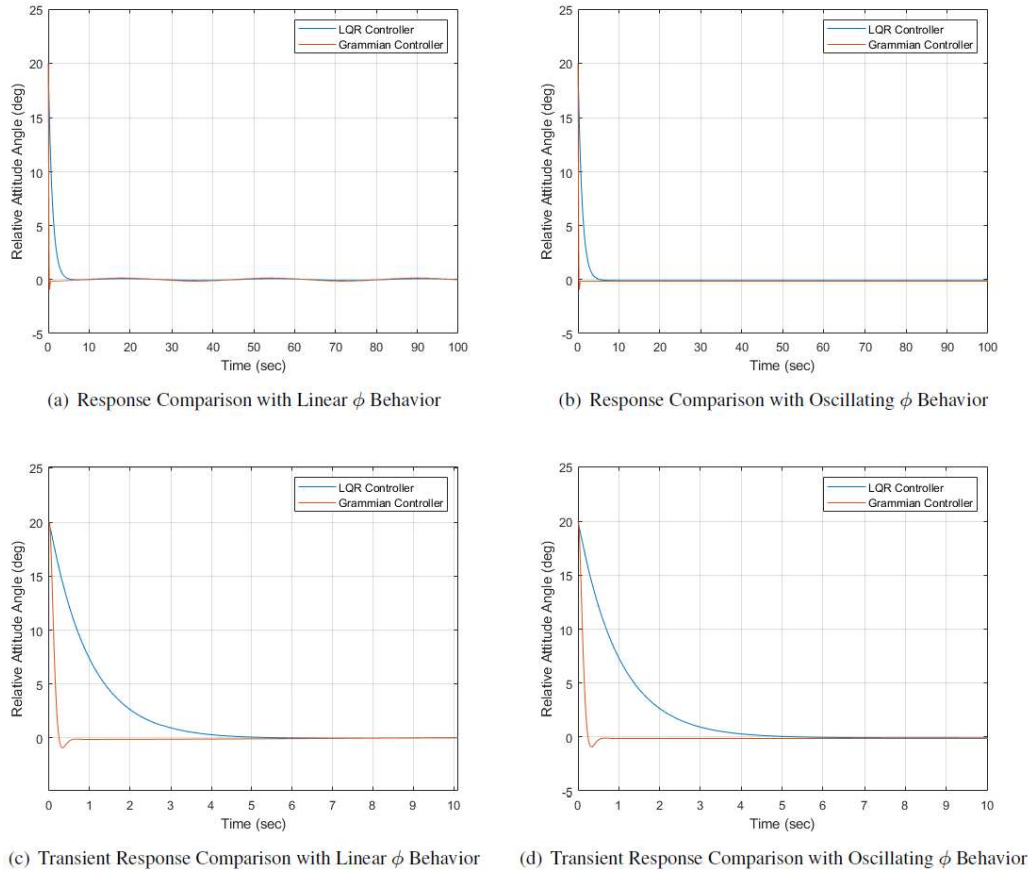

(a) Response Comparison with Linear ϕ Behavior

(b) Response Comparison with Oscillating ϕ Behavior

(c) Transient Response Comparison with Linear ϕ Behavior

(d) Transient Response Comparison with Oscillating ϕ Behavior

Figure 6.6 Comparison of Time-Varying LQR and Grammian Controllers by Relative Angle ε Behavior for the 2D Case.

6.2. 3D Case

The following simulations address the system in its 3D Case. They examine numerous behaviors of the system, including open-loop dynamics, equilibrium behavior, closed-loop dynamics, and actuator dynamics.

6.2.1. Open-Loop Dynamics

By using Equations (24), and (26), the natural, open-loop, motion of the 3D Case of the system is simulated. Several open-loop motion simulations will be presented to show different aspects of the open-loop behavior.

In the first, the spacecraft are set to start as shown in Figure 4.1 and experience single axis rotations of equal speed. The first case is motion only about the spacecraft $\hat{I}$ and $\hat{\imath}$ axes. The initial angular velocity is set to 10 deg/sec. The results are shown in Figure 6.7.

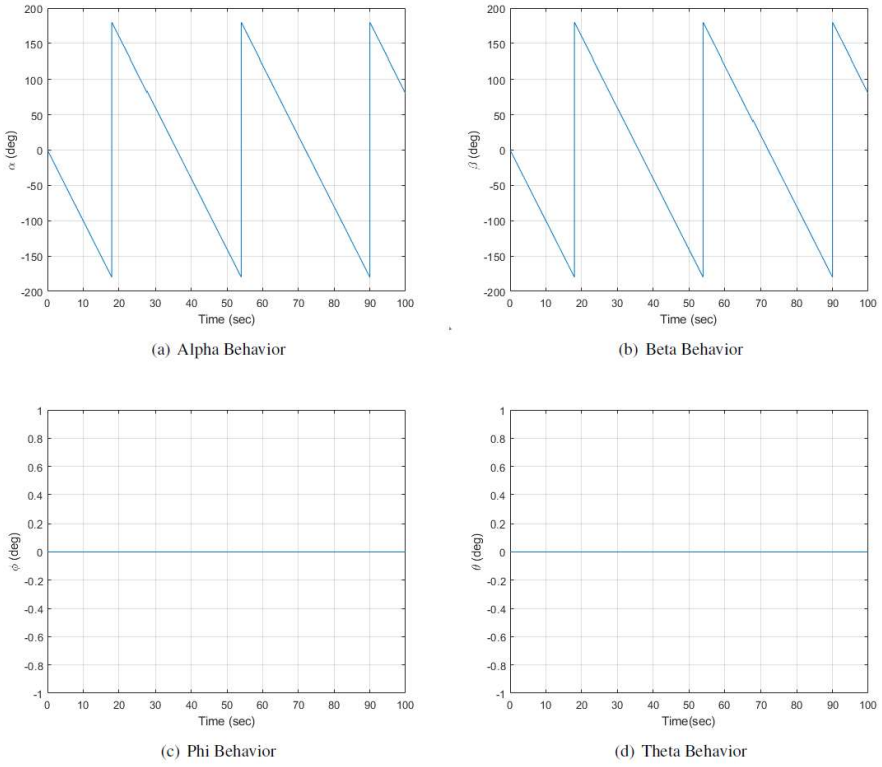

Figure 6.7 Open-Loop First Axis Rotation Simulation for 3D Case

As expected, both spacecraft first axis angles, α and β, show constant increase behavior, while the second axis angles are still. The spacecraft do not interact, because in this configuration (like in Figure 4.1), their long axes are aligned and no moments are produced due to the electrostatic charges.

The second case is rotation only about the spacecraft $\hat{f}$ and $\hat{\jmath}$ axes, with the same starting orientation as in the previous case. The initial angular velocity for both craft is set to 10 deg/sec and the results are shown in Figure 6.8.

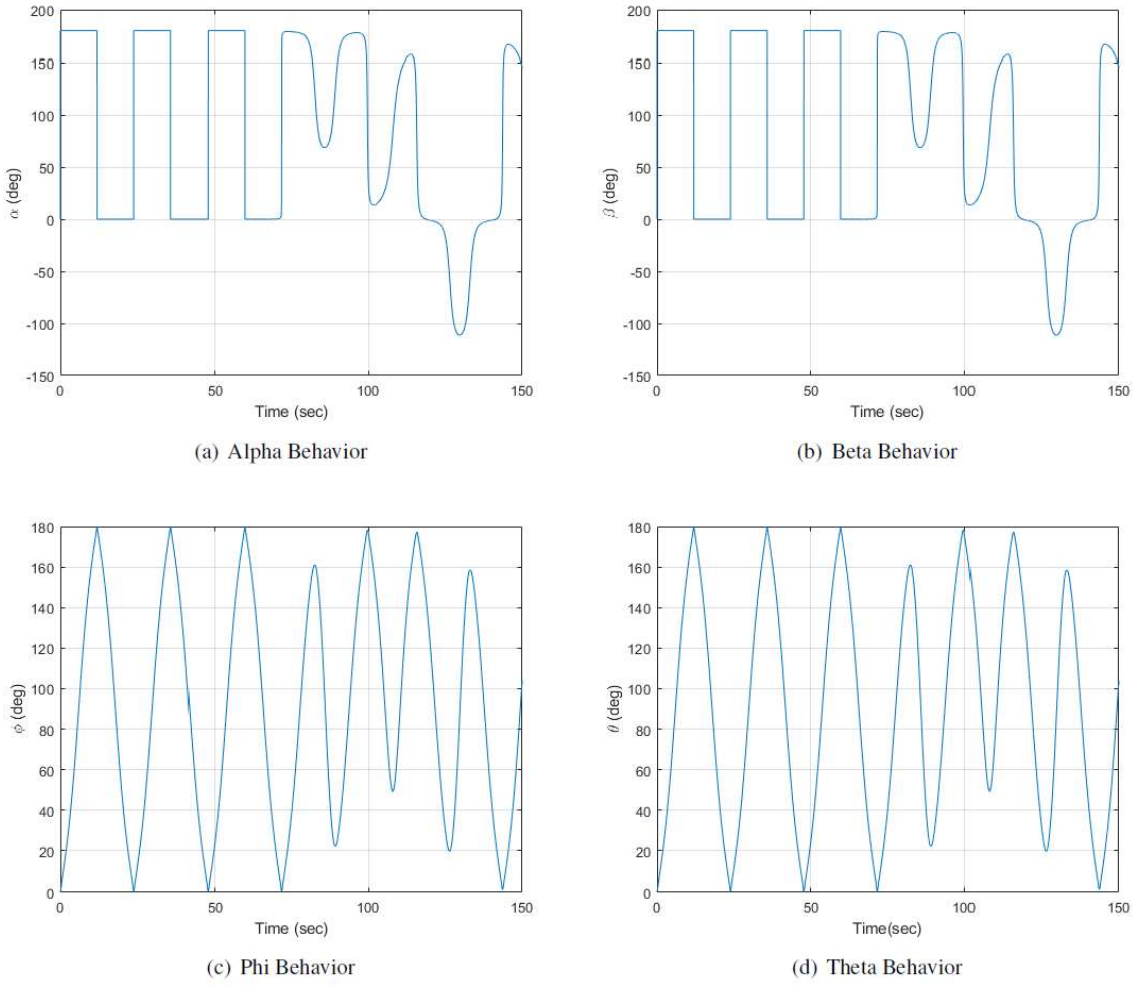

Figure 6.8 Open-Loop Second Axis Rotation Simulation for 3D Case

Initially, Figure 6.8 shows the system behaving as expected, with the second-axis angles evolving with time, subject to disturbance by the electrostatic torque, while the first-axis angles remain constant (the switching behavior shown is an artifact of the attitude coordinate system). However, at approximately 75 seconds into the simulation, the small differences in the attitudes of the two spacecraft allow the electrostatic torque to induce a change in their motion.

Finally, a more interesting set of initial conditions are used for the final simulation. This is with the chief spacecraft beginning with $\varphi = \frac{\pi}{2}$ and $\alpha = 0$ and the deputy beginning at $\theta = \frac{\pi}{2}$ and $\beta = \frac{\pi}{2}$. This initial condition is shown in Figure 6.9, for ease of visualization. The chief's initial angular velocity is set to $\vec{\omega}_{C0} = [0 \quad 10 \quad 0]^T$ deg/sec and the deputy's is set to $\vec{\omega}_{D0} = [0 \quad 30 \quad 0]^T$ deg/sec. The results are shown in Figure 6.10.

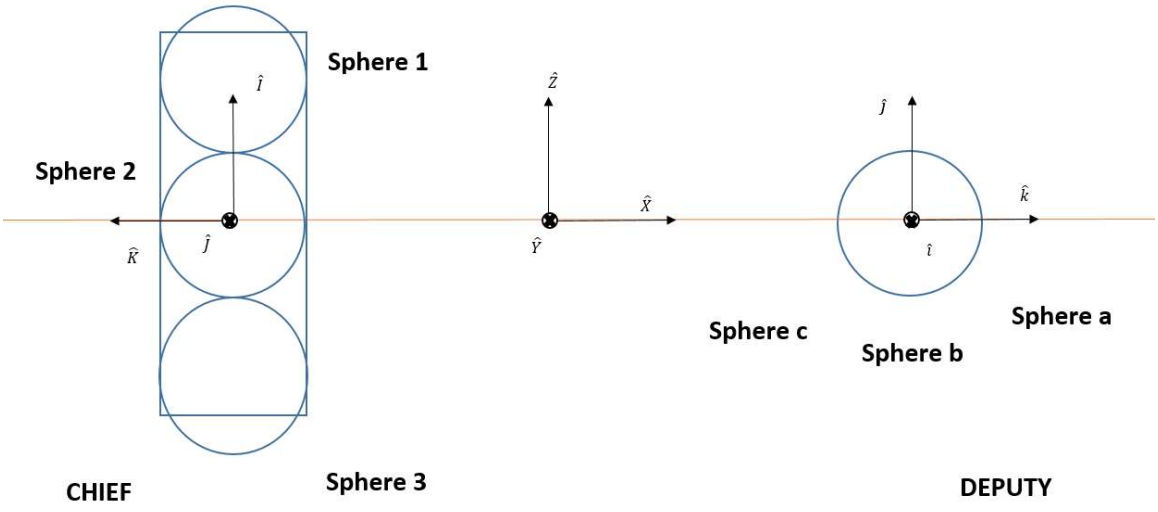

Figure 6.9 Open-Loop Perpendicular Initial Condition

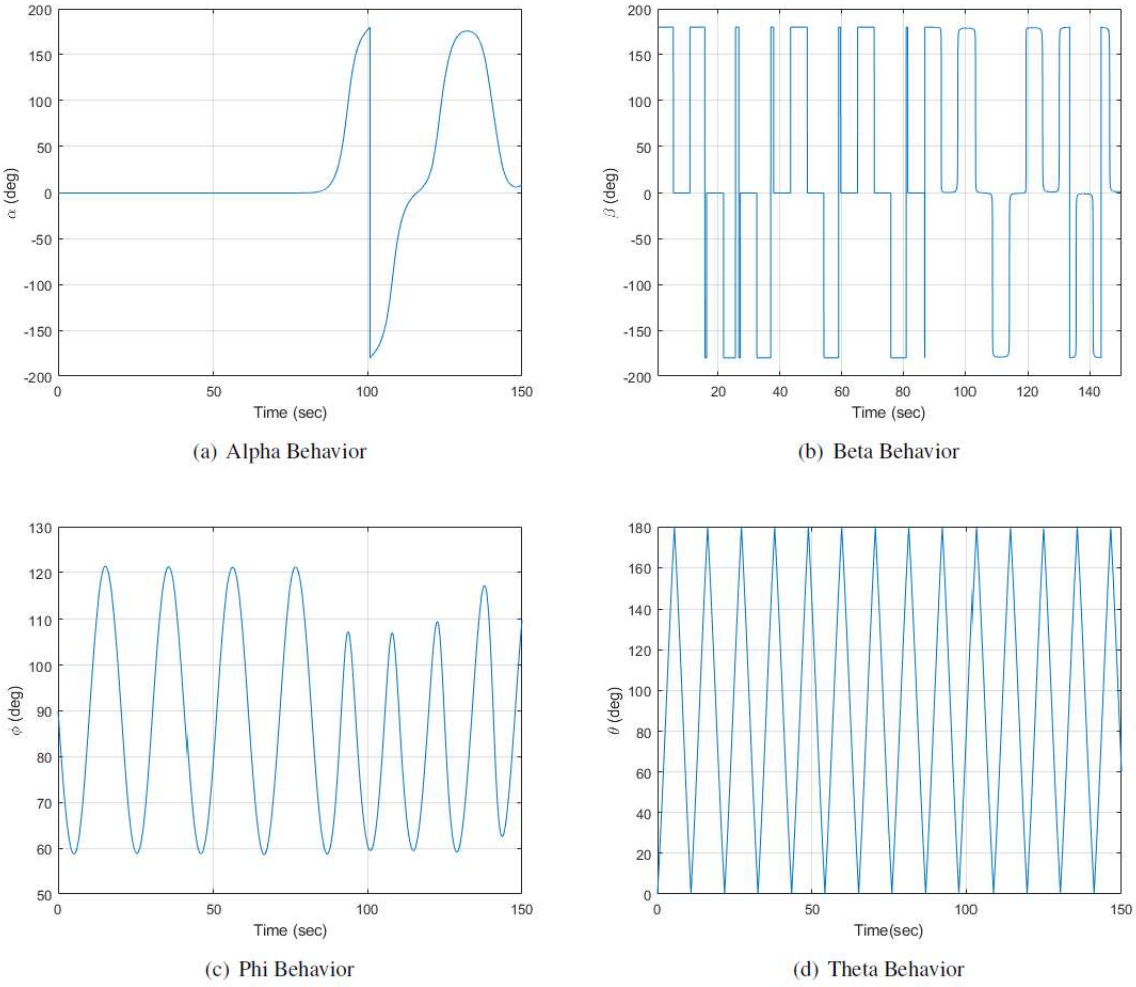

Figure 6.10 Open-Loop Perpendicular Simulation for 3D Case

Figure 6.10 shows some very interesting behavior. Initially, the deputy spins about its $\hat{\jmath}$ axis purely, but around 90 seconds, it begins to develop a slight motion about the reference $\hat{X}$ axis, which is visible in the β plot. Prior to this, the β variations on the plot were artifacts of the attitude representation, as mentioned previously. The chief spacecraft shows more interesting dynamics, overall. Due to electrostatic interactions with the spinning deputy, its motion shows oscillation, rather than simple spinning. This occurs fairly consistently until about 90 seconds, at which point interactions with the

deputy induce motion in the chief's α response, which leads to corresponding changes in the chief's φ response.

6.2.2. Equilibrium States

Using Equation (24), several equilibrium states have been found for this system. Here, we will present two cases. In the first case, the two spacecraft have initial attitude $[\alpha \quad \varphi]^T = \left[0 \quad \frac{\pi}{4}\right]^T$ radians and $[\beta \quad \theta]^T = \left[0 \quad \frac{\pi}{4}\right]^T$ radians, and are set to rotate together about the $\hat{Z}$ axis with an angular speed of 10 deg/sec.

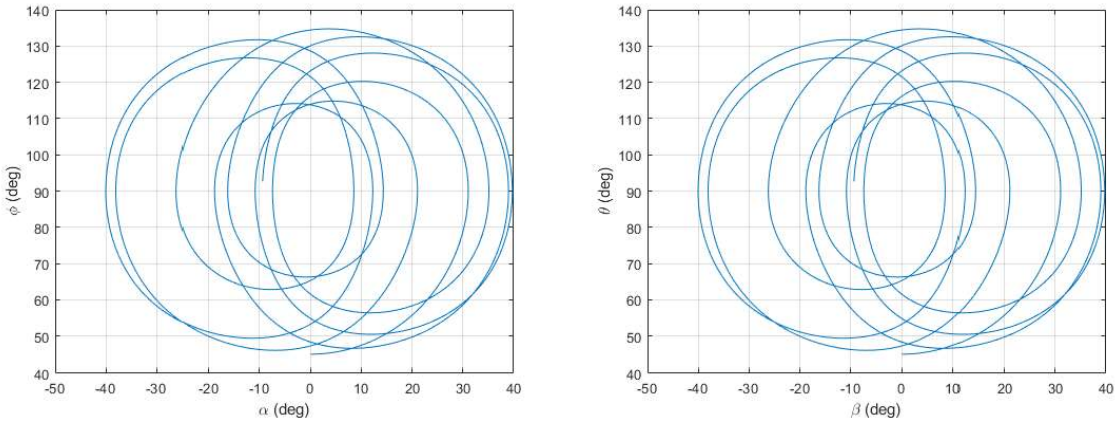

(a) Equilibrium Response of Chief Spacecraft

(b) Equilibrium Response of Deputy Spacecraft

Figure 6.11 First Equilibrium State

As can be seen from Figure 6.11, the two spacecraft's attitudes oscillate with an identical pattern. This shows that, with this starting state, they maintain the same relative attitude and relative angular velocity. Therefore, the relative system experiences an equilibrium here.

The second equilibrium state that will be presented is with the two spacecraft at starting attitudes $[\alpha \quad \varphi]^T = \left[0 \quad \frac{\pi}{3}\right]^T$ radians and $[\beta \quad \theta]^T = \left[0 \quad \frac{\pi}{3}\right]^T$ radians. Their

initial angular velocities are both 30 deg/sec about the $\hat{X}$ axis.

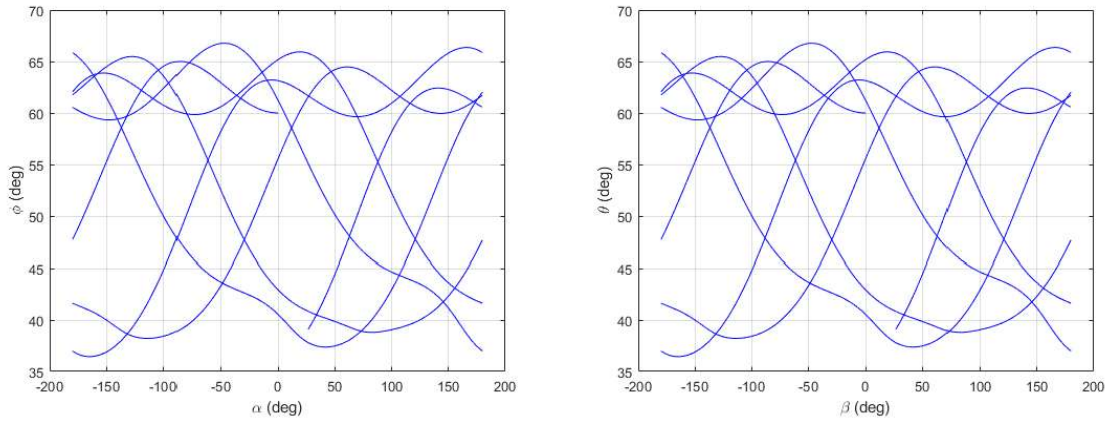

(a) Equilibrium Response of Chief Spacecraft

(b) Equilibrium Response of Deputy Spacecraft

Figure 6.12 Second Equilibrium State

While the equilibrium condition shown in Figure 6.12 is certainly more chaotic for the individual spacecraft than the previous one, the point must be made again that their behavior is identical, which therefore shows that the relative system experiences equilibrium at this condition. Note that, for this equilibrium plot, all the lines represent a single simulation case. Horizontal lines showing the first-axis rotation angles crossing 180 degrees have been removed for clarity.

6.2.3. Closed-Loop Behavior

The closed-loop system is here simulated for a simple case, with the attitude of the chief held fixed at $[\alpha \quad \varphi]^T = \left[0 \quad \frac{\pi}{2}\right]^T$. This attitude is assumed to be maintained by a traditional attitude control system, using either reaction wheels or attitude thrusters. Meanwhile, the deputy spacecraft is simulated with the controller mentioned above. The simulation is conducted with the deputy spacecraft having an initial attitude vector of

$[\beta \quad \theta]^T = \left[\frac{-5\pi}{9} \quad \frac{\pi}{4}\right]^T$ radians, and an initial angular velocity of $\vec{\omega}_{CD} = \left[0 \quad \frac{\pi}{36} \quad \frac{\pi}{36}\right]^T$ radians per second. The geometric parameters and equilibrium charges for this simulation are the same as those used above. The nonlinear controller given in Equation (36) is applied to the system, using the h function $h(\Phi_{CD}) = 0.8sin^2(\Phi_{CD}^2)$. The resulting simulation output is shown in Figure 6.14.

6.2.4. Actuator Dynamics

Finally, the actuator dynamics for the closed-loop simulation presented above were simulated. This was done by taking the state history from the above simulation and using it as input to Equations (42) and (43) to plot the required electrostatic charges to achieve the control torques that created that state trajectory presented above. For this simulation, the electrostatic charges on the chief spacecraft, as well as the free electrostatic charge on the deputy spacecraft (q_b), were set to the usual value of 1 mC. The results of this simulation are presented in Figure 6.13.

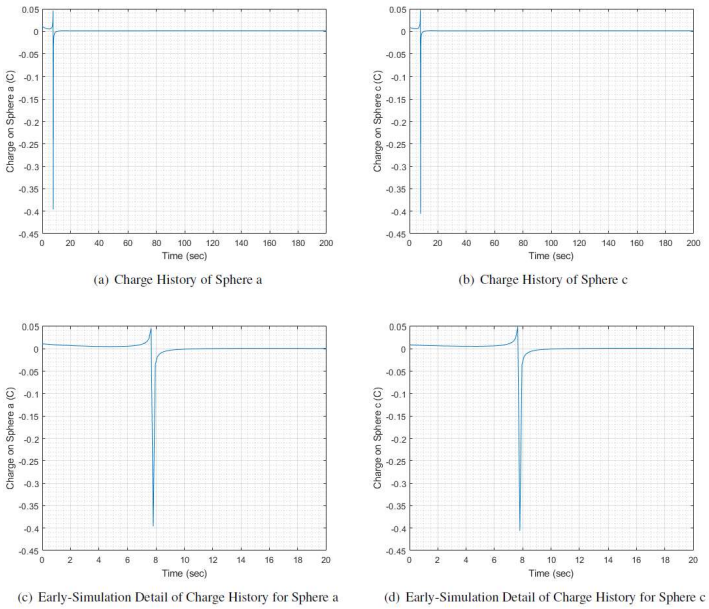

Figure 6.13 Charge History of Sphere a and Sphere c for Closed-Loop 3D Case

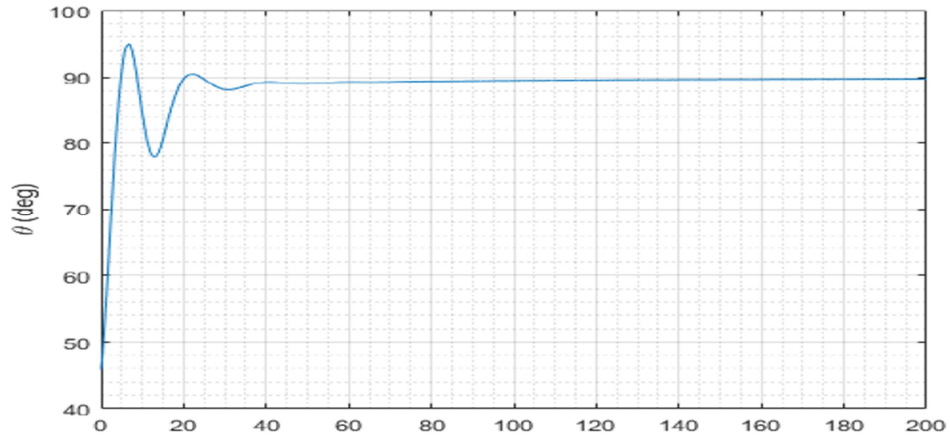

(a) Theta Behavior

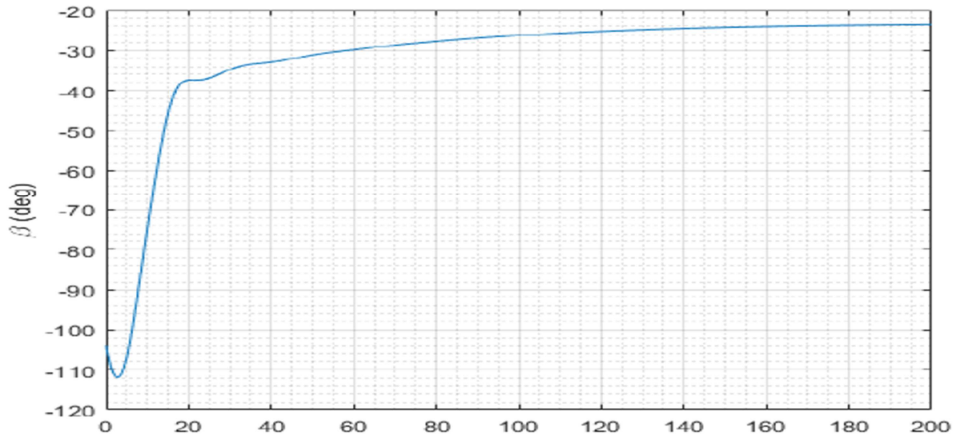

(b) Beta Behavior

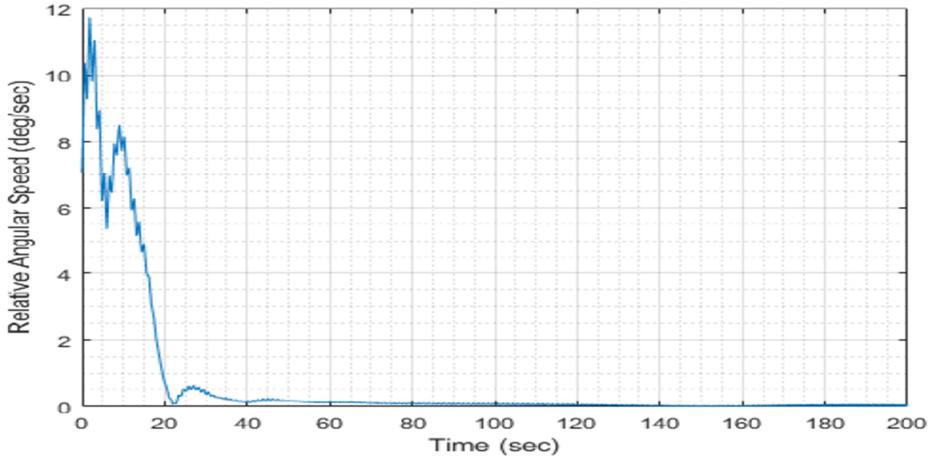

(c) Angular Speed Behavior

Figure 6.14 Closed-Loop Simulation for 3D Case

Figure 6.13 shows that, overall, the responses of the two charges for this case are very similar. However, a closer inspection of the plots will reveal a few salient differences. First, sphere c shows a much flatter curve at the beginning of the simulation than sphere a does, while sphere a has flatter post-spike behavior than sphere c does. Additionally, while the difference in each sphere's positive spike, at about 7.6 sec, is quite small, the difference in their negative spikes, at about 7.9 sec, is a bit larger. Sphere c reaches about -0.405 C at the bottom of its negative spike, while sphere a reaches only -0.395 C. It is worth noting from both plots that the majority of the control effort is spent in a very small time interval, in the two seconds containing the spikes, with the rest of the simulation having much more moderate changes in the required charge dynamics. Comparing with Figure 6.14, this seems to be associated with arresting the initial overshoot of the θ angle of the deputy spacecraft. After this point, the spacecraft control is accomplished with far smaller charge values and far less variation in them, with the charges eventually settling close to their equilibrium value of 1 mC.

To determine the practicality of these actuator dynamics, it is most important to analyze the greatest change in the required charge in the lowest time. That is to say, the spikes at 7.5 s to 8 s. To achieve the large drop in charge required of sphere a, the charge must change at a rate of -2.9878 $\frac{C}{s}$, or -2.9878 A. Sphere c requires a charge change rate of -3.0655 A. Considering the actuation system to be a beam of charged particles, as in (Schaub & Stevenson, 2013), this may be unattainable. High-powered laboratory-grade electron guns can achieve this level of power, but the size and complexity of these devices make them unusable for this application (Pikin, Beebe, & Raparia, 2013). Most more compact electron guns have emission currents in the range of a few hundred mA

(Lee, Kim, Ghergherehchi, et al., 2014). However, another method to impart the necessary charges, a less aggressive control law, or more optimal initial conditions for the case may ameliorate this problem.

7. Conclusion and Future Work

The information presented in this thesis show that the system under consideration, under the given assumptions, is controllable. A collection of several different control laws has been presented, both for the case when the spacecraft rotations are constrained to the plane of the two craft, and for the case when they are allowed to freely rotate in three dimensions. The controllers demonstrate that stabilization of the system can be achieved in reasonable times, with the longest taking about two minutes. While performance of these controllers is not yet optimal, their utility toward stabilizing the system is well demonstrated. Finally, analysis was shown to demonstrate one of the practical requirements of one of these controllers for use by determining the dynamics that the controller would require of the system's actuators: the surface charges of the discretized regions of the spacecraft's outer surface.

This analysis shows that, overall, the charges required to implement this control law are not exceptionally large for most of the simulation presented; mostly varying in a small neighborhood of the equilibrium charge values. However, the nimble dynamics required in earlier portions of the flight merit further investigation before this control system can be implemented on a real-world system, as the required beam current for charging with electron beams is currently too high.

Future work may also consider optimizing the performance of the presented controllers, or finding others whose performance is naturally better for this system, requiring less aggressive actuator dynamics. Additionally, further studies may wish to extend this research into the case where a larger formation of spacecraft is investigated, making fuller use of the swarm-controller introduced for the 3D Case, or finding a

higher-performing controller for this expanded system. Finally, when the attitude control system is more mature, future work should investigate the coupling effects between translational and rotational motion control using the electrostatic actuator, allowing all six degrees of freedom of each spacecraft to be controlled for a large formation.

REFERENCES

Aslanov, V., & Schaub, H., (2019). Detumbling attitude control analysis considering an electrostatic pusher configuration, *Journal of Guidance, Control, and Dynamics*, Vol. 42, Issue 4, pp. 900-909

Aslanov, V., & Yudintsev, V., (2018). Motion control of space tug during debris removal by a coulomb force, *Journal of Guidance, Control, and Dynamics*, Vol. 41, Issue 7, pp. 1476–1484. DOI:10.2514/1.G003251

Bennett, T., & Schaub, H., (2015). Touchless electrostatic three-dimensional detumbling of large axi-symmetric debris, *AAS Journal of the Astronautical Sciences*, Vol. 62, pp. 233-253

Bennett, T., & Schaub, H., (2018). Contactless electrostatic detumbling of axi-symmetric GEO objects with nominal pushing or pulling, *Advances in Space Research*, Vol. 62, Issue 11, pp. 2977-2987

Curtis, H. D., (2005). *Orbital mechanics for engineering students.* Ch. 9, ERAU.

Desoer and Callier, (1990). *Linear system theory*. Pp. 231-232, Springer.

Galjanic, J., Seo, D., & Nazari, M. (2019). Relative attitude regulation control using electrostatic torques and cylindrical models. *Proceedings of the 2019 AAS/AIAA astrodynamics specialist conference*, pp. 4125-4136.

Galjanic, J., & Seo, D., (2020). 3D attitude synchronization control with coulomb interactions, *Proceedings of the 2020 AAS/AIAA astrodynamics specialist conference*

Hespanha, J., (2009). *Linear system theory.* Pp. 101-102, Princeton University Press.

Hogan, E., & Schaub, H., (2013). Relative motion control for two-spacecraft electrostatic orbit corrections, *Journal of Guidance, Control, and Dynamics*, Vol. 36, Issue 1, pp. 240–249. DOI:10.2514/1.56118

Lee, J., Kim, H., Ghergherehchi, M., Shin, S., Lee, Y., & Yeon, Y., (2014). Design and analysis of an electron beam in an electron gun for x-ray radiotherapy. *Proceedings of the 5th international particle accelerator conference,* DOI: 10.18429/JACoW-IPAC2014-MOPRI040

National Aeronautics and Space Administration, Jet Propulsion Laboratory, (n.d.). Precision formation flying. *Office of the Chief Scientist and Chief Technologist*. Retrieved from https://scienceandtechnology.jpl.nasa.gov/precision-formation-flying

Pikin, A., Beebe, E., & Raparia, D., (2013). Simulation and optimization of a 10 A electron gun with electrostatic compression for the electron beam ion source. *Review of Scientific Instruments*, Vol. 84, Issue 3.

Rugh W., (1996). Linear system theory, 2nd ed. Ch.9, Prentice Hall

Schaub, H., & Stevenson, D., (2013). Prospects of relative attitude control using coulomb actuation, *AAS Journal of the Astronautical Sciences*, Vol. 60, pp. 258–277.

Song, W., Tang, Y., Hong, Y., & Hu, X. (2017). Relative attitude formation control of multi-agent systems, *International Journal of Robust and Nonlinear Control,* Vol. 27, Issue 18.

Stevenson, D., & Schaub, H., (2013). Multi-sphere method for modeling spacecraft electrostatic forces and torques, *Advances in Space Research*, Vol. 51, Issue 1, pp. 10-20.

Wie, B. (2008). *Space vehicle dynamics and control: 2nd ed.* Ch.1. AIAA, DOI: 10.2514/4.860119

APPENDIX A – DERIVATION OF TORQUE EXPRESSIONS FOR 2D CASE

In order to derive the total electrostatic torque on one of the spacecraft in this study, we must start from Equation (15), the expression for the electrostatic torque about one body due to the interactions between a charged region on it and another charged region off of it. This equation is reproduced here for convenience.

$$\vec{M}_G = \vec{r}_{G2} \times \frac{k_C q_1 q_2 \hat{r}_{12}}{\|\vec{r}_{12}\|^2}$$

Note that, in this equation, 1 and 2 do not yet refer to the charged regions in our particular system, but instead refer to two general electrostatically-charged regions that are interacting, with G denoting the center of mass of the rotating body. In order to use this equation for this system, it must be summed, twice, over the set of electrostatically charged interacting regions in the system. For instance, for the deputy spacecraft, the regions indicated as 1 in Equation (15) are the spheres on the chief spacecraft and the regions indicated as 2 are the spheres on the deputy spacecraft. Also, G is the center of sphere b for the deputy.

Taking this double-sum, the following equation results.

$$\vec{M}_D = k_C \sum_{n=a}^{c} q_n \sum_{v=1}^{3} \frac{q_v}{\|\vec{r}_{v,n}\|^3} \vec{r}_{b,n} \times \vec{r}_{v,n} \tag{44}$$

where $n \in \{a \quad b \quad c\}$ is the set of spheres on the deputy spacecraft, $v \in \{1 \quad 2 \quad 3\}$ is the set of spheres on the chief spacecraft, and the vectors follow the conventions established in Chapter 3. Once this equation is expanded, the following expression results.

$$\vec{M}_D = k_C \left(\frac{q_1 q_a (\vec{r}_{b,a} \times \vec{r}_{1,a})}{\|\vec{r}_{1,a}\|^3} + \frac{q_1 q_b (\vec{r}_{b,b} \times \vec{r}_{1,b})}{\|\vec{r}_{1,b}\|^3} + \frac{q_1 q_c (\vec{r}_{b,c} \times \vec{r}_{1,c})}{\|\vec{r}_{1,c}\|^3} + \frac{q_2 q_a (\vec{r}_{b,a} \times \vec{r}_{2,a})}{\|\vec{r}_{2,a}\|^3} + \frac{q_2 q_b (\vec{r}_{b,b} \times \vec{r}_{2,b})}{\|\vec{r}_{2,b}\|^3} + \frac{q_2 q_c (\vec{r}_{b,c} \times \vec{r}_{2,c})}{\|\vec{r}_{2,c}\|^3} + \frac{q_3 q_a (\vec{r}_{b,a} \times \vec{r}_{3,a})}{\|\vec{r}_{3,a}\|^3} + \frac{q_3 q_b (\vec{r}_{b,b} \times \vec{r}_{3,b})}{\|\vec{r}_{3,b}\|^3} + \frac{q_3 q_c (\vec{r}_{b,c} \times \vec{r}_{3,c})}{\|\vec{r}_{3,c}\|^3} \right) \quad (45)$$

Take note that, in this equation, the terms involving sphere b will go to zero, since $\vec{r}_{b,b}$ is the zero vector. Taking this into account, the following terms remain.

$$\vec{M}_D = k_C \left(\frac{q_1 q_a (\vec{r}_{b,a} \times \vec{r}_{1,a})}{\|\vec{r}_{1,a}\|^3} + \frac{q_1 q_c (\vec{r}_{b,c} \times \vec{r}_{1,c})}{\|\vec{r}_{1,c}\|^3} + \frac{q_2 q_a (\vec{r}_{b,a} \times \vec{r}_{2,a})}{\|\vec{r}_{2,a}\|^3} + \frac{q_2 q_c (\vec{r}_{b,c} \times \vec{r}_{2,c})}{\|\vec{r}_{2,c}\|^3} + \frac{q_3 q_a (\vec{r}_{b,a} \times \vec{r}_{3,a})}{\|\vec{r}_{3,a}\|^3} + \frac{q_3 q_c (\vec{r}_{b,c} \times \vec{r}_{3,c})}{\|\vec{r}_{3,c}\|^3} \right) \quad (46)$$

Thus, constructing the torque expression becomes a simple matter of evaluating the position vector expressions in Equation (46). This requires expressions for the relative position vectors between the spheres. Taken in reference coordinates and using the kinematic angles θ and φ, the position of each sphere relative to sphere 2 is given by the following.

$$\vec{r}_1 = \begin{bmatrix} l\cos\varphi \\ 0 \\ l\sin\varphi \end{bmatrix}, \qquad \vec{r}_2 = \begin{bmatrix} 0 \\ 0 \\ 0 \end{bmatrix}, \qquad \vec{r}_3 = \begin{bmatrix} -l\cos\varphi \\ 0 \\ -l\sin\varphi \end{bmatrix}$$

$$\vec{r}_a = \begin{bmatrix} d + l\cos\theta \\ 0 \\ l\sin\theta \end{bmatrix}, \ \vec{r}_b = \begin{bmatrix} d \\ 0 \\ 0 \end{bmatrix}, \ \vec{r}_c = \begin{bmatrix} d - l\cos\theta \\ 0 \\ -l\sin\theta \end{bmatrix} \quad (47)$$

Verifying these position vectors is left as an exercise for the reader. The relative position vectors between the charge-carrying spheres are then constructed by subtraction:

$$\vec{r}_{1,a} = \begin{bmatrix} d + l\cos\theta - l\cos\varphi \\ 0 \\ l\sin\theta - l\sin\varphi \end{bmatrix}, \qquad \vec{r}_{1,c} = \begin{bmatrix} d - l\cos\theta - l\cos\varphi \\ 0 \\ -l\sin\theta - l\sin\varphi \end{bmatrix}$$

$$\vec{r}_{3,a} = \begin{bmatrix} d + l\cos\theta + l\cos\varphi \\ 0 \\ l\sin\theta + l\sin\varphi \end{bmatrix}, \qquad \vec{r}_{3,c} = \begin{bmatrix} d - l\cos\theta + l\cos\varphi \\ 0 \\ -l\sin\theta + l\sin\varphi \end{bmatrix}$$

$$\vec{r}_{2,a} = \begin{bmatrix} d + l\cos\theta \\ 0 \\ l\sin\theta \end{bmatrix}, \qquad \vec{r}_{2,c} = \begin{bmatrix} d - l\cos\theta \\ 0 \\ -l\sin\theta \end{bmatrix}, \qquad \vec{r}_{b,a} = \begin{bmatrix} l\cos\theta \\ 0 \\ l\sin\theta \end{bmatrix}$$

$$\vec{r}_{b,c} = \begin{bmatrix} -l\cos\theta \\ 0 \\ -l\sin\theta \end{bmatrix} \tag{48}$$

Note that, not all relative position vectors were necessary to construct; only those that appear in Equation (46). Two operations must be conducted with these position vectors: certain ones' magnitudes must be computed and the cross products of certain pairs must be computed. First, we will compute the magnitudes, shown below.

$$\left\|\vec{r}_{1,a}\right\| = \sqrt{(d + l\cos\theta - l\cos\varphi)^2 + (l\sin\theta - l\sin\varphi)^2}$$

$$\left\|\vec{r}_{2,a}\right\| = \sqrt{(d - l\cos\theta)^2 + (-l\sin\theta)^2}$$

$$\left\|\vec{r}_{3,a}\right\| = \sqrt{(d + l\cos\theta + l\cos\varphi)^2 + (l\sin\theta + l\sin\varphi)^2}$$

$$\left\|\vec{r}_{1,c}\right\| = \sqrt{(d - l\cos\theta - l\cos\varphi)^2 + (-l\sin\theta - l\sin\varphi)^2}$$

$$\left\|\vec{r}_{2,c}\right\| = \sqrt{(d - l\cos\theta)^2 + (-l\sin\theta)^2}$$

$$\left\|\vec{r}_{3,c}\right\| = \sqrt{(d - l\cos\theta + l\cos\varphi)^2 + (-l\sin\theta + l\sin\varphi)^2} \tag{49}$$

Note that, since vector magnitudes are invariant under frame transformation, taking the magnitudes from the vectors' reference frame expressions is valid for our purposes. Similarly, the reference frame expression can be used for the cross products to construct a body-fixed frame torque expression in the special case represented by this system. Since the $\hat{Y}$, $\hat{J}$, and $\hat{\jmath}$ vectors are always parallel for the 2D Case, and noting that all of the

relative position vectors have zero second-axis component, all cross products will result in vectors whose only nonzero component is the second-axis component. Since the second axes of all three coordinate frames in this study are assumed to align for the 2D Case, these cross products are valid for any of these frames. Thus, the cross products are evaluated to be the following, using the substitution $\varepsilon = \theta - \varphi$.

$$\vec{r}_{b,a} \times \vec{r}_{1,a} =$$

$$\begin{bmatrix} 0 \\ dl\ sin\ \theta + l^2 sin\ \theta\ cos\ \theta - l^2 sin\ \theta\ cos\ \varphi - l^2 sin\ \theta\ cos\ \theta + l^2 cos\ \theta\ sin\ \varphi \\ 0 \end{bmatrix} =$$

$$\begin{bmatrix} 0 \\ dl\ sin\ (\varepsilon + \varphi) - l^2 sin\ \varepsilon \\ 0 \end{bmatrix}$$

$$\vec{r}_{b,a} \times \vec{r}_{3,a} =$$

$$\begin{bmatrix} 0 \\ dl\ sin\ \theta + l^2 sin\ \theta\ cos\ \theta + l^2 sin\ \theta\ cos\ \varphi - l^2 sin\ \theta\ cos\ \theta - l^2 cos\ \theta\ sin\ \varphi \\ 0 \end{bmatrix} =$$

$$\begin{bmatrix} 0 \\ dl\ sin\ (\varepsilon + \varphi) + l^2 sin\ \varepsilon \\ 0 \end{bmatrix}$$

$$\vec{r}_{b,a} \times \vec{r}_{2,a} = \begin{bmatrix} 0 \\ dl\ sin\ \theta + l^2 sin\ \theta\ cos\ \theta - l^2 sin\ \theta\ cos\ \theta \\ 0 \end{bmatrix} = \begin{bmatrix} 0 \\ dl\ sin\ (\varepsilon + \varphi) \\ 0 \end{bmatrix}$$

$$\vec{r}_{b,c} \times \vec{r}_{1,c} =$$

$$\begin{bmatrix} 0 \\ -dl\ sin\ \theta + l^2 sin\ \theta\ cos\ \theta + l^2 sin\ \theta\ cos\ \varphi - l^2 sin\ \theta\ cos\ \theta - l^2 cos\ \theta\ sin\ \varphi \\ 0 \end{bmatrix} =$$

$$\begin{bmatrix} 0 \\ -dl\ sin\ (\varepsilon + \varphi) + l^2 sin\ \varepsilon \\ 0 \end{bmatrix}$$

$$\vec{r}_{b,c} \times \vec{r}_{3,c} =$$

$$\begin{bmatrix} 0 \\ -dl\ sin\ \theta + l^2 sin\ \theta\ cos\ \theta - l^2 sin\ \theta\ cos\ \varphi - l^2 sin\ \theta\ cos\ \theta + l^2 cos\ \theta\ sin\ \varphi \\ 0 \end{bmatrix} =$$

$$\begin{bmatrix} 0 \\ -dl\ sin\ (\varepsilon + \varphi) - l^2 sin\ \varepsilon \\ 0 \end{bmatrix}$$

$$\vec{r}_{b,c} \times \vec{r}_{2,c} = \begin{bmatrix} 0 \\ -dl\ sin\ \theta + l^2 sin\ \theta\ cos\ \theta - l^2 sin\ \theta\ cos\ \theta \\ 0 \end{bmatrix} = \begin{bmatrix} 0 \\ -dl\ sin\ (\varepsilon + \varphi) \\ 0 \end{bmatrix} \quad (50)$$

With these terms computed, the final electrostatic torque expression for the deputy spacecraft is found by substituting Equations (49) and (50) into Equation (46). This results in Equation (19) from the main thesis. Treating the single nonzero component of the vector torque as a scalar, it is denoted L_D.

To derive the equivalent equation for the chief spacecraft, it is necessary to reverse the double-sum in Equation (44), this time treating the spheres of the deputy spacecraft as the first interacting object and the spheres of the chief as the second interacting object. This is given by the following expression.

$$\vec{M}_C = k_C \sum_{v=1}^{3} q_v \sum_{n=a}^{c} \frac{q_n}{\|\vec{r}_{n,v}\|^3} \vec{r}_{2,v} \times \vec{r}_{n,v} \quad (51)$$

Which, when expanded, gives the following expression.

$$\vec{M}_C = k_C \left(\frac{q_1 q_a (\vec{r}_{2,1} \times \vec{r}_{a,1})}{\|\vec{r}_{a,1}\|^3} + \frac{q_1 q_b (\vec{r}_{2,1} \times \vec{r}_{b,1})}{\|\vec{r}_{b,1}\|^3} + \frac{q_1 q_c (\vec{r}_{2,1} \times \vec{r}_{c,1})}{\|\vec{r}_{c,1}\|^3} + \frac{q_2 q_a (\vec{r}_{2,2} \times \vec{r}_{a,2})}{\|\vec{r}_{a,2}\|^3} \right.$$

$$\left. + \frac{q_2 q_b (\vec{r}_{2,2} \times \vec{r}_{b,2})}{\|\vec{r}_{b,2}\|^3} + \frac{q_2 q_c (\vec{r}_{2,2} \times \vec{r}_{c,2})}{\|\vec{r}_{c,2}\|^3} + \frac{q_3 q_a (\vec{r}_{2,3} \times \vec{r}_{a,3})}{\|\vec{r}_{a,3}\|^3} + \frac{q_3 q_b (\vec{r}_{2,3} \times \vec{r}_{b,3})}{\|\vec{r}_{b,3}\|^3} + \frac{q_3 q_c (\vec{r}_{2,3} \times \vec{r}_{c,3})}{\|\vec{r}_{c,3}\|^3} \right) \quad (52)$$

Like its deputy counterpart, several terms in this equation go to zero, due to the presence of the zero vector $\vec{r}_{2,2}$. Removing these, we are left with:

$$\vec{M}_C = k_C \left(\frac{q_1 q_a (\vec{r}_{2,1} \times \vec{r}_{a,1})}{\|\vec{r}_{a,1}\|^3} + \frac{q_1 q_b (\vec{r}_{2,1} \times \vec{r}_{b,1})}{\|\vec{r}_{b,1}\|^3} + \frac{q_1 q_c (\vec{r}_{2,1} \times \vec{r}_{c,1})}{\|\vec{r}_{c,1}\|^3} + \frac{q_3 q_a (\vec{r}_{2,3} \times \vec{r}_{a,3})}{\|\vec{r}_{a,3}\|^3} + \frac{q_3 q_b (\vec{r}_{2,3} \times \vec{r}_{b,3})}{\|\vec{r}_{b,3}\|^3} + \frac{q_3 q_c (\vec{r}_{2,3} \times \vec{r}_{c,3})}{\|\vec{r}_{c,3}\|^3} \right) \tag{53}$$

To finish deriving the chief spacecraft's electrostatic torque expression, we must, once again, evaluate these position vector expressions. These can be done using the same vectors presented in Equation (47). The required relative position vectors can then be constructed by subtraction, as before.

$$\vec{r}_{a,1} = \begin{bmatrix} -d - l\cos\theta + l\cos\varphi \\ 0 \\ -l\sin\theta + l\sin\varphi \end{bmatrix}, \quad \vec{r}_{c,1} = \begin{bmatrix} -d + l\cos\theta + l\cos\varphi \\ 0 \\ l\sin\theta + l\sin\varphi \end{bmatrix}$$

$$\vec{r}_{a,3} = \begin{bmatrix} -d - l\cos\theta - l\cos\varphi \\ 0 \\ -l\sin\theta - l\sin\varphi \end{bmatrix}, \quad \vec{r}_{c,3} = \begin{bmatrix} -d + l\cos\theta - l\cos\varphi \\ 0 \\ l\sin\theta - l\sin\varphi \end{bmatrix}$$

$$\vec{r}_{b,1} = \begin{bmatrix} -d + l\cos\varphi \\ 0 \\ l\sin\varphi \end{bmatrix}, \quad \vec{r}_{b,3} = \begin{bmatrix} -d - l\cos\varphi \\ 0 \\ -l\sin\varphi \end{bmatrix}, \quad \vec{r}_{2,1} = \begin{bmatrix} l\cos\varphi \\ 0 \\ l\sin\varphi \end{bmatrix}$$

$$\vec{r}_{2,3} = \begin{bmatrix} -l\cos\varphi \\ 0 \\ -l\sin\varphi \end{bmatrix} \tag{54}$$

For evaluating the required vector magnitudes, there is a bit of material that we can reuse from the deputy derivation. Namely, since the vectors $\vec{r}_{a,1}$, $\vec{r}_{c,1}$, $\vec{r}_{a,3}$, and $\vec{r}_{c,3}$ are the exact negatives of vectors $\vec{r}_{1,a}$, $\vec{r}_{1,c}$, $\vec{r}_{3,a}$, and $\vec{r}_{3,c}$, respectively, the magnitude expressions of the latter may be used in place of those of the former. This is because vector

magnitude is independent of vector orientation. Thus, the remaining magnitudes to compute can be evaluated as the following.

$$\left\|\vec{r}_{b,1}\right\| = \sqrt{(-d + l\,cos\,\varphi)^2 + (l\,sin\,\varphi)^2}$$

$$\left\|\vec{r}_{b,3}\right\| = \sqrt{(-d - l\,cos\,\varphi)^2 + (-l\,sin\,\varphi)^2} \tag{55}$$

Finally, the cross product terms must be computed. For the same reason as described above for the deputy spacecraft, this can be done on with the vectors as they are, without transformation. The resulting terms are as follows.

$$\vec{r}_{2,1} \times \vec{r}_{a,1} =$$

$$\begin{bmatrix} 0 \\ -ld\,\sin\varphi\ - l^2 sin\,\varphi\,cos\,\theta + l^2 sin\,\varphi\,cos\,\varphi + l^2 cos\,\varphi\,sin\,\theta - l^2 sin\,\varphi\,cos\,\varphi \\ 0 \end{bmatrix} =$$

$$\begin{bmatrix} 0 \\ -ld\,\sin\varphi + l^2 sin\,\varepsilon \\ 0 \end{bmatrix}$$

$$\vec{r}_{2,1} \times \vec{r}_{c,1} =$$

$$\begin{bmatrix} 0 \\ -ld\,\sin\varphi\ + l^2 sin\,\varphi\,cos\,\theta + l^2 sin\,\varphi\,cos\,\varphi - l^2 cos\,\varphi\,sin\,\theta - l^2 sin\,\varphi\,cos\,\varphi \\ 0 \end{bmatrix} =$$

$$\begin{bmatrix} 0 \\ -ld\,\sin\varphi - l^2 sin\,\varepsilon \\ 0 \end{bmatrix}$$

$$\vec{r}_{2,1} \times \vec{r}_{b,1} = \begin{bmatrix} 0 \\ -ld\,\sin\varphi\ + l^2 sin\,\varphi\,cos\,\varphi - l^2 sin\,\varphi\,cos\,\varphi \\ 0 \end{bmatrix} = \begin{bmatrix} 0 \\ -ld\,\sin\varphi \\ 0 \end{bmatrix}$$

$$\vec{r}_{2,3} \times \vec{r}_{a,3} =$$

$$\begin{bmatrix} 0 \\ ld \sin\varphi \ + l^2 sin\,\varphi\, cos\,\theta + l^2 sin\,\varphi\, cos\,\varphi - l^2 cos\,\varphi\, sin\,\theta - l^2 sin\,\varphi\, cos\,\varphi \\ 0 \end{bmatrix} =$$

$$\begin{bmatrix} 0 \\ ld \sin\varphi - l^2 sin\,\varepsilon \\ 0 \end{bmatrix}$$

$$\vec{r}_{2,3} \times \vec{r}_{c,3} =$$

$$\begin{bmatrix} 0 \\ ld \sin\varphi \ - l^2 sin\,\varphi\, cos\,\theta + l^2 sin\,\varphi\, cos\,\varphi + l^2 cos\,\varphi\, sin\,\theta - l^2 sin\,\varphi\, cos\,\varphi \\ 0 \end{bmatrix} =$$

$$\begin{bmatrix} 0 \\ ld \sin\varphi + l^2 sin\,\varepsilon \\ 0 \end{bmatrix}$$

$$\vec{r}_{2,3} \times \vec{r}_{b,3} = \begin{bmatrix} 0 \\ ld \sin\varphi \ + l^2 sin\,\varphi\, cos\,\varphi - l^2 sin\,\varphi\, cos\,\varphi \\ 0 \end{bmatrix} = \begin{bmatrix} 0 \\ ld \sin\varphi \\ 0 \end{bmatrix} \qquad (56)$$

Finally, Equations (49), (55), and (56) are substituted into Equation (53) to derive the electrostatic torque expression for the chief spacecraft, given as Equation (20) in the main draft. Treating the single nonzero component of the vector torque as a scalar, it is denoted L_C.

APPENDIX B – DERIVATION OF OPEN-LOOP DYNAMICS FOR 2D CASE

Using the electrostatic torque expressions derived in Appendix A, it is now a simple matter to derive the open-loop dynamics of the 2D Case system. Taking the nonzero components of the torque vectors $\vec{M}_D$ and $\vec{M}_C$ as L_D and L_C, respectively, the dynamics of the two spacecraft, rotating in a single plane, can be written as the following.

$$L_D = I_t\ddot{\theta}, \quad L_C = I_t\ddot{\varphi} \tag{57}$$

recalling that the two spacecraft's moments-of-inertia are identical, due to the assumption of identical construction. Additionally, note that, since the coordinate frame axes $\hat{Y}$, $\hat{J}$, and $\hat{\jmath}$ (which these equations are taken about) are always parallel for the 2D Case. This means that these equations can be added and subtracted directly.

Since it is desired to obtain an expression for the open-loop dynamics in terms of the relative attitude angle $\varepsilon = \theta - \varphi$, this is a useful property. Taking the time derivative of ε twice, we observe that $\ddot{\varepsilon} = \ddot{\theta} - \ddot{\varphi}$. Therefore, by rearranging Equation (57) and subtracting, the following results.

$$\ddot{\varepsilon} = \frac{L_D - L_C}{I_t} \tag{58}$$

To fully capture the system dynamics, they can be modelled in nonlinear state-space form as the following.

$$\vec{e} = \begin{bmatrix} \varepsilon \\ \dot{\varepsilon} \end{bmatrix}, \ \dot{\vec{e}} = \begin{bmatrix} \dot{\varepsilon} \\ \frac{L_D - L_C}{I_t} \end{bmatrix} = \begin{bmatrix} \dot{\varepsilon} \\ f(\varepsilon, \varphi) \end{bmatrix} \tag{59}$$

To fully expand this equation, Equations (19) and (20) must be substituted into

this state-space model. This results in the following expression.

$$f(\varepsilon,\varphi)=\frac{k_C}{I_t}\left(\frac{q_1q_a(dl\,sin\,(\varepsilon+\varphi)-2l^2sin\,\varepsilon+ld\,\sin\varphi)}{((d+l\,cos\,(\varepsilon+\varphi)-l\,cos\,\varphi)^2+(l\,sin\,(\varepsilon+\varphi)-l\,sin\,\varphi)^2)^{3/2}}\right.$$

$$+\frac{q_1q_c(-dl\,sin\,(\varepsilon+\varphi)+2l^2sin\,\varepsilon+ld\,\sin\varphi)}{((d-l\,cos\,(\varepsilon+\varphi)-l\,cos\,\varphi)^2+(-l\,sin\,(\varepsilon+\varphi)-l\,sin\,\varphi)^2)^{3/2}}$$

$$+\frac{q_2q_a(dl\,sin\,(\varepsilon+\varphi))}{((d-l\,cos\,(\varepsilon+\varphi))^2+(-l\,sin\,(\varepsilon+\varphi))^2)^{3/2}}$$

$$+\frac{q_2q_c(-dl\,sin\,(\varepsilon+\varphi))}{((d+l\,cos\,(\varepsilon+\varphi))^2+(-l\,sin\,(\varepsilon+\varphi))^2)^{3/2}}$$

$$+\frac{q_3q_a(dl\,sin\,(\varepsilon+\varphi)+2l^2sin\,\varepsilon-ld\,\sin\varphi)}{((d+l\,cos\,(\varepsilon+\varphi)+l\,cos\,\varphi)^2+(l\,sin\,(\varepsilon+\varphi)+l\,sin\,\varphi)^2)^{3/2}}$$

$$+\frac{q_3q_c(2l^2\,sin\,\varepsilon-ld\,sin\,\varphi-ld\,\sin\,(\varepsilon+\varphi))}{((d-l\,cos\,(\varepsilon+\varphi)+l\,cos\,\varphi)^2+(-l\,sin\,(\varepsilon+\varphi)+l\,sin\,\varphi)^2)^{3/2}}$$

$$-\frac{q_1q_b(-ld\,\sin\varphi)}{((-d+l\,cos\,\varphi)^2+(l\,sin\,\varphi)^2)^{3/2}}$$

$$\left.-\frac{q_3q_b(ld\,sin\,\varphi)}{((-d-l\,cos\,\varphi)^2+(-l\,sin\,\varphi)^2)^{3/2}}\right)$$

Which is Equation (21) from the main thesis.

APPENDIX C – LINEARIZATION OF OPEN-LOOP DYNAMICS FOR 2D CASE

The first step of using the controllers presented in this thesis for the 2D Case is to linearize the open-loop dynamics of the system. As described in Chapter 3, this is done by taking the Jacobian of the nonlinear state-space equation about the equilibrium point $\vec{e}_e = [0 \quad 0]^T$ and substituting the result into Equation (17). We start with the following definition.

$$\vec{f}(\vec{e}) = \begin{bmatrix} \dot{\varepsilon} \\ f(\varepsilon, \varphi) \end{bmatrix} \tag{60}$$

The Jacobian is then comprised of four partial derivatives, evaluated about the equilibrium state. These are the following.

$$\frac{\partial f_1}{\partial \varepsilon} = 0, \quad \frac{\partial f_1}{\partial \dot{\varepsilon}} = 1, \quad \frac{\partial f_2}{\partial \varepsilon} = g(\varphi), \quad \frac{\partial f_2}{\partial \dot{\varepsilon}} = 0 \tag{61}$$

Where the third partial derivative is given by the following.

$$\begin{aligned} g(\varphi) = \frac{k_C}{I_t}\Bigg(& \frac{q_{1,e}q_{a,e}(D_1N\prime_1 - N_1D\prime_1)}{((d+l\cos(\varepsilon+\varphi)-l\cos\varphi)^2+(l\sin(\varepsilon+\varphi)-l\sin\varphi)^2)^3} \\ & + \frac{q_{1,e}q_{c,e}(D_2N\prime_2 - N_2D\prime_2)}{((d-l\cos(\varepsilon+\varphi)-l\cos\varphi)^2+(-l\sin(\varepsilon+\varphi)-l\sin\varphi)^2)^3} + \frac{q_{2,e}q_{a,e}(D_3N\prime_3 - N_3D\prime_3)}{((d-l\cos(\varepsilon+\varphi))^2+(-l\sin(\varepsilon+\varphi))^2)^3} \\ & + \frac{q_{2,e}q_{c,e}(D_4N\prime_4 - N_4D\prime_4)}{((d+l\cos(\varepsilon+\varphi))^2+(-l\sin(\varepsilon+\varphi))^2)^3} + \frac{q_{3,e}q_{a,e}(D_5N\prime_5 - N_5D\prime_5)}{((d+l\cos(\varepsilon+\varphi)+l\cos\varphi)^2+(l\sin(\varepsilon+\varphi)+l\sin\varphi)^2)^3} \\ & + \frac{q_{3,e}q_{c,e}(D_6N\prime_6 - N_6D\prime_6)}{((d-l\cos(\varepsilon+\varphi)+l\cos\varphi)^2+(-l\sin(\varepsilon+\varphi)+l\sin\varphi)^2)^3} + \frac{q_{1,e}q_{b,e}(D_7N\prime_7 - N_7D\prime_7)}{((-d+l\cos\varphi)^2+(l\sin\varphi)^2)^3} \\ & + \frac{q_3q_b(D_8N\prime_8 - N_8D\prime_8)}{((-d-l\cos\varphi)^2+(-l\sin\varphi)^2)^3}\Bigg)\Bigg|_{\varepsilon=0} \end{aligned} \tag{62}$$

Where the *N* and *D* terms are defined by the following.

$$N_1 = dl\ sin\ (\varepsilon + \varphi) - 2l^2 sin\ \varepsilon + ld \sin \varphi$$

$$N'_1 = dl\ cos\ (\varepsilon + \varphi) - 2l^2 cos\ \varepsilon$$

$$D_1 = ((d + l\ cos\ (\varepsilon + \varphi) - l\ cos\ \varphi)^2 + (l\ sin\ (\varepsilon + \varphi) - l\ sin\ \varphi)^2)^{3/2}$$

$$D'_1 = 3\sqrt[3]{D_1}\big((l\ sin\ (\varepsilon + \varphi) - l\ sin\ \varphi) l\ cos\ (\varepsilon + \varphi) - (d + l\ cos\ (\varepsilon + \varphi) - l\ cos\ \varphi)\ l\ sin\ (\varepsilon + \varphi)\ \big)$$

$$N_2 = -dl\ sin\ (\varepsilon + \varphi) + 2l^2 sin\ \varepsilon + ld \sin \varphi$$

$$N'_2 = -ld\ cos\ (\varepsilon + \varphi) + 2\ l^2 cos\ \varepsilon$$

$$D_2 = ((d - l\ cos\ (\varepsilon + \varphi) - l\ cos\ \varphi)^2 + (-l\ sin\ (\varepsilon + \varphi) - l\ sin\ \varphi)^2)^{3/2}$$

$$D'_2 = 3\sqrt[3]{D_2}\big((d - l\ cos\ (\varepsilon + \varphi) - l\ cos\ \varphi)\ l\ sin\ (\varepsilon + \varphi) - (-l\ sin\ (\varepsilon + \varphi) - l\ sin\ \varphi)\ l\ cos\ (\varepsilon + \varphi)\big)$$

$$N_3 = dl\ sin\ (\varepsilon + \varphi)$$

$$N'_3 = ld\ cos\ (\varepsilon + \varphi)$$

$$D_3 = ((d - l\ cos\ (\varepsilon + \varphi))^2 + (-l\ sin\ (\varepsilon + \varphi))^2)^{3/2}$$

$$D'_3 = 3\sqrt[3]{D_3}\big((d - l\ cos\ (\varepsilon + \varphi))\ l\ sin\ (\varepsilon + \varphi) - (-l\ sin\ (\varepsilon + \varphi))\ l\ cos\ (\varepsilon + \varphi)\big)$$

$$N_4 = -dl\ sin\ (\varepsilon + \varphi)$$

$$N'_4 = -ld\ cos\ (\varepsilon + \varphi)$$

$$D_4 = ((d + l\ cos\ (\varepsilon + \varphi))^2 + (-l\ sin\ (\varepsilon + \varphi))^2)^{3/2}$$

$$D'_4 = 3\sqrt[3]{D_4}(-(d + l\ cos\ (\varepsilon + \varphi))\ l\ sin\ (\varepsilon + \varphi) - (-l\ sin\ (\varepsilon + \varphi))\ l\ cos\ (\varepsilon + \varphi))$$

$$N_5 = dl\ sin\ (\varepsilon + \varphi) + 2l^2 sin\ \varepsilon - ld \sin \varphi$$

$$N'_5 = ld\ cos\ (\varepsilon + \varphi) + 2\ l^2 cos\ \varepsilon$$

$$D_5 = ((d + l\ cos\ (\varepsilon + \varphi) + l\ cos\ \varphi)^2 + (l\ sin\ (\varepsilon + \varphi) + l\ sin\ \varphi)^2)^{3/2}$$

$$D'_5 = 3\sqrt[3]{D_5}(-(d + l\ cos\ (\varepsilon + \varphi) + l\ cos\ \varphi)\ l\ sin\ (\varepsilon + \varphi) + (l\ sin\ (\varepsilon + \varphi) + l\ sin\ \varphi)\ l\ cos\ (\varepsilon + \varphi))$$

$$N_6 = 2l^2\ sin\ \varepsilon - ld\ sin\ \varphi - ld \sin\ (\varepsilon + \varphi)$$

$$N'_6 = 2\ l^2 cos\ \varepsilon - ld\ cos\ (\varepsilon + \varphi)$$

$$D_6 = ((d - l\ cos\ (\varepsilon + \varphi) + l\ cos\ \varphi)^2 + (-l\ sin\ (\varepsilon + \varphi) + l\ sin\ \varphi)^2)^{3/2}$$

$$D'_6 = 3\sqrt[3]{D_6}\big((d - l\ cos\ (\varepsilon + \varphi) + l\ cos\ \varphi)\ l\ sin\ (\varepsilon + \varphi) - (-l\ sin\ (\varepsilon + \varphi) + l\ sin\ \varphi)\ l\ cos\ (\varepsilon + \varphi)\big)$$

$$N_7 = ld \sin \varphi$$

$$N'_7 = 0$$

$$D_7 = ((-d + l\ cos\ \varphi)^2 + (l\ sin\ \varphi)^2)^{3/2}$$

$$D'_7 = 0$$

$$N_8 = -ld\ sin\ \varphi$$

$$N'_8 = 0$$

$$D_8 = ((-d - l\ cos\ \varphi)^2 + (-l\ sin\ \varphi)^2)^{3/2}$$

$$D'_8 = 0$$

Substituting and evaluating the derivatives results in the following, which is Equation

(27) from the main thesis.

$$g(\varphi) = \frac{k_C}{I_t}\left(\frac{q_{1,e}q_{a,e}(6l^2 sin^2\varphi - 2l^2 + ld\ cos\ \varphi)}{d^3}\right.$$

$$+ \frac{q_{1,e}q_{c,e}(2l^2 - ld\ cos\ \varphi\ )}{((d - 2l\ cos\ \varphi)^2 + (-2l\ sin\ \varphi)^2)^{3/2}}$$

$$+ \frac{q_{2,e}q_{a,e}(ld\ cos\ \varphi\ ((d - l\ cos\ \varphi)^2 + (-l\ sin\ \varphi)^2)^{3/2})}{((d - l\ cos\ \varphi)^2 + (-l\ sin\ \varphi)^2)^3}$$

$$- \frac{3\ q_{2,e}q_{a,e}\ l^2d^2\ sin^2\varphi\ ((d - l\ cos\ \varphi)^2 + (-l\ sin\ \varphi)^2)^{1/2}}{((d - l\ cos\ \varphi)^2 + (-l\ sin\ \varphi)^2)^3}$$

$$+ \frac{q_{2,e}q_{c,e}(-ld\ cos\ \varphi\ ((d + l\ cos\ \varphi)^2 + (-l\ sin\ \varphi)^2)^{3/2})}{((d + l\ cos\ \varphi)^2 + (-l\ sin\ \varphi)^2)^3}$$

$$+ \frac{3q_{2,e}q_{c,e}\ l^2d^2sin^2\varphi\ ((d + l\ cos\ \varphi)^2 + (-l\ sin\ \varphi)^2)^{1/2}}{((d + l\ cos\ \varphi)^2 + (-l\ sin\ \varphi)^2)^3}$$

$$+ \frac{q_{3,e}q_{a,e}(ld\ cos\ \varphi + 2l^2)}{((d + 2l\ cos\ \varphi)^2 + (2l\ sin\ \varphi)^2)^{3/2}}$$

$$\left. + \frac{q_{3,e}q_{c,e}(6l^2 sin^2\varphi + 2l^2 - ld\ cos\ \varphi)}{d^3}\right)$$

APPENDIX D – DERIVATION OF TORQUE EXPRESSIONS FOR 3D CASE

The electrostatic torque expressions for the 3D Case, like the 2D Case, are derived using Equation (15), under double-sums to include the interactions of each pair of charged regions. However, in this Case, the dimensionality of the position vectors is different, owing to the higher dimensionality of the system.

Starting with the torque experienced by the deputy spacecraft, we begin with Equation (44), the double-sum of Equation (15) that was introduced in Appendix A, reproduced here for convenience.

$$\vec{M}_D = k_C \sum_{n=a}^{c} q_n \sum_{v=1}^{3} \frac{q_v}{\left\|\vec{r}_{v,n}\right\|^3} \vec{r}_{b,n} \times \vec{r}_{v,n}$$

where all symbols are as defined above. As shown before, expanding this double-sum fully results in the following expression.

$$\begin{aligned}\vec{M}_D = k_C \Bigg(& \frac{q_1 q_a \left(\vec{r}_{b,a} \times \vec{r}_{1,a}\right)}{\left\|\vec{r}_{1,a}\right\|^3} + \frac{q_1 q_b \left(\vec{r}_{b,b} \times \vec{r}_{1,b}\right)}{\left\|\vec{r}_{1,b}\right\|^3} + \frac{q_1 q_c \left(\vec{r}_{b,c} \times \vec{r}_{1,c}\right)}{\left\|\vec{r}_{1,c}\right\|^3} + \frac{q_2 q_a \left(\vec{r}_{b,a} \times \vec{r}_{2,a}\right)}{\left\|\vec{r}_{2,a}\right\|^3} \\ & + \frac{q_2 q_b \left(\vec{r}_{b,b} \times \vec{r}_{2,b}\right)}{\left\|\vec{r}_{2,b}\right\|^3} + \frac{q_2 q_c \left(\vec{r}_{b,c} \times \vec{r}_{2,c}\right)}{\left\|\vec{r}_{2,c}\right\|^3} + \frac{q_3 q_a \left(\vec{r}_{b,a} \times \vec{r}_{3,a}\right)}{\left\|\vec{r}_{3,a}\right\|^3} \\ & + \frac{q_3 q_b \left(\vec{r}_{b,b} \times \vec{r}_{3,b}\right)}{\left\|\vec{r}_{3,b}\right\|^3} + \frac{q_3 q_c \left(\vec{r}_{b,c} \times \vec{r}_{3,c}\right)}{\left\|\vec{r}_{3,c}\right\|^3} \Bigg)\end{aligned}$$

Note, however, that all three terms involving q_b will drop from this equation, as for the 2D Case. This is because the $\vec{r}_{b,b}$ vector in the cross product in each is the vector from the center of sphere b to the center of sphere b, also known as the zero vector. This results in each of these terms evaluating to zero. Thus, the remaining terms are the same as for

the 2D Case, as shown below.

$$\vec{M}_D = k_C \left(\frac{q_1 q_a (\vec{r}_{b,a} \times \vec{r}_{1,a})}{\|\vec{r}_{1,a}\|^3} + \frac{q_1 q_c (\vec{r}_{b,c} \times \vec{r}_{1,c})}{\|\vec{r}_{1,c}\|^3} + \frac{q_2 q_a (\vec{r}_{b,a} \times \vec{r}_{2,a})}{\|\vec{r}_{2,a}\|^3} + \frac{q_2 q_c (\vec{r}_{b,c} \times \vec{r}_{2,c})}{\|\vec{r}_{2,c}\|^3} + \frac{q_3 q_a (\vec{r}_{b,a} \times \vec{r}_{3,a})}{\|\vec{r}_{3,a}\|^3} + \frac{q_3 q_c (\vec{r}_{b,c} \times \vec{r}_{3,c})}{\|\vec{r}_{3,c}\|^3} \right)$$

Thus, the derivation becomes a matter of evaluating the vector operations in this equation from here on. Given the 1-2-1 Euler angle sequence used in this study, with the third angle dropped due to the cylindrical shapes of the spacecraft (see Section 4.2.2 for details), the six position vectors of the charged regions on the spacecraft, reckoned from the center of sphere 2 in reference coordinates, are as follows.

$$\vec{r}_1 = \begin{bmatrix} l\cos\varphi \\ l\sin\varphi\sin\alpha \\ l\sin\varphi\cos\alpha \end{bmatrix}, \qquad \vec{r}_2 = \begin{bmatrix} 0 \\ 0 \\ 0 \end{bmatrix}, \qquad \vec{r}_3 = \begin{bmatrix} -l\cos\varphi \\ -l\sin\varphi\sin\alpha \\ -l\sin\varphi\cos\alpha \end{bmatrix}$$

$$\vec{r}_a = \begin{bmatrix} d + l\cos\theta \\ l\sin\theta\sin\beta \\ l\sin\theta\cos\beta \end{bmatrix}, \ \vec{r}_b = \begin{bmatrix} d \\ 0 \\ 0 \end{bmatrix}, \ \vec{r}_c = \begin{bmatrix} d - l\cos\theta \\ -l\sin\theta\sin\beta \\ -l\sin\theta\cos\beta \end{bmatrix} \tag{63}$$

Verification of these position vectors is left as an exercise to the reader. Using these six position vectors, the relative position vector of each charged region from each other one (that is used in the torque expression) is easily constructed by subtracting one from the other.

$$\vec{r}_{1,a} = \begin{bmatrix} d + l\cos\theta - l\cos\varphi \\ l\sin\theta\sin\beta - l\sin\varphi\sin\alpha \\ l\sin\theta\cos\beta - l\sin\varphi\cos\alpha \end{bmatrix}, \qquad \vec{r}_{1,c} = \begin{bmatrix} d - l\cos\theta - l\cos\varphi \\ -l\sin\theta\sin\beta - l\sin\varphi\sin\alpha \\ -l\sin\theta\cos\beta - l\sin\varphi\cos\alpha \end{bmatrix}$$

$$\vec{r}_{3,a} = \begin{bmatrix} d + l\cos\theta + l\cos\varphi \\ l\sin\theta\sin\beta + l\sin\varphi\sin\alpha \\ l\sin\theta\cos\beta + l\sin\varphi\cos\alpha \end{bmatrix}, \qquad \vec{r}_{3,c} = \begin{bmatrix} d - l\cos\theta + l\cos\varphi \\ -l\sin\theta\sin\beta + l\sin\varphi\sin\alpha \\ -l\sin\theta\cos\beta + l\sin\varphi\cos\alpha \end{bmatrix}$$

$$\vec{r}_{2,a} = \begin{bmatrix} d + l\cos\theta \\ l\sin\theta\sin\beta \\ l\sin\theta\cos\beta \end{bmatrix}, \qquad \vec{r}_{2,c} = \begin{bmatrix} d - l\cos\theta \\ -l\sin\theta\sin\beta \\ -l\sin\theta\cos\beta \end{bmatrix}, \qquad \vec{r}_{b,a} = \begin{bmatrix} l\cos\theta \\ l\sin\theta\sin\beta \\ l\sin\theta\cos\beta \end{bmatrix}$$

$$\vec{r}_{b,c} = \begin{bmatrix} -l\cos\theta \\ -l\sin\theta\sin\beta \\ -l\sin\theta\cos\beta \end{bmatrix} \tag{64}$$

Since the magnitudes of vectors are invariant under pure rotation, the magnitudes of these vectors can be taken prior to transformation into the deputy spacecraft's body-fixed frame. This will result in simpler expressions than if they had been taken after transformation. The resulting vector magnitudes, for the relevant vectors, are presented below.

$$\left\|\vec{r}_{1,a}\right\| = ((d + l\cos\theta - l\cos\varphi)^2 + (l\sin\theta\sin\beta - l\sin\varphi\sin\alpha)^2 + (l\sin\theta\cos\beta - l\sin\varphi\cos\alpha)^2)^{1/2}$$

$$\left\|\vec{r}_{1,a}\right\| = \sqrt{d^2 + 2l(d\cos\varphi - d\cos\theta - l\cos\theta\cos\varphi + l - \Omega - \Gamma)}$$

$$\left\|\vec{r}_{1,c}\right\| = ((d - l\cos\theta - l\cos\varphi)^2 + (-l\sin\theta\sin\beta - l\sin\varphi\sin\alpha)^2 + (-l\sin\theta\cos\beta - l\sin\varphi\cos\alpha)^2)^{1/2}$$

$$\left\|\vec{r}_{1,c}\right\| = \sqrt{d^2 + 2l(d\cos\varphi + d\cos\theta + l\cos\theta\cos\varphi + l + \Omega + \Gamma)}$$

$$\left\|\vec{r}_{3,a}\right\| = ((d + l\cos\theta + l\cos\varphi)^2 + (l\sin\theta\sin\beta + l\sin\varphi\sin\alpha)^2 + (l\sin\theta\cos\beta + l\sin\varphi\cos\alpha)^2)^{1/2}$$

$$\left\|\vec{r}_{3,a}\right\| = \sqrt{d^2 - 2l(d\cos\varphi + d\cos\theta - l\cos\theta\cos\varphi - l - \Omega - \Gamma)}$$

$$\left\|\vec{r}_{3,c}\right\| = ((d - l\cos\theta + l\cos\varphi)^2 + (-l\sin\theta\sin\beta + l\sin\varphi\sin\alpha)^2$$

$$+ (-l\sin\theta\cos\beta + l\sin\varphi\cos\alpha)^2)^{1/2}$$

$$\left\|\vec{r}_{3,c}\right\| = \sqrt{d^2 - 2l(d\cos\varphi - d\cos\theta + l\cos\theta\cos\varphi - l + \Omega + \Gamma)}$$

$$\left\|\vec{r}_{2,a}\right\| = \sqrt{(d + l\cos\theta)^2 + (l\sin\theta\sin\beta)^2 + (l\sin\theta\cos\beta)^2}$$

$$\left\|\vec{r}_{2,a}\right\| = \sqrt{d^2 - 2\,ld\cos\theta + l^2}$$

$$\left\|\vec{r}_{2,c}\right\| = \sqrt{(d - l\cos\theta)^2 + (-l\sin\theta\sin\beta)^2 + (-l\sin\theta\cos\beta)^2}$$

$$\left\|\vec{r}_{2,c}\right\| = \sqrt{d^2 + 2\,ld\cos\theta + l^2}$$

$$\Omega = l\sin\theta\sin\beta\sin\varphi\sin\alpha$$

$$\Gamma = l\sin\theta\cos\beta\sin\varphi\cos\alpha \tag{65}$$

Finally, the cross-product terms in the torque expression must be computed. In order to do this, the vectors must be converted into the deputy spacecraft's body-fixed frame and the relevant cross-products must be evaluated. To accomplish the conversion from reference to body-fixed coordinates, the general DCM for the deputy's attitude with respect to the reference frame must be determined. Using the 1-2-1 Euler angles for the deputy spacecraft and Equation (4), this DCM can be determined to be the following.

$$Q_D = \begin{bmatrix}\cos\theta & 0 & -\sin\theta \\ 0 & 1 & 0 \\ \sin\theta & 0 & \cos\theta\end{bmatrix}\begin{bmatrix}1 & 0 & 0 \\ 0 & \cos\beta & \sin\beta \\ 0 & -\sin\beta & \cos\beta\end{bmatrix} =$$

$$\begin{bmatrix}\cos\theta & \sin\theta\sin\beta & -\sin\theta\cos\beta \\ 0 & \cos\beta & \sin\beta \\ \sin\theta & -\cos\theta\sin\beta & \cos\theta\cos\beta\end{bmatrix} \tag{66}$$

Using this DCM, the vectors in Equation (64) can be converted to the deputy's body-fixed frame as follows.

$$Q_D\vec{r}_{1,a} = \begin{bmatrix} cos\,\theta\,(d + l\,cos\,\theta - l\,cos\,\varphi) - \sin\theta\cos\beta(l\,sin\,\theta\,cos\,\beta - l\,sin\,\varphi\,cos\,\alpha) \\ \cos\beta(l\,sin\,\theta\,sin\,\beta - l\,sin\,\varphi\,sin\,\alpha) + \sin\beta(l\,sin\,\theta\,cos\,\beta - l\,sin\,\varphi\,cos\,\alpha) \\ \sin\theta(d + l\,cos\,\theta - l\,cos\,\varphi) + \cos\theta\cos\beta(l\,sin\,\theta\,cos\,\beta - l\,sin\,\varphi\,cos\,\alpha) \end{bmatrix}$$

$$+ \begin{bmatrix} \sin\theta\sin\beta(l\,sin\,\theta\,sin\,\beta - l\,sin\,\varphi\,sin\,\alpha) \\ 0 \\ -\cos\theta\sin\beta(l\,sin\,\theta\,sin\,\beta - l\,sin\,\varphi\,sin\,\alpha) \end{bmatrix}$$

$Q_D\vec{r}_{1,c}$

$$= \begin{bmatrix} cos\,\theta\,(d - l\,cos\,\theta - l\,cos\,\varphi) - \sin\theta\cos\beta(-l\,sin\,\theta\,cos\,\beta - l\,sin\,\varphi\,cos\,\alpha) \\ \cos\beta(-l\,sin\,\theta\,sin\,\beta - l\,sin\,\varphi\,sin\,\alpha) + \sin\beta(-l\,sin\,\theta\,cos\,\beta - l\,sin\,\varphi\,cos\,\alpha) \\ \sin\theta(d - l\,cos\,\theta - l\,cos\,\varphi) + \cos\theta\cos\beta(-l\,sin\,\theta\,cos\,\beta - l\,sin\,\varphi\,cos\,\alpha) \end{bmatrix}$$

$$+ \begin{bmatrix} \sin\theta\sin\beta(-l\,sin\,\theta\,sin\,\beta - l\,sin\,\varphi\,sin\,\alpha) \\ 0 \\ -\cos\theta\sin\beta(-l\,sin\,\theta\,sin\,\beta - l\,sin\,\varphi\,sin\,\alpha) \end{bmatrix}$$

$$Q_D\vec{r}_{3,a} = \begin{bmatrix} cos\,\theta\,(d + l\,cos\,\theta + l\,cos\,\varphi) - \sin\theta\cos\beta(l\,sin\,\theta\,cos\,\beta + l\,sin\,\varphi\,cos\,\alpha) \\ \cos\beta(l\,sin\,\theta\,sin\,\beta + l\,sin\,\varphi\,sin\,\alpha) + \sin\beta(l\,sin\,\theta\,cos\,\beta + l\,sin\,\varphi\,cos\,\alpha) \\ \sin\theta(d + l\,cos\,\theta + l\,cos\,\varphi) + \cos\theta\cos\beta(l\,sin\,\theta\,cos\,\beta + l\,sin\,\varphi\,cos\,\alpha) \end{bmatrix}$$

$$+ \begin{bmatrix} \sin\theta\sin\beta(l\,sin\,\theta\,sin\,\beta + l\,sin\,\varphi\,sin\,\alpha) \\ 0 \\ -\cos\theta\sin\beta(l\,sin\,\theta\,sin\,\beta + l\,sin\,\varphi\,sin\,\alpha) \end{bmatrix}$$

$Q_D\vec{r}_{3,c}$

$$= \begin{bmatrix} cos\,\theta\,(d - l\,cos\,\theta + l\,cos\,\varphi) - \sin\theta\cos\beta(-l\,sin\,\theta\,cos\,\beta + l\,sin\,\varphi\,cos\,\alpha) \\ \cos\beta(-l\,sin\,\theta\,sin\,\beta + l\,sin\,\varphi\,sin\,\alpha) + \sin\beta(-l\,sin\,\theta\,cos\,\beta + l\,sin\,\varphi\,cos\,\alpha) \\ \sin\theta(d - l\,cos\,\theta + l\,cos\,\varphi) + \cos\theta\cos\beta(-l\,sin\,\theta\,cos\,\beta + l\,sin\,\varphi\,cos\,\alpha) \end{bmatrix}$$

$$+ \begin{bmatrix} \sin\theta\sin\beta(-l\,sin\,\theta\,sin\,\beta + l\,sin\,\varphi\,sin\,\alpha) \\ 0 \\ -\cos\theta\sin\beta(-l\,sin\,\theta\,sin\,\beta + l\,sin\,\varphi\,sin\,\alpha) \end{bmatrix}$$

$$Q_D\vec{r}_{2,a}$$

$$= \begin{bmatrix} \cos\theta(d + l\cos\theta) + \sin\theta\sin\beta(l\sin\theta\sin\beta) - \sin\theta\cos\beta(l\sin\theta\cos\beta) \\ \cos\beta(l\sin\theta\sin\beta) + \sin\beta(l\sin\theta\cos\beta) \\ \sin\theta(d + l\cos\theta) - \cos\theta\sin\beta(l\sin\theta\sin\beta) + \cos\theta\cos\beta(l\sin\theta\cos\beta) \end{bmatrix}$$

$$Q_D\vec{r}_{2,c}$$

$$= \begin{bmatrix} \cos\theta(d - l\cos\theta) + \sin\theta\sin\beta(-l\sin\theta\sin\beta) - \sin\theta\cos\beta(-l\sin\theta\cos\beta) \\ \cos\beta(-l\sin\theta\sin\beta) + \sin\beta(-l\sin\theta\cos\beta) \\ \sin\theta(d - l\cos\theta) - \cos\theta\sin\beta(-l\sin\theta\sin\beta) + \cos\theta\cos\beta(-l\sin\theta\cos\beta) \end{bmatrix}$$

$$Q_D\vec{r}_{b,a} = \begin{bmatrix} l \\ 0 \\ 0 \end{bmatrix},\ Q_D\vec{r}_{b,c} = \begin{bmatrix} -l \\ 0 \\ 0 \end{bmatrix} \tag{67}$$

Note that, for $\vec{r}_{1,a}$, $\vec{r}_{1,c}$, $\vec{r}_{3,a}$, and $\vec{r}_{3,c}$, the vectors were only presented as a sum of vectors to accommodate them on the page without decreasing the font size to unreadable levels. Using these vectors' deputy frame expressions, the cross-product terms are then computed as follows.

$$\vec{r}_{b,a} \times \vec{r}_{1,a} = \begin{bmatrix} 0 \\ -l\sin\theta\left(d - l\cos\varphi + \cos\theta\left(l - l\sin^2\beta + l\cos^2\beta\right)\right) + l\cos\theta\,\Lambda \\ l\left(-l\cos\beta\sin\varphi\sin\alpha + 2l\sin\theta\sin\beta\cos\beta - l\sin\varphi\cos\alpha\sin\beta\right) \end{bmatrix}$$

$$\vec{r}_{b,a} \times \vec{r}_{3,a} = \begin{bmatrix} 0 \\ -l\sin\theta\left(d + l\cos\varphi + \cos\theta\left(l - l\sin^2\beta + l\cos^2\beta\right)\right) - l\cos\theta\,\Lambda \\ l\left(l\cos\beta\sin\varphi\sin\alpha + 2l\sin\theta\sin\beta\cos\beta + l\sin\varphi\cos\alpha\sin\beta\right) \end{bmatrix}$$

$$\vec{r}_{b,a} \times \vec{r}_{2,a} = \begin{bmatrix} 0 \\ -l\left(d\sin\theta + l\cos\theta\sin\theta - l\sin\theta\cos\theta\sin^2\beta + l\sin\theta\cos\theta\cos^2\beta\right) \\ 2l^2\sin\theta\sin\beta\cos\beta \end{bmatrix}$$

$$\vec{r}_{b,c} \times \vec{r}_{1,c} = \begin{bmatrix} 0 \\ -l\sin\theta\left(-d + l\cos\varphi + \cos\theta\left(l - l\sin^2\beta + l\cos^2\beta\right)\right) - l\cos\theta\,\Lambda \\ l\left(l\cos\beta\sin\varphi\sin\alpha + 2l\sin\theta\sin\beta\cos\beta + l\sin\varphi\cos\alpha\sin\beta\right) \end{bmatrix}$$

$$\vec{r}_{b,c} \times \vec{r}_{3,c} = \begin{bmatrix} 0 \\ -l\ sin\ \theta \left(-d - l\ cos\ \varphi + cos\ \theta\ (l - l\ sin^2\beta + l\ cos^2\beta)\right) + l\ cos\ \theta\ \Lambda \\ l\ (-l\ cos\ \beta\ sin\ \varphi\ sin\ \alpha + 2l\ sin\ \theta\ sin\ \beta\ cos\ \beta - l\ sin\ \varphi\ cos\ \alpha\ sin\ \beta) \end{bmatrix}$$

$$\vec{r}_{b,c} \times \vec{r}_{2,c}$$

$$= \begin{bmatrix} 0 \\ -l\ (-d\ sin\ \theta + l\ cos\ \theta\ sin\ \theta - l\ sin\ \theta\ cos\ \theta\ sin^2\beta + l\ sin\ \theta\ cos\ \theta\ cos^2\beta) \\ 2l^2 sin\ \theta\ sin\ \beta\ cos\ \beta \end{bmatrix}$$

$$\Lambda = sin\ \beta\ sin\ \varphi\ sin\ \alpha - cos\ \beta\ sin\ \varphi\ cos\ \alpha \tag{68}$$

Substituting Equations (65) and (68) into the torque expression then yields the electrostatic torque on the deputy, presented in the main thesis as Equation (22).

To derive the corresponding expression for the chief spacecraft follows a very similar path. As with the 2D Case, the torque expression is given by the following double-sum, Equation (51), reproduced here for convenience.

$$\vec{M}_C = k_C \sum_{v=1}^{3} q_v \sum_{n=a}^{c} \frac{q_n}{\left\|\vec{r}_{n,v}\right\|^3} \vec{r}_{2,v} \times \vec{r}_{n,v}$$

Similar to how the deputy derivation was conducted, we start with the expansion of this equation, given below.

$$\vec{M}_C = k_C \left(\frac{q_1 q_a \left(\vec{r}_{2,1} \times \vec{r}_{a,1}\right)}{\left\|\vec{r}_{a,1}\right\|^3} + \frac{q_1 q_b \left(\vec{r}_{2,1} \times \vec{r}_{b,1}\right)}{\left\|\vec{r}_{b,1}\right\|^3} + \frac{q_1 q_c \left(\vec{r}_{2,1} \times \vec{r}_{c,1}\right)}{\left\|\vec{r}_{c,1}\right\|^3} + \frac{q_2 q_a \left(\vec{r}_{2,2} \times \vec{r}_{a,2}\right)}{\left\|\vec{r}_{a,2}\right\|^3} \right.$$

$$+ \frac{q_2 q_b \left(\vec{r}_{2,2} \times \vec{r}_{b,2}\right)}{\left\|\vec{r}_{b,2}\right\|^3} + \frac{q_2 q_c \left(\vec{r}_{2,2} \times \vec{r}_{c,2}\right)}{\left\|\vec{r}_{c,2}\right\|^3} + \frac{q_3 q_a \left(\vec{r}_{2,3} \times \vec{r}_{a,3}\right)}{\left\|\vec{r}_{a,3}\right\|^3}$$

$$\left. + \frac{q_3 q_b \left(\vec{r}_{2,3} \times \vec{r}_{b,3}\right)}{\left\|\vec{r}_{b,3}\right\|^3} + \frac{q_3 q_c \left(\vec{r}_{2,3} \times \vec{r}_{c,3}\right)}{\left\|\vec{r}_{c,3}\right\|^3} \right)$$

Like its deputy spacecraft counterpart, three of the terms from this expression go to zero. These are the terms that involve q_2, as the $\vec{r}_{2,2}$ vector is the zero vector. Therefore, the remaining terms are the following, like in the 2D Case.

$$\vec{M}_C = k_C \left(\frac{q_1 q_a \left(\vec{r}_{2,1} \times \vec{r}_{a,1}\right)}{\left\|\vec{r}_{a,1}\right\|^3} + \frac{q_1 q_b \left(\vec{r}_{2,1} \times \vec{r}_{b,1}\right)}{\left\|\vec{r}_{b,1}\right\|^3} + \frac{q_1 q_c \left(\vec{r}_{2,1} \times \vec{r}_{c,1}\right)}{\left\|\vec{r}_{c,1}\right\|^3} + \frac{q_3 q_a \left(\vec{r}_{2,3} \times \vec{r}_{a,3}\right)}{\left\|\vec{r}_{a,3}\right\|^3} + \frac{q_3 q_b \left(\vec{r}_{2,3} \times \vec{r}_{b,3}\right)}{\left\|\vec{r}_{b,3}\right\|^3} + \frac{q_3 q_c \left(\vec{r}_{2,3} \times \vec{r}_{c,3}\right)}{\left\|\vec{r}_{c,3}\right\|^3} \right)$$

Using the general position vectors in Equation (63), the required relative position vectors are, like their deputy counterparts, constructed by subtraction.

$$\vec{r}_{a,1} = \begin{bmatrix} -d - l\cos\theta + l\cos\varphi \\ -l\sin\theta\sin\beta + l\sin\varphi\sin\alpha \\ -l\sin\theta\cos\beta + l\sin\varphi\cos\alpha \end{bmatrix}, \qquad \vec{r}_{c,1} = \begin{bmatrix} -d + l\cos\theta + l\cos\varphi \\ l\sin\theta\sin\beta + l\sin\varphi\sin\alpha \\ l\sin\theta\cos\beta + l\sin\varphi\cos\alpha \end{bmatrix}$$

$$\vec{r}_{a,3} = \begin{bmatrix} -d - l\cos\theta - l\cos\varphi \\ -l\sin\theta\sin\beta - l\sin\varphi\sin\alpha \\ -l\sin\theta\cos\beta - l\sin\varphi\cos\alpha \end{bmatrix}, \qquad \vec{r}_{c,3} = \begin{bmatrix} -d + l\cos\theta - l\cos\varphi \\ l\sin\theta\sin\beta - l\sin\varphi\sin\alpha \\ l\sin\theta\cos\beta - l\sin\varphi\cos\alpha \end{bmatrix}$$

$$\vec{r}_{b,1} = \begin{bmatrix} -d + l\cos\varphi \\ l\sin\varphi\sin\alpha \\ l\sin\varphi\cos\alpha \end{bmatrix}, \qquad \vec{r}_{b,3} = \begin{bmatrix} -d - l\cos\varphi \\ -l\sin\varphi\sin\alpha \\ -l\sin\varphi\cos\alpha \end{bmatrix}, \qquad \vec{r}_{2,1} = \begin{bmatrix} l\cos\varphi \\ l\sin\varphi\sin\alpha \\ l\sin\varphi\cos\alpha \end{bmatrix}$$

$$\vec{r}_{2,3} = \begin{bmatrix} -l\cos\varphi \\ -l\sin\varphi\sin\alpha \\ -l\sin\varphi\cos\alpha \end{bmatrix} \tag{69}$$

Next, as before, we take the vector magnitudes that are needed in the denominator of the terms in the torque expression. Luckily, since four of these vectors, $\vec{r}_{a,1}$, $\vec{r}_{c,1}$, $\vec{r}_{a,3}$, and $\vec{r}_{c,3}$, are negatives of four vectors from the deputy derivation ($\vec{r}_{1,a}$, $\vec{r}_{1,c}$, $\vec{r}_{3,a}$, and $\vec{r}_{3,c}$, respectively), the magnitudes of these from the deputy case can be used, as vector

magnitudes are independent of vector orientation. The remaining magnitudes are as follows.

$$\left\|\vec{r}_{b,1}\right\| = \sqrt{(-d + l\,cos\,\varphi)^2 + (l\,sin\,\varphi\,sin\,\alpha)^2 + (l\,sin\,\varphi\,cos\,\alpha)^2}$$

$$\left\|\vec{r}_{b,1}\right\| = \sqrt{d^2 - 2ld\,cos\,\varphi + l^2}$$

$$\left\|\vec{r}_{b,3}\right\| = \sqrt{(-d - l\,cos\,\varphi)^2 + (-l\,sin\,\varphi\,sin\,\alpha)^2 + (-l\,sin\,\varphi\,cos\,\alpha)^2}$$

$$\left\|\vec{r}_{b,3}\right\| = \sqrt{d^2 + 2ld\,cos\,\varphi + l^2} \tag{70}$$

With these magnitudes computed, the vectors of Equation (69) must be converted to the chief's body-fixed frame, as the deputy's vectors needed to be converted for it. To accomplish this conversion, the chief spacecraft's general attitude DCM is constructed similarly to how the deputy's was.

$$Q_C = \begin{bmatrix} \cos\varphi & 0 & -\sin\varphi \\ 0 & 1 & 0 \\ \sin\varphi & 0 & \cos\varphi \end{bmatrix} \begin{bmatrix} 1 & 0 & 0 \\ 0 & \cos\alpha & \sin\alpha \\ 0 & -\sin\alpha & \cos\alpha \end{bmatrix} =$$

$$\begin{bmatrix} \cos\varphi & \sin\varphi\,\sin\alpha & -\sin\varphi\,\cos\alpha \\ 0 & \cos\alpha & \sin\alpha \\ \sin\varphi & -\cos\varphi\,\sin\alpha & \cos\varphi\,\cos\alpha \end{bmatrix} \tag{71}$$

The transformed relative position vectors are then found to be given by the following:

$$Q_C\vec{r}_{a,1}$$

$$= \begin{bmatrix} \cos\varphi\,(-d - l\,cos\,\theta + l\,cos\,\varphi) - \sin\varphi\,\cos\alpha(-l\,sin\,\theta\,cos\,\beta + l\,sin\,\varphi\,cos\,\alpha) \\ \cos\alpha(-l\,sin\,\theta\,sin\,\beta + l\,sin\,\varphi\,sin\,\alpha) + \sin\alpha(-l\,sin\,\theta\,cos\,\beta + l\,sin\,\varphi\,cos\,\alpha) \\ \sin\varphi(-d - l\,cos\,\theta + l\,cos\,\varphi) + \cos\varphi\,\cos\alpha(-l\,sin\,\theta\,cos\,\beta + l\,sin\,\varphi\,cos\,\alpha) \end{bmatrix}$$

$$+ \begin{bmatrix} \sin\varphi\,\sin\alpha(-l\,sin\,\theta\,sin\,\beta + l\,sin\,\varphi\,sin\,\alpha) \\ 0 \\ -\cos\varphi\,\sin\alpha(-l\,sin\,\theta\,sin\,\beta + l\,sin\,\varphi\,sin\,\alpha) \end{bmatrix}$$

$$Q_C\vec{r}_{c,1}$$

$$= \begin{bmatrix} cos\ \varphi\ (-d + l\ cos\ \theta + l\ cos\ \varphi) - \sin\varphi\cos\alpha(l\ sin\ \theta\ cos\ \beta + l\ sin\ \varphi\ cos\ \alpha) \\ \cos\alpha(l\ sin\ \theta\ sin\ \beta + l\ sin\ \varphi\ sin\ \alpha) + \sin\alpha(l\ sin\ \theta\ cos\ \beta + l\ sin\ \varphi\ cos\ \alpha) \\ \sin\varphi(-d + l\ cos\ \theta + l\ cos\ \varphi) + \cos\varphi\cos\alpha(l\ sin\ \theta\ cos\ \beta + l\ sin\ \varphi\ cos\ \alpha) \end{bmatrix}$$

$$+ \begin{bmatrix} \sin\varphi\sin\alpha(l\ sin\ \theta\ sin\ \beta + l\ sin\ \varphi\ sin\ \alpha) \\ 0 \\ -\cos\varphi\sin\alpha(l\ sin\ \theta\ sin\ \beta + l\ sin\ \varphi\ sin\ \alpha) \end{bmatrix}$$

$$Q_C\vec{r}_{a,3}$$

$$= \begin{bmatrix} cos\ \varphi\ (-d - l\ cos\ \theta - l\ cos\ \varphi) - \sin\varphi\cos\alpha(-l\ sin\ \theta\ cos\ \beta - l\ sin\ \varphi\ cos\ \alpha) \\ \cos\alpha(-l\ sin\ \theta\ sin\ \beta - l\ sin\ \varphi\ sin\ \alpha) + \sin\alpha(-l\ sin\ \theta\ cos\ \beta - l\ sin\ \varphi\ cos\ \alpha) \\ \sin\varphi(-d - l\ cos\ \theta - l\ cos\ \varphi) + \cos\varphi\cos\alpha(-l\ sin\ \theta\ cos\ \beta - l\ sin\ \varphi\ cos\ \alpha) \end{bmatrix}$$

$$+ \begin{bmatrix} \sin\varphi\sin\alpha(-l\ sin\ \theta\ sin\ \beta - l\ sin\ \varphi\ sin\ \alpha) \\ 0 \\ -\cos\varphi\sin\alpha(-l\ sin\ \theta\ sin\ \beta - l\ sin\ \varphi\ sin\ \alpha) \end{bmatrix}$$

$$Q_C\vec{r}_{c,3}$$

$$= \begin{bmatrix} cos\ \varphi\ (-d + l\ cos\ \theta - l\ cos\ \varphi) - \sin\varphi\cos\alpha(l\ sin\ \theta\ cos\ \beta - l\ sin\ \varphi\ cos\ \alpha) \\ \cos\alpha(l\ sin\ \theta\ sin\ \beta - l\ sin\ \varphi\ sin\ \alpha) + \sin\alpha(l\ sin\ \theta\ cos\ \beta - l\ sin\ \varphi\ cos\ \alpha) \\ \sin\varphi(-d + l\ cos\ \theta - l\ cos\ \varphi) + \cos\varphi\cos\alpha(l\ sin\ \theta\ cos\ \beta - l\ sin\ \varphi\ cos\ \alpha) \end{bmatrix}$$

$$+ \begin{bmatrix} \sin\varphi\sin\alpha(l\ sin\ \theta\ sin\ \beta - l\ sin\ \varphi\ sin\ \alpha) \\ 0 \\ -\cos\varphi\sin\alpha(l\ sin\ \theta\ sin\ \beta - l\ sin\ \varphi\ sin\ \alpha) \end{bmatrix}$$

$$Q_C\vec{r}_{b,1}$$

$$= \begin{bmatrix} \cos\varphi(-d + l\ cos\ \varphi) + \sin\varphi\sin\alpha(l\ sin\ \varphi\ sin\ \alpha) - \sin\varphi\cos\alpha(l\ sin\ \varphi\ cos\ \alpha) \\ \cos\alpha(l\ sin\ \varphi\ sin\ \alpha) + \sin\alpha(l\ sin\ \varphi\ cos\ \alpha) \\ \sin\varphi(-d + l\ cos\ \varphi) - \cos\varphi\sin\alpha(l\ sin\ \varphi\ sin\ \alpha) + \cos\varphi\cos\alpha(l\ sin\ \varphi\ cos\ \alpha) \end{bmatrix}$$

$$Q_C\vec{r}_{b,3}$$

$$= \begin{bmatrix} \cos\varphi(-d - l\ cos\ \varphi) + \sin\varphi\sin\alpha(-l\ sin\ \varphi\ sin\ \alpha) - \sin\varphi\cos\alpha(-l\ sin\ \varphi\ cos\ \alpha) \\ \cos\alpha(-l\ sin\ \varphi\ sin\ \alpha) + \sin\alpha(-l\ sin\ \varphi\ cos\ \alpha) \\ \sin\varphi(-d - l\ cos\ \varphi) - \cos\varphi\sin\alpha(-l\ sin\ \varphi\ sin\ \alpha) + \cos\varphi\cos\alpha(-l\ sin\ \varphi\ cos\ \alpha) \end{bmatrix}$$

$$Q_C\vec{r}_{2,1} = \begin{bmatrix} l \\ 0 \\ 0 \end{bmatrix},\ Q_C\vec{r}_{2,3} = \begin{bmatrix} -l \\ 0 \\ 0 \end{bmatrix} \tag{72}$$

With these vectors transformed, their necessary cross products can be taken, resulting in the following expressions.

$$\vec{r}_{2,1} \times \vec{r}_{a,1} = \begin{bmatrix} 0 \\ -l\ sin\ \varphi \left(-d - l\ cos\ \theta + cos\ \varphi\ (l + l\ sin^2\alpha + l\ cos^2\alpha)\right) - l\ cos\ \varphi\ \Xi \\ l\ (-l\ cos\ \alpha\ sin\ \theta\ sin\ \beta + 2l\ sin\ \varphi\ sin\ \alpha\ cos\ \alpha - l\ sin\ \theta\ cos\ \beta\ sin\ \alpha) \end{bmatrix}$$

$$\vec{r}_{2,1} \times \vec{r}_{c,1} = \begin{bmatrix} 0 \\ -l\ sin\ \varphi \left(-d + l\ cos\ \theta + cos\ \varphi\ (l - l\ sin^2\alpha + l\ cos^2\alpha)\right) - l\ cos\ \varphi\ \Xi \\ l\ (l\ cos\ \alpha\ sin\ \theta\ sin\ \beta + 2l\ sin\ \varphi\ sin\ \alpha\ cos\ \alpha + l\ sin\ \theta\ cos\ \beta\ sin\ \alpha) \end{bmatrix}$$

$$\vec{r}_{2,1} \times \vec{r}_{b,1}$$

$$= \begin{bmatrix} 0 \\ -l\ (-d\ sin\ \varphi + l\ cos\ \varphi\ sin\ \varphi - l\ sin\ \varphi\ cos\ \varphi\ sin^2\alpha + l\ sin\ \varphi\ cos\ \varphi\ cos^2\alpha) \\ 2l^2 sin\ \varphi\ sin\ \alpha\ cos\ \alpha \end{bmatrix}$$

$$\vec{r}_{2,3} \times \vec{r}_{a,3} = \begin{bmatrix} 0 \\ -l\ sin\ \varphi \left(d + l\ cos\ \theta + cos\ \varphi\ (l + l\ sin^2\alpha - l\ cos^2\alpha)\right) + l\ cos\ \varphi\ \Xi \\ l\ (l\ cos\ \alpha\ sin\ \theta\ sin\ \beta + 2l\ sin\ \varphi\ sin\ \alpha\ cos\ \alpha + l\ sin\ \theta\ cos\ \beta\ sin\ \alpha) \end{bmatrix}$$

$$\vec{r}_{2,3} \times \vec{r}_{c,3} = \begin{bmatrix} 0 \\ -l\ sin\ \varphi \left(d - l\ cos\ \theta + cos\ \varphi\ (l - l\ sin^2\alpha + l\ cos^2\alpha)\right) + l\ cos\ \varphi\ \Xi \\ l\ (-l\ cos\ \alpha\ sin\ \theta\ sin\ \beta + 2l\ sin\ \varphi\ sin\ \alpha\ cos\ \alpha - l\ sin\ \theta\ cos\ \beta\ sin\ \alpha) \end{bmatrix}$$

$$\vec{r}_{2,3} \times \vec{r}_{b,3}$$

$$= \begin{bmatrix} 0 \\ -l\ (d\ sin\ \varphi + l\ cos\ \varphi\ sin\ \varphi - l\ sin\ \varphi\ cos\ \varphi\ sin^2\alpha + l\ sin\ \varphi\ cos\ \varphi\ cos^2\alpha) \\ 2l^2 sin\ \varphi\ sin\ \alpha\ cos\ \alpha \end{bmatrix}$$

$$\Xi = sin\ \beta\ sin\ \theta\ sin\ \alpha - cos\ \alpha\ sin\ \theta\ cos\ \beta \tag{73}$$

Finally, as before, substitution of Equations (70) and (73) into the torque expression results in the chief electrostatic torque, presented in the main thesis as Equation (23).

APPENDIX E – DERIVATION OF OPEN-LOOP KINETIC EQUATION FOR 3D CASE

With the electrostatic torque expressions defined, deriving the open-loop dynamics of the 3D Case is a simple matter. Using Equation (13) for the kinetic equations of the two spacecraft, we begin with the following equations. Note that the subscripts on the moment of inertia terms indicate the spacecraft whose body-fixed frame they were calculated in. Due to the assumption of identical construction, their numerical values are the same.

$$\dot{\vec{\omega}}_D = I_D^{-1}\left(\vec{M}_D - \vec{\omega}_D \times I_D\vec{\omega}_D\right)$$
$$\dot{\vec{\omega}}_C = I_C^{-1}\left(\vec{M}_C - \vec{\omega}_C \times I_C\vec{\omega}_C\right) \quad (74)$$

It is desired to obtain the kinetic equation for the relative system in terms of the relative angular velocity of the deputy spacecraft with respect to the chief spacecraft. That is to say, in terms of $\vec{\omega}_{CD} = \vec{\omega}_D - \vec{\omega}_C$. Taking the derivative of this angular velocity with respect to time, the following results: $\dot{\vec{\omega}}_{CD} = \dot{\vec{\omega}}_D - \dot{\vec{\omega}}_C$. Thus, in principle, the derivative of the relative angular velocity is the difference of the derivatives of the two spacecraft angular velocities. However, this cannot be computed by simply subtracting the spacecraft kinetic equations. This is because the two angular velocities are expressed in their respective spacecraft's body-fixed frames. Thus, they must be resolved into a single frame to conduct this subtraction. For computational simplicity, the chief spacecraft's frame was selected to be the common frame. To transform the derivative of the deputy's angular velocity into the chief's body-fixed frame, the DCM of the relative attitude of the deputy with respect to the chief is used. That is to say, $E_{CD} = Q_D Q_C^T$. This

is used to transform the deputy's equation, resulting in the following expression.

$$E_{CD}^{T}\dot{\vec{\omega}}_D = E_{CD}^{T}I_D^{-1}\left(\vec{M}_D - \vec{\omega}_D \times I_D\vec{\omega}_D\right) \tag{75}$$

Then, the chief kinetic equation is subtracted from this to construct the relative system kinetic equation, as follows.

$$\dot{\vec{\omega}}_{CD} = E_{CD}^{T}I_D^{-1}\left(\vec{M}_D - \vec{\omega}_D \times I_D\vec{\omega}_D\right) - I_C^{-1}\left(\vec{M}_C - \vec{\omega}_C \times I_C\vec{\omega}_C\right) \tag{76}$$

Next, $\vec{\omega}_D$ is expressed as a function of the relative angular velocity and the chief angular velocity, taking frames into account. This substitution is given by $\vec{\omega}_D = E_{CD}(\vec{\omega}_{CD} + \vec{\omega}_C)$. Applying this to Equation (76) results in the following.

$$\begin{aligned}\dot{\vec{\omega}}_{CD} = E_{CD}^{T}I_D^{-1}\Big(\vec{M}_D - E_{CD}(\vec{\omega}_{CD} + \vec{\omega}_C) \times I_D E_{CD}(\vec{\omega}_{CD} + \vec{\omega}_C)\Big)\\ -I_C^{-1}\left(\vec{M}_C - \vec{\omega}_C \times I_C\vec{\omega}_C\right)\end{aligned} \tag{77}$$

Finally, the cross products are resolved into matrix products using the skew-symmetric operator introduced in the main thesis, resulting in the final relative system kinetic equation. Note that this equation can be closed-loop or open-loop, depending on whether the torque terms consist only of open-loop torques, or of open- and closed-loop torques. This is Equation (24) from the main thesis.

$$\dot{\vec{\omega}}_{CD} = E_{CD}^{T}I_D^{-1}\left(\vec{M}_D - E_{CD}(\widetilde{\vec{\omega}_{CD}} + \vec{\omega}_C)I_D\left(E_{CD}(\vec{\omega}_{CD} + \vec{\omega}_C)\right)\right) - I_C^{-1}\left(\vec{M}_C - \widetilde{\omega}_C I_C\vec{\omega}_C\right)$$

APPENDIX F – DERIVATION OF CONTROL TORQUE EXPRESSION FOR 3D CASE

This Appendix will derive the control torque expression, presented in the main thesis as Equation (36), from the control law, presented in the main thesis as Equation (35). Thus, the control law is reprinted here for convenience.

$$\vec{\omega}_D = \vec{\omega}_D^d + h'(\Phi_{CD})\vec{k}_{CD}$$

This control law is unlike most; it specifies an angular velocity to follow, not the torque that must be used to create it. So, a torque expression was generated from it by using Euler's equation for rigid body rotations, Equation (12), which is reprinted below for convenience.

$$\vec{M}_G = I\dot{\vec{\omega}} + \vec{\omega} \times I\vec{\omega}$$

In order to input the control law into Euler's equation, its derivative must be taken and the desired angular velocity $\vec{\omega}_D^d$ must be defined. The second task is the simpler one. For the purposes of this research, it is desired to make the deputy spacecraft track the motion of the chief spacecraft. Therefore, the desired angular velocity is the angular velocity of the chief, $\vec{\omega}_C$. Making this substitution results in the following.

$$\vec{\omega}_D = \vec{\omega}_C + h'(\Phi_{CD})\vec{k}_{CD}$$

Which is then differentiated with respect to time, resulting in the following.

$$\dot{\vec{\omega}}_D = \dot{\vec{\omega}}_C + \dot{\Phi}_{CD}h''(\Phi_{CD})\vec{k}_{CD} + h'(\Phi_{CD})\dot{\vec{k}}_{CD}$$

Finally, substituting this derivative and the original control law into Euler's equation results in the control torque expression for this controller, as presented in the main thesis.

$$\vec{M}_D^{CL} = I_D \left(\dot{\vec{\omega}}_C + \dot{\Phi}_{CD} h''(\Phi_{CD}) \vec{k}_{CD} + h'(\Phi_{CD}) \dot{\vec{k}}_{CD} \right) + \left(\vec{\omega}_C + h'(\Phi_{CD}) \vec{k}_{CD} \right) \times I_D \left(\vec{\omega}_C + h'(\Phi_{CD}) \vec{k}_{CD} \right)$$

APPENDIX G – DERIVATION OF ACTUATOR DYNAMICS SOLUTION FOR 3D CASE

As stated in the main thesis, the actuator dynamics solution was created by equating the electrostatic torque expression for the deputy spacecraft to the control torque expression and solving for the charges q_a and q_c. This was done under the constraint of assuming the chief spacecraft charges q_1, q_2, and q_3 to be constant. Under these circumstances, the equation becomes a linear system of equations, expressed in matrix form, of the deputy charges. This is expressed as the following.

$$\begin{bmatrix} \eta & \chi \\ \mu & \lambda \end{bmatrix} \begin{bmatrix} q_a \\ q_c \end{bmatrix} = \begin{bmatrix} \vec{M}_{D,2}^{CL} \\ \vec{M}_{D,3}^{CL} \end{bmatrix}$$

where η, χ, μ, and λ are as defined in the main thesis. Approaching this with the well-described theory of linear systems of equations, one must merely pre-multiply the equation by the inverse of the 2x2 matrix on the left to solve it. This results in the following expression.

$$\begin{bmatrix} q_a \\ q_c \end{bmatrix} = \frac{1}{\eta\lambda - \mu\chi} \begin{bmatrix} \lambda & -\chi \\ -\mu & \eta \end{bmatrix} \begin{bmatrix} \vec{M}_{D,2}^{CL} \\ \vec{M}_{D,3}^{CL} \end{bmatrix}$$

When multiplied out into scalar equations, this results in the solution presented in the main thesis as Equations (42) and (43).